Amine detection in aquatic organisms: receptor evolution, neuronal circuits and behavior in the model organism zebrafish

---

Inaugural-Dissertation

zur Erlangung des Doktorgrades
der Mathematisch-Naturwissenschaftlichen Fakultät
der Universität zu Köln

---

vorgelegt von

Milan Dieris

aus Berlin

Köln, 2018

Berichterstatter:	Prof. Dr. Sigrun Korsching
	Prof. Dr. Peter Kloppenburg
Tag der mündlichen Prüfung:	11.12.2017

ABSTRACT

Olfactory cues are responsible for the generation of diverse behaviors in the animal kingdom. Olfactory receptors are expressed by specialized sensory neurons (OSNs) in the olfactory epithelium. Upon odorant binding to the olfactory receptor, these neurons are activated. The information is transferred to the olfactory bulb glomeruli, which represent the first relay station for olfactory processing in the brain.

Most olfactory receptors are G-protein coupled receptors and form large gene families. One type of olfactory receptors is the trace amine-associated receptor family (TAAR). TAARs generally recognize amines. One particular member of the zebrafish TAAR family, TAAR13c, is a high-affinity receptor for the death-associated odor cadaverine, which induces aversive behavior.

Here, we identified the cell type of amine-sensitive OSNs in the zebrafish nose, which show typical properties of ciliated neurons. We used OSN type-specific markers to unambiguously characterize zebrafish TAAR13c OSNs. Using the neuronal activity marker pERK we could show that low concentrations of cadaverine activate a specific, invariant glomerulus in the dorso-lateral cluster of glomeruli (dlG) in the olfactory bulb of zebrafish. This cluster was also shown to process amine stimuli in general, a feature that is conserved in the neoteleost stickleback.

Apart from developing a technique to measure neuronal activity in the adult olfactory epithelium, we also established the use of GCaMP6-expressing zebrafish to measure neuronal activity in the larval brain. This will be helpful in deciphering neuronal circuits involved in odor processing in future experiments.

Although adult zebrafish display aversive behavior in response to cadaverine, we found zebrafish larvae to be attracted to cadaverine in a similar behavioral assay. This shift of behavior in the ontogeny of zebrafish has to be further investigated.

A TAAR13c gene knock-out could provide important insights into the neuronal processing of diamine stimuli and the role of TAAR13c for the generation of behavioral outputs. Here we used an alternative CRISPR/Cas9 approach to partially knock out the TAAR13c gene. The DNA sequence between two gRNA target sites was deleted from the genome. Further studies will have to characterize this knock-out.

The evolutionary origin of TAARs has not been conclusively described yet. Using a large scale analysis of 81 fish genomes we provide new insights into TAAR evolution. We found that TAARs together with its close sister group, TARLs, which drastically expanded in lamprey, originate in a duplication of the HTR4 gene after the emergence of chordates, but before the divergence of jawed from jawless fish. Class II TAARs are present only in the jawed vertebrate lineage. Contrary to our expectations we found TAAR13 to be retained in neoteleosts. Class II TAARs are characterized by early as well as late gene loss events at several points in fish evolution and single members often show family- or species-specific expansions.

ZUSAMMENFASSUNG

Über das gesamte Tierreich lösen Duftstoffe eine Reihe verschiedenster Verhalten aus. Olfaktorische Rezeptoren werden von spezialisierten sensorischen Neuronen (ORNs) im Riechepithel exprimiert. Durch Bindung eines Duftstoffes an den Rezeptor werden diese Neurone aktiviert. Die Reizinformation wird in sogenannte Glomeruli im olfaktorischen Bulbus (OB) weitergeleitet. Dieser repräsentiert die erste Schaltzentrale für olfaktorische Informationsverarbeitung im Gehirn.

Die meisten olfaktorischen Rezeptoren sind G-Protein gekoppelte Rezeptoren und formen große Genfamilien. Eine dieser Familien ist die Familie der Trace Amin Assoziierten Rezeptoren (TAARs). Typische Liganden für TAARs sind Amine. Ein spezifisches Mitglied der Zebrafisch TAAR Familie, TAAR13c, ist ein hoch-affiner Rezeptor für Cadaverin, welches eine Komponente von Verwesungsgeruch ist und aversives Verhalten auslöst.

Hier identifizieren wir den Zelltyp von Amin-sensitiven Zebrafisch ORNs, welche zu den ziliierten ORNs gehören. Wir benutzen Zelltyp-spezifische Marker um TAAR13c-exprimierende ORNs eindeutig zu charakterisieren. Mit dem neuronalen Aktivitätsmarker pERK identifizieren wir einen einzelnen Glomerulus im dorso-lateralen Cluster des OB, welcher durch niedrige Cadaverin Konzentrationen aktiviert wird. Dieses Cluster ist auch verantwortlich für die Verarbeitung von anderen Amin Duftstoffen, ein Merkmal, das auch im Stichling, einem Neoteleosten, konserviert ist.

Neben der Entwicklung einer Methode zur Messung neuronaler Aktivität im adulten Riechepithel, haben wir ebenso ein Protokoll zur Messung neuronaler Aktivität mittels GCaMP6 im larvalen Gehirn etabliert. Diese Technik kann zur Entschlüsselung neuronaler Netzwerke genutzt werden, die mit der Verarbeitung von Geruchsstoffen assoziiert sind.

Obwohl adulte Zebrafische aversives Verhalten in Antwort auf Cadaverin Stimuli zeigen, konnten wir dieses Verhalten nicht in der Larve beobachten. Stattdessen wurden die Larven von dem Duftstoff angezogen. Der Wechsel von attraktiver zu aversiver Verhaltensantwort im Lebenszyklus eines Zebrafisches muss noch näher untersucht werden.

Ein TAAR13c Gen-Knockout kann wichtige Erkenntnisse bezüglich der neuronalen Informationsverarbeitung und der Rolle von Cadaverin in der Generierung von Verhalten liefern. Hier haben wir ein alternatives CRISPR/Cas9 Protokoll verwendet, um einen Teil der TAAR13c

Gensequenz aus dem Genom herauszuschneiden. Dabei wurde der zwischen zwei Target-Sites befindliche DNA Abschnitt deletiert. Dieser Knock-out muss in weiteren Experimenten charakterisiert werden.

Der evolutionäre Ursprung der TAARs ist nicht abschließend geklärt. Daher wurden hier durch eine umfangreiche Suche in 81 Fischgenomen neue Erkenntnisse bezüglich der TAAR Evolution gewonnen. TAARs und ihre Schwestergruppe, TARLs, haben ihren Ursprung in einer Duplikation des HTR4 Gens. Diese fand nach dem Auftreten der ersten Chordaten, jedoch vor der Aufspaltung von kieferlosen und kiefertragenden Fischen statt. TAARs der Klasse II sind ausschließlich in kiefertragenden Fischen zu finden. TAAR13 wurde entgegen unserer Erwartungen auch in Neoteleosten gefunden. Klasse II TAARs zeichnen sich durch diverse frühe und späte Genverluste zu verschiedenen Zeitpunkten in der Evolution der Fische aus. Häufig zeigen einzelne Mitglieder der Klasse II TAARs spezies- oder familienspezifische Expansionen.

TABLE OF CONTENTS

1 INTRODUCTION

Animals rely on their sensory systems to perceive and evaluate environmental stimuli. While the senses of sight, hearing, touch, taste and olfaction belong to the classical senses often described in the human and animal physiology, the sense of balance, noci-, proprio-, magneto-, and electroception also represent senses that are present in the animal kingdom, but are less extensively studied.

The ability to find and utilize energy sources is crucial for all living organisms. Chemoception - the ability to perceive chemicals through adequate receptor molecules or mechanisms – enables a motile organism to move towards an energy source and is present from bacteria to higher eukaryotes. The idea of specialized receptors enabling an organism to sense an attractant and move towards its source phrased in the late 1960s (Adler, 1969). The author suggested that *E. coli* bacteria lacking chemotactic response to a certain attractant might carry a mutation in the respective receptor.

Positive and negative chemotaxis (attraction and aversion/avoidance, respectively) in response to environmental stimuli represent a conserved concept in the evolution of not only prokaryotes, but also eukaryotes, where the complexity of chemosensory systems increased massively in parallel along with the complexity of the organisms themselves. The chemical senses are conceptually conserved from flatworms over flies and fish to frogs and felines. In insects and vertebrates these senses are olfaction and taste. They both rely on environmental stimuli, binding to specific receptor molecules and thereby activating a downstream neuronal signaling cascade, which can lead to alterations in the animal's behavior.

One of the major questions currently under investigation in the field concerns the evolution of olfactory receptors and receptor repertoires. Novel techniques like next generation sequencing led to the publication of hundreds of animal genomes. This allows large-scale studying of receptor evolution covering entire branches of the tree of life, including early-derived as well as evolutionary young species. This could lead us to understanding the evolutionary origin of olfaction as a specialized chemosensory sense. The other major question concerns the neuronal basis of a functional olfactory system. The aim is to get a better understanding of how odor molecules are perceived and how the brain processes these stimuli to generate behavior

responses. This is an interesting field of study and, while many exciting discoveries have been made recently, still poses many unanswered questions.

1.1 Function and general anatomy of the olfactory organ is conserved from fish to mammals

Animals, including humans, are able to process and discriminate a vast amount of different olfactory stimuli. Most olfactory stimuli do not consist of a single compound, but are complex mixtures of different active compounds. The smell of a rose for example is made up by a mixture of 275 different components (Ohloff, 1994). Although the number of olfactory stimuli that humans are able to discriminate remains a subject of discussion, conservative estimates suggest more than a billion discriminable odorant mixtures (Bushdid et al., 2014, Gerkin and Castro, 2015). This underlines the remarkable functional complexity of the olfactory system.

In mammals, as well as fish, the olfactory system harbors specialized sensory neurons located in epithelial sensory surfaces. These neurons, also referred to as olfactory sensory neurons (OSNs), choose to express a single olfactory receptor, from a variety of olfactory receptor families. The "one neuron - one receptor" rule represents the first principle of organization in olfactory systems. Although there are reported exceptions (Sato et al., 2007, Hanchate et al., 2015), this rule seems to be valid for mature OSNs of mouse (Serizawa et al., 2000, Serizawa et al., 2004) as well as zebrafish (Barth et al., 1997). The total number of different olfactory receptors expressed in an animal´s OSNs constitutes their receptor repertoire.

The axons of olfactory sensory neurons project to the olfactory bulb (OB), where axons from neurons expressing the same receptor converge onto glomeruli. The principle of axonal convergence, "one receptor - one glomerulus", represents the second principle of olfactory system organization. It has been described in the mammalian olfactory system (Takeuchi and Sakano, 2014) as well as in fish (Ahuja et al., 2013, Ahuja et al., 2014). Odorants bind to their respective receptors, creating an action potential that is carried to the olfactory bulb glomeruli. The glomeruli are innervated by specialized interneurons, i.e. mitral cells, and the signal is transported to higher brain areas, where odor evaluation takes place and adequate behavioral responses are generated.

The principal structure of the olfactory system with the basic building blocks (receptors, OSNs, glomeruli, and central nervous system) is conserved from insects to mammals. In mammals, reptiles, and amphibians the olfactory system underwent a segregation and comprises an additional olfactory surface, the vomeronasal organ (VNO). Sensory neurons in the VNO have different properties and primarily express receptors for the detection of pheromones (Karlson and Luscher, 1959, Dulac and Axel, 1995, Wagner et al., 2006). The ontogenetic development of the additional olfactory subsystem has been described in an metamorphic amphibian (*Xenopus laevis*), whose olfactory receptor repertoires in the different subsystems also allow implications on the transition of the olfactory system from water to land living animals (Gliem et al., 2013, Syed et al., 2017). In fish, which only have one olfactory organ, the olfactory epithelium, a partial segregation within the sensory surface can be observed. Pheromone and amino acid-sensing OSNs are present in the apical layer, while the OSNs harboring the classical olfactory receptors and a family of amine sensing receptors are present in the basal layer of the epithelium. These cell populations also have distinct projection targets in the olfactory bulb (Sato et al., 2005, Braubach et al., 2012).

1.2 Olfactory receptor types and their ligands

The perception of olfactory stimuli is mediated by a variety of different receptor types. Apart from classical odorant receptors (OR), sensory neurons in the main olfactory epithelium of mammals also express genes of other receptor families, namely the trace amine-associated receptors (TAAR), and the recently identified non-GPCR receptor family MS4A, which is co-expressed with the guanylate cyclase GC-D. The vomeronasal organ (VNO) has its own subset of olfactory receptors expressed, including vomeronasal type 1 receptors (V1R), vomeronasal type 2 receptors (V2R) and formyl peptide receptor-related receptors (FPR). In fish, which do not possess a VNO, V1Rs and V2Rs are expressed in the main olfactory epithelium alongside with ORs, TAARs and others (Bear et al., 2016). Even though mouse and zebrafish lineages have been evolving separately for around 430 million years since the divergence of tetrapods from fish (Blair and Hedges, 2005), their receptor repertoires exhibit a high degree of molecular conservation (Saraiva et al., 2015).

A schematic representation of the relevant olfactory receptor families present in zebrafish is given below.

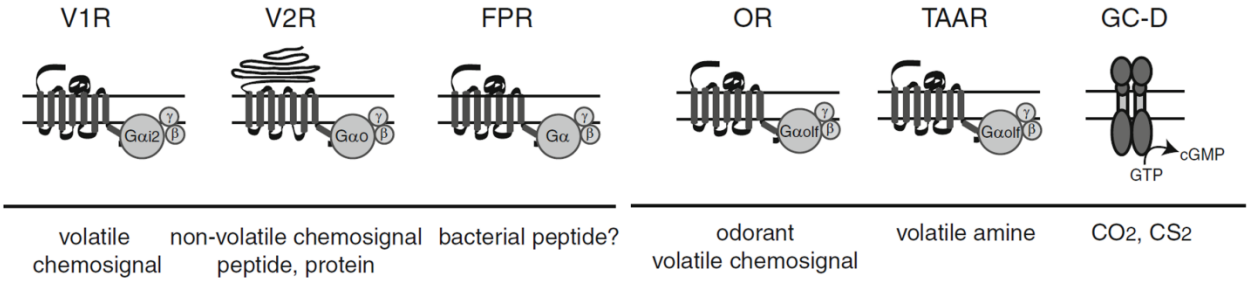

Figure 1.1: The olfactory receptor types and their general ligands, modified from (Ihara et al., 2013)

Odorant receptors (OR)

In 1991 the later Nobel laureates Linda Buck and Richard Axel discovered a large family of GPCRs in rats, which was proposed to function as odorant receptors and therefore abbreviated ORs (Buck and Axel, 1991). The mouse genome contains more than 1000 OR genes alone, not counting the many pseudogenes, underlining the relevance of olfaction for this species (Zhang and Firestein, 2002, Mombaerts, 2004). The zebrafish genome contains about 150 ORs and, like in the mouse, zebrafish OR genes are clustered in the genome (Sullivan et al., 1996, Alioto and

Ngai, 2005). ORs are GPCRs, which use a specialized stimulatory alpha-subunit, $G\alpha_{olf}$, and show a high degree of sequence diversity in their proposed ligand binding regions within their transmembrane domains, which enable them to detect a large spectrum of molecularly differing odors and odor compounds. In zebrafish OR expressing OSNs were shown to be mainly ciliated type OSNs (Sato et al., 2005) and mostly, but not always, follow the "one neuron - one receptor" rule of monogenic receptor expression (Sato et al., 2007).

V1Rs/ORA

Mammalian vomeronasal receptors type 1 (V1Rs) belong to the rhodopsin-like GPCR family and were thought to be represented in the teleost fish nose by a single gene (Pfister and Rodriguez, 2005) or gene pair (Shi and Zhang, 2007), until a novel V1R-like gene family with six members and orthologous to mammalian V1Rs was identified in various fish genomes (Saraiva and Korsching, 2007). These genes, also referred to as ORA genes (olfactory receptor class-A related), form a clade that includes the mammalian V1Rs and seem to be conserved over large episodes of fish evolution. With few exceptions ORA genes have only one coding exon. A recent genome study showed, that the V1R-like ORA repertoire is even larger in ancestral ray-finned species, pointing out at least Two gene loss events early in the ray-finned fish lineage (Zapilko and Korsching, 2016). In zebrafish one of the ORA genes, *ora1*, has been deorphanized. *Ora1* recognizes 4-hydroxyphenylacetic acid, which stimulates oviposition and thereby acts as a reproductive pheromone (Behrens et al., 2014). Another of the ORA genes, *ora4*, was shown to be expressed in crypt cells, a specialized sparse population of OSNs (Oka et al., 2012).

V2Rs/OlfC

Tetrapod vomeronasal receptors type 2 (V2Rs) were independently described as putative pheromone receptors by three different groups only two years after the discovery of V1Rs (Herrada and Dulac, 1997, Matsunami and Buck, 1997, Ryba and Tirindelli, 1997). V2Rs belong to the class C of GPCRs, and are closely related to the mammalian metabotropic glutamate receptors. This is also the reason why the teleost V2R-corresponding receptor gene family has been termed OlfC. The genomes of zebrafish, bitterling and a few other species have been reported to possess around 50-60 genes of the V2R-related OlfC gene family, while other fish

species have substantially less of these receptor genes (Alioto and Ngai, 2006, Hashiguchi and Nishida, 2006, Hashiguchi and Nishida, 2009). V2R/OlfC proteins consist of around 800 amino acids and characteristically possess a long extracellular N-terminus, which most presumably harbors the agonist binding site. While mammalian V2Rs have been shown to be activated by peptides, e.g. MHC-peptides, or even proteins with a high sensitivity (Leinders-Zufall et al., 2004, Leinders-Zufall et al., 2009, Leinders-Zufall et al., 2014), some teleost OlfC receptors were shown to recognize amino acids (Luu et al., 2004).

Trace amine-associated receptors (TAARs)

TAARs are a family of rhodopsin-like GPCRs, that were initially thought to detect low levels of aminergic neurotransmitter-like signaling molecules in the brain (therefore termed trace amine-associated receptors), but were then found to be primarily expressed in the olfactory epithelium of mice (Liberles and Buck, 2006). TAAR genes are mono-exonic with very rare exceptions and, like ORs, are represented in gene clusters. With six members in humans and 15 members in mice their repertoire in tetrapods is generally small when compared to the several hundred to over 1000 OR genes present in the respective genomes (Malnic et al., 2004, Godfrey et al., 2004). In teleost fish TAARs underwent a rather big expansion (Hussain et al., 2009). Zebrafish for instance possess one of the largest TAAR repertoires known to date, with 112 members. Zebrafish is an earlier derived teleost, TAAR gene repertoires of later derived neoteleosts are generally smaller and indeed complete subfamily gene losses in neoteleost species have been suggested (Hussain et al., 2009). The evolutionary origin and fate of TAARs and its subfamilies in vertebrate evolution have not been defined with certainty.

Like ORs, TAARs are usually expressed by ciliated OSNs and their mode of generating a response is described to rely on a $G\alpha_{olf}$ mediated cAMP signaling cascade (Zhang et al., 2013). Several mammalian TAARs have been deorphanized and many of them seem to be involved in the generation of either attractive or aversive responses (Dewan et al., 2013, Li and Liberles, 2015). Among the structurally diverse ligands for mammalian TAARs are predator odors, as well as biogenic amines and amines of other sources (Ferrero et al., 2011, Ferrero et al., 2012, Pacifico et al., 2012). Zebrafish TAAR13c is a high-affinity receptor for the death-associated odor cadaverine, which is a diamine generated by bacterial decarboxylation of basic amino acids

during the process of decay (Sabo et al., 1974). TAAR13c mediates the aversive response to the odor (Hussain et al., 2013). Other zebrafish TAARs have been described to respond to different diamines in heterologous expression systems (Li et al., 2015).

The evolutionary origin of TAARs as olfactory receptors is still a matter of discussion. It was suggested that TAARs already are present in jawless vertebrates (Hashiguchi and Nishida, 2007) and indeed one study has claimed, that TAARs are expressed in OSNs of the olfactory epithelium of the sea lamprey, Petromyzon marinus, a jawless vertebrate (Libants et al., 2009). However, another study argues that TAARs evolved after the emergence of jawed vertebrates and that the lamprey genes fall into another receptor class, because they lack key components of the signature TAAR amino acid motif (Lindemann and Hoener, 2005, Hussain et al., 2009). While several studies have focused on mammals (Eyun et al., 2016), the situation for fish remains only partially resolved.

Several studies suggest that TAARs originate from a duplication of the serotonin receptor gene HTR4, although the time point of this event has not been specified yet (Hashiguchi and Nishida, 2007, Spielman et al., 2015). TAARs therefore secondarily gained their function as olfactory receptors, while their ancestral genes have served as neurotransmitter genes in the central nervous system. This is supported by the observation that TAAR 1, the most ancestral TAAR gene found in tetrapods and also teleosts, is not expressed in the olfactory epithelium (Liberles and Buck, 2006, Hussain et al., 2009). TAAR 1 was instead shown to be expressed in certain brain areas in mice and is involved in the regulation of addiction behaviors (Liu et al., 2017a).

Phylogenetic studies have shown that TAARs evolved into three classes, class I-III, two of which are present in tetrapods as well as teleosts, class I and II. The third class (III) is present only in fish, representing a lineage specific expansion of this receptor family (Hussain et al., 2009). The data also suggested that class II TAARs are completely lost in neoteleost fish, although the number of genomes analyzed so far has been quite low.

Other receptor types

In recent work an adenosine-sensing GPCR has been identified in zebrafish (Wakisaka et al., 2017). This receptor, termed A2c, is expressed in a specialized type of OSNs and seems to be involved in food-finding behavior.

MS4A receptors have been identified as a non-GPCR family of olfactory receptors in mice, which recognize pheromones and fatty acids (Greer et al., 2016). In mice MS4As are expressed in a special type of OSNs projecting to the necklace glomeruli. These four transmembrane spanning receptors, which are also present in the zebrafish genome (Zuccolo et al., 2010), are co-expressed with guanylate cyclase-D and, as they do not define as GPCRs, rely on an alternative signal transduction pathway using cGMP. Interestingly, several MS4A receptors are co-expressed in single OSNs, indicating a novel mechanism for olfactory detection and encoding.

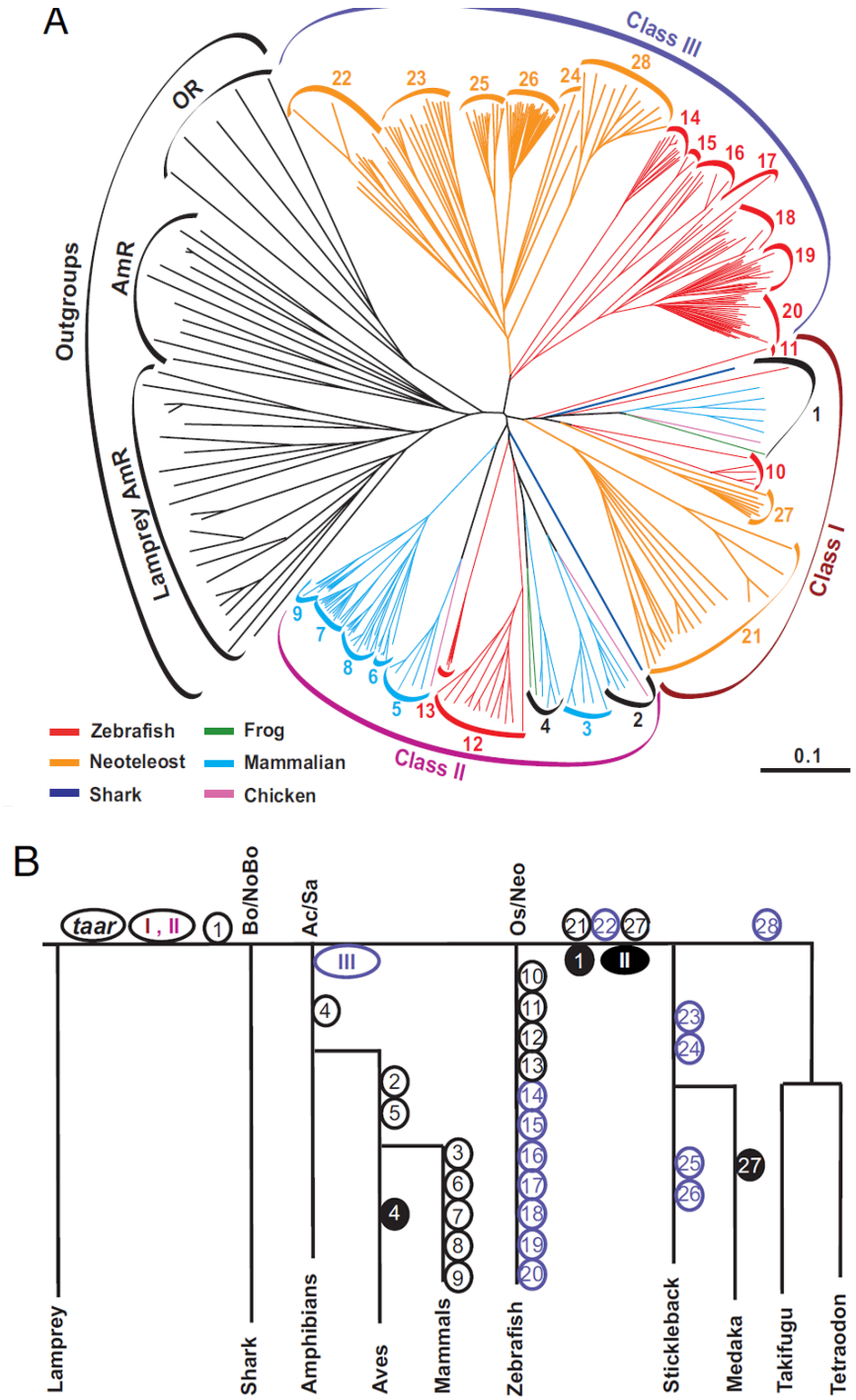

Figure 1.2: Evolution of TAARS A) Phylogenetic tree of TAAR family members in selected species of tetrapods, teleosts and earlier vertebrates. B) Gene gain (open circles) and loss (filled circles) events in the evolution of TAARs. Emergence of a new TAAR class is indicated by ovals. (Hussain et al., 2009)

1.3 Olfactory sensory neurons

The specialized neurons expressing olfactory receptors are called olfactory sensory neurons (OSNs). The two major OSN populations, microvillous and ciliated OSNs, make up the vast majority of all sensory neurons present in the OE and can be found in tetrapods as well as fish. In zebrafish there are at least five types of OSNs that have been described to date. Presumably, there are more OSN types that have not been described yet. They differ from each other in morphological and functional aspects. This includes their cell shape, olfactory receptor expression, signal transduction and axonal projection targets. A schematic overview of the OSN types known to date in zebrafish is depicted in Figure 1.3.

All OSNs are embedded into the sensory epithelium that forms the lamellar structure of the nose. Furthermore, the OE comprises supporting cells and different types of basal cells (stem cells and OSN progenitors) at the base of the lamellae.

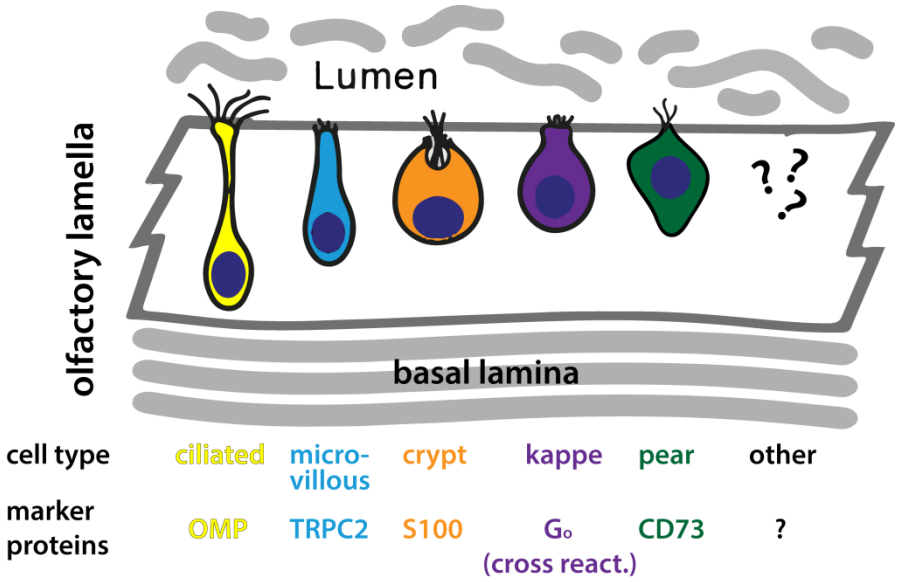

Figure 1.3: OSN types in the olfactory epithelium of zebrafish

Microvillous OSNs are located in the apical layer of the epithelium and possess microvilli that contain the olfactory receptors. This population is characterized by expression of transient receptor potential channel member C2 (TRPC2), which plays a role in the signal transduction cascade (Von Niederhausern et al., 2013). Microvillous OSNs are known to express V2Rs (Cao et al., 1998, Speca et al., 1999) and project mainly to the lateral and ventral olfactory bulb regions of zebrafish (Sato et al., 2005). These regions as well as the microvillous OSNs themselves have

been shown to respond primarily to amino acids (Friedrich and Korsching, 1997, Lipschitz and Michel, 2002, Koide et al., 2009).

The cell body of ciliated OSNs is located at more basal positions in the olfactory lamellae. Ciliated OSNs have an elongated slender shape and a long dendrite harboring cilia that contain the olfactory receptors. They express olfactory marker protein (OMP) and are characterized by $G_{\alpha olf}$ expression, which is a stimulatory G-protein characteristic for olfactory signal transduction (Jones and Reed, 1989, Hansen et al., 2003). This type of OSNs is known to express ORs (Buck and Axel, 1991) as well as TAARs (Zhang et al., 2013). In zebrafish their axons mainly project to the medial and dorsal olfactory bulb (Sato et al., 2005).

To date, three minor OSN populations that have been described in zebrafish, crypt, kappe, and pear OSNs. Their total number in the olfactory epithelium, as compared to the ciliated and microvillous OSNs, is very small. Whether all of these types also exist in species other than (zebra-)fish is mostly unknown.

Crypt neurons have a unique globose shape and are positioned very apically in the olfactory lamellae, i.e. close to the lumen (Hansen and Zeiske, 1998). They carry cilia as well as microvilli, which are located in the characteristic crypt-like structure, and, as has been shown in the zebrafish nose, express ORA4 as their olfactory receptor (Oka et al., 2012). This was the first example of a cell type with its entire population expressing only one specific olfactory receptor. Crypt neurons have been shown to be present in other fish species as well, including marine teleosts (Schmachtenberg, 2006) and shark (Ferrando et al., 2006). They are characterized by S100 immunoreactivity (Germana et al., 2004). In zebrafish crypt neurons project to a large mediodorsal glomerulus, mdG2 (Ahuja et al., 2013) and have been shown to be involved in olfactory imprinting and recognition of kin odor (Biechl et al., 2016).

Kappe neurons also sit at a very apical position in the olfactory lamellae and are morphologically distinguishable from crypt neurons by their characteristic “cap”-like knot on the apical end. They carry microvilli, are characterized by G_o-immunoreactivity and their axons project to the mdG5 glomerulus in the medio-dorsal cluster of glomeruli (Ahuja et al., 2014). The olfactory receptor expressed by kappe neurons has not been identified yet.

A fifth type of OSNs has been recently identified by their expression of the novel adenosine receptor A2c (Wakisaka et al., 2017). Because of their characteristic shape, this type of OSNs has

been termed “pear” OSNs. They too are located apically in the lamellae and project to a large lateral glomerulus, lG2, which is activated upon stimulation with adenosine as well as AMP, ADP, and ATP (Friedrich and Korsching, 1998, Wakisaka et al., 2017). Pear OSNs are therefore thought to be involved in feeding behavior.

The recent discoveries of alternative receptor molecules and new types of sensory neurons infer that the current list of OSN-types and receptor families may still be incomplete. Discoveries of further OSN types and olfactory receptor molecules remain a distinct possibility.

1.4 Canonical olfactory signal transduction and neuronal activity markers

The binding of an odorant molecule to the odorant receptor, which is located in the cell membrane of an OSN´s sensory cilia, triggers a signaling cascade leading to a local membrane depolarization and finally to formation of an action potential.

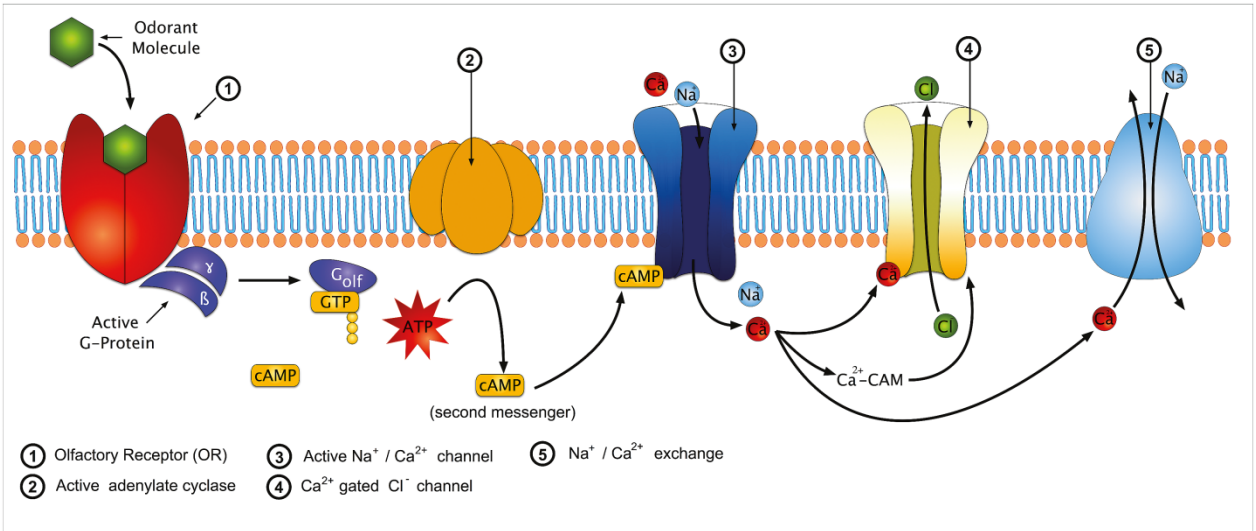

Figure 1.4: Olfactory signal transduction via a stimulatory G-protein and the second messenger cAMP, modified from (Silva Teixeira et al., 2016)

In the inactivated state the olfactory receptor is coupled to an olfactory-specific heterotrimeric G-protein, consisting of the α-subunit ($G\alpha_{olf}$) and the βγ-subunit complex. In that state the α-subunit binds GDP. Upon odorant binding the receptor changes its conformation, the Gα subunit exchanges GDP for GTP, and is released from the complex (Jones and Reed, 1989). It then activates adenylate cyclase III (AC3), which leads to the ATP-dependent production of cyclic AMP (cAMP) as a second messenger molecule (Bakalyar and Reed, 1990). cAMP activates cyclic nucleotide-gated ion channels (CNG) in the membrane, which allow the influx of sodium and calcium ions across the membrane (Dhallan et al., 1990). A knockout of any of these key components causes anosmia (Brunet et al., 1996, Belluscio et al., 1998, Wong et al., 2000). A rise in intracellular calcium concentrations furthermore opens calcium-gated chloride channels (ANO2) amplifying the membrane depolarization by chloride efflux (Kleene, 1993, Stephan et al., 2009). Taken together these events can spark an action potential along the axon of the sensory neuron, transmitting the odorant information to the glomerular relay station in the olfactory bulb. Specific phosphodiesterases (PDE), which interact with Calmodulin (CAM), degrade cAMP and

thereby terminate the olfactory signaling in the OSN (Yan et al., 1996). This cascade represents the classical olfactory signal transduction pathway for ORs and TAARs.

Calcium is an important regulator of the neuronal odorant response. Calcium indirectly inhibits AC3 through phosphorylation by Ca^{2+}/CaM-dependent protein kinase II, leading to an attenuation of the olfactory signal (Wei et al., 1996, Wei et al., 1998). Entering calcium also reduces the sensitivity of the CNG channel to cAMP, thus leading to a desensitization of the neuron (Chen and Yau, 1994, Munger et al., 2001). At the same time Ca^{2+}/CaM activates PDE, which depletes cAMP levels and is crucial for odorant response termination (Boekhoff and Breer, 1992).

Immediate early genes (IEG), like c-fos, arc, or egr1, have been used as neuronal activity markers in response to odor stimulation in the olfactory system (Bepari et al., 2012). C-fos is commonly used as an activity marker. As other IEGs, it is upregulated in response to neuronal firing (Dragunow and Faull, 1989). Odor exposure, and therefore neuronal activity in the olfactory pathway, has a direct influence on the expression of olfactory receptors through IEGs (Calfun et al., 2016). Olfactory stimulation has even been used to identify receptor-ligand pairs through transcriptional profiling (von der Weid et al., 2015). On the other hand, IEGs have been shown to be downregulated upon olfactory deprivation (Kress and Wullimann, 2012). Although c-fos is an accepted marker to trace neuronal activity, it has a poor temporal resolution and requires long stimulation times to visualize activity in response to olfactory stimuli.

Phosphorylation of the extracellular signal-regulated kinase (ERK) has been used as an alternative marker for neuronal activity in the olfactory system as well as the brain of mouse and zebrafish (Miwa and Storm, 2005, Hussain et al., 2013, Randlett et al., 2015). Phosphorylated ERK (pERK) is part of the MAP-kinase phosphorylation cascade, which has been shown to be activated upon stimulation of GPCRs in a large variety of cell types and species. Thus, this pathway constitutes a second, alternative signal transduction cascade besides the classical path through cAMP (Wetzker and Bohmer, 2003). The phosphorylation cascade leads to the expression of regulatory transcription factors. Used as readout of neuronal activity, pERK provides an improved temporal resolution. Its signal is maximal within few minutes after stimulation, while IEGs require at least half an hour to reach maximum transcript levels (Bepari et al., 2012).

1.5 Functional organization of the zebrafish olfactory bulb

After an action potential is produced in the sensory neuron, the signal is transported along the axon to reach the olfactory bulb. There, the axons of OSNs expressing the same olfactory receptor converge into so-called glomeruli (Treloar et al., 2002, Sato et al., 2007), which represent the first information relay station of the central nervous system. Glomeruli are formed by incoming OSN axon terminals. Apical dendrites of mitral cells receive synaptic input from OSNs and the information is transmitted to higher brain centers (Fuller et al., 2006). Mitral cell output is modulated by several types of interneurons, some of them located in the glomerular layer and some in deeper layers of the olfactory bulb (juxtaglomerular, periglomerular, and granule cells) (Edwards and Michel, 2002, Bundschuh et al., 2012). The mode of action in this network is not yet fully understood.

The glomeruli in the zebrafish olfactory bulb are organized in densely packed clusters and there is a number of relatively large glomeruli, that can be identified across individuals (Baier and Korsching, 1994, Braubach et al., 2012). It is not known to what extent the architecture and organization of the glomerular clusters in the olfactory bulb is conserved in the fish lineage.

Different OSN types are represented by glomeruli of distinct position within the olfactory bulb (see also Figure 1.5). Ciliated OSNs project mainly to the dorsal and ventromedial portion of the olfactory bulb, while microvillous OSNs project mainly to the ventral and lateral portion of the olfactory bulb (Sato et al., 2005). Furthermore, crypt neurons, which express the V1R-related receptor ORA4, have been shown to project to the large mediodorsal glomerulus mdG2 (Ahuja et al., 2013), while kappe neurons project to the adjacent mdG5 glomerulus (Ahuja et al., 2014).

Because each olfactory receptor binds only specific ligands, different sets of glomeruli are activated upon stimulation with a certain odor blend. The presence of such a glomerular odor map has been illustrated for mammals (Mori et al., 2006, Mori and Sakano, 2011, Shirasu et al., 2014). Early functional studies indicated that this concept also applies to zebrafish (Friedrich and Korsching, 1997, Friedrich and Korsching, 1998, Fuss and Korsching, 2001). According to these studies amino acid odors are processed by the lateral cluster of glomeruli, the prostaglandin PGF2α is processed by a specific ventral glomerulus (as confirmed recently by Yabuki et al. (2016)) and nucleotides are processed by the lateral glomerulus lG2 (see also Wakisaka et al.

(2017)). For glomerular representations of other odor classes there exists only preliminary evidence (Friedrich and Korsching, 1998).

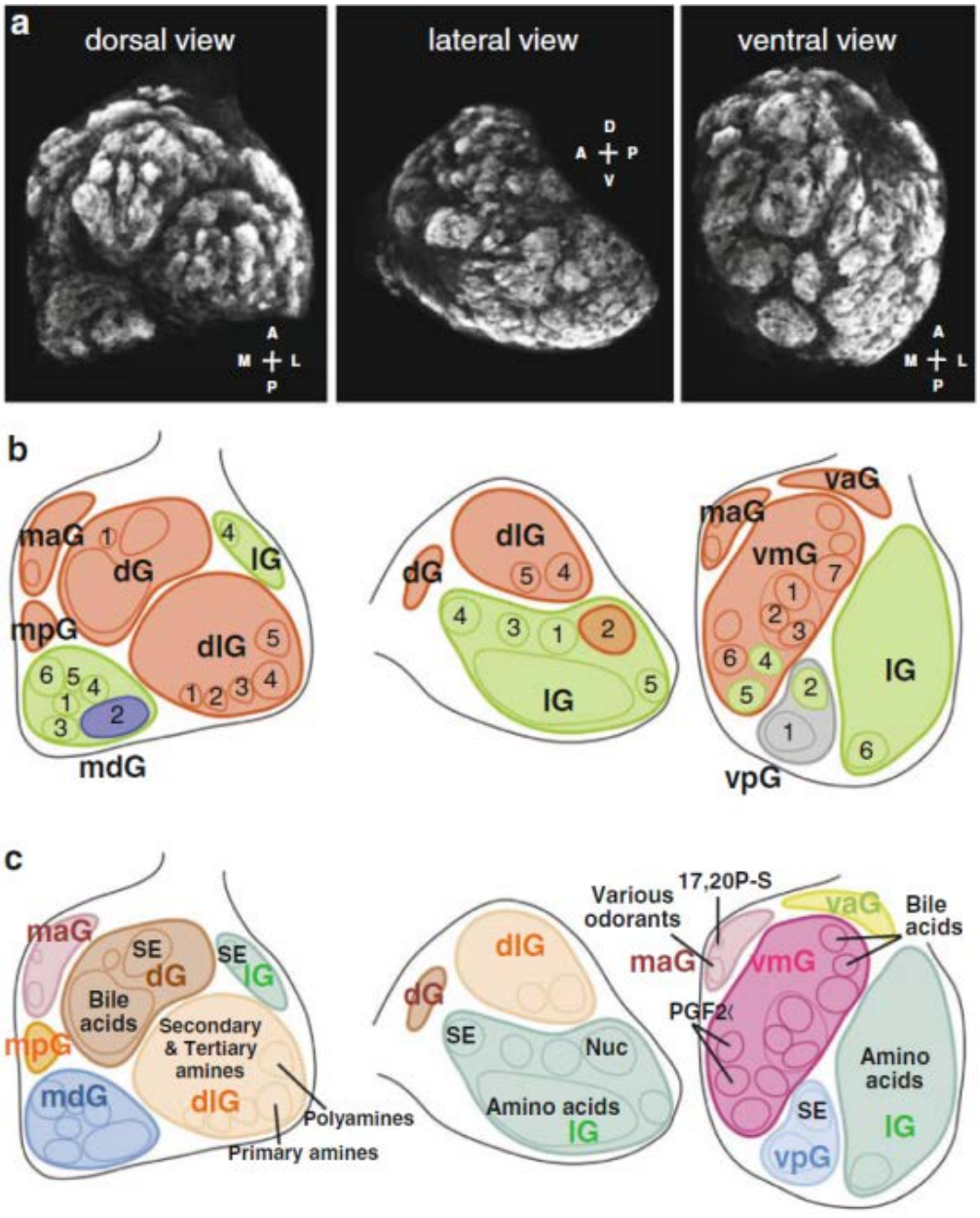

Figure 1.5: Glomerular organization of the zebrafish olfactory bulb: A) Staining for SV2 visualizes the position and cluster patterning of olfactory glomeruli. B) Axonal projection targets of ciliated (red), microvillous (green), and crypt (blue) OSNs. C) Odor map in the OB reveals response profiles of different odorant classes. (maG = medioanterior glomeruli, mpG = medioposterior glomeruli, mdG = mediodorsal glomeruli, dG = dorsal glomeruli, dlG = dorsolateral glomeruli, lG = lateral glomeruli, vaG = ventroanterior glomeruli, vmG = ventromedial glomeruli, vpG = ventroposterior glomeruli (Yoshihara, 2014)

1.6 Olfactory processing in the higher brain of zebrafish

Different brain areas are associated with different tasks. Brains of mammals, and especially humans, are characterized by the extraordinary abilities of their neocortex, while other vertebrates such as fish cannot rely on such a powerful, mind-forming tool. In contrast, many other brain compartments are evolutionary conserved from fish to humans and can be found as functioning homologous counterparts, like the olfactory bulb, hypothalamus, habenula, or cerebellum. Even if there is no direct homology, there are similarities of zebrafish brain regions to mammalian counterparts, like for example the limbic system or the thalamus (Rink and Wullimann, 2001, Mueller, 2012). Some of these regions are involved in similar processing tasks and behavioral outputs in both fish and higher tetrapods.

Once the mitral cells pick up the olfactory information in the OB, they transfer it to various higher brain centers. Axonal projection targets of mitral cells have been studied using dye tracing as well as genetic labeling approaches and have led to the identification of several brain regions involved in olfactory processing (Rink and Wullimann, 2004, Miyasaka et al., 2009, Miyasaka et al., 2014).

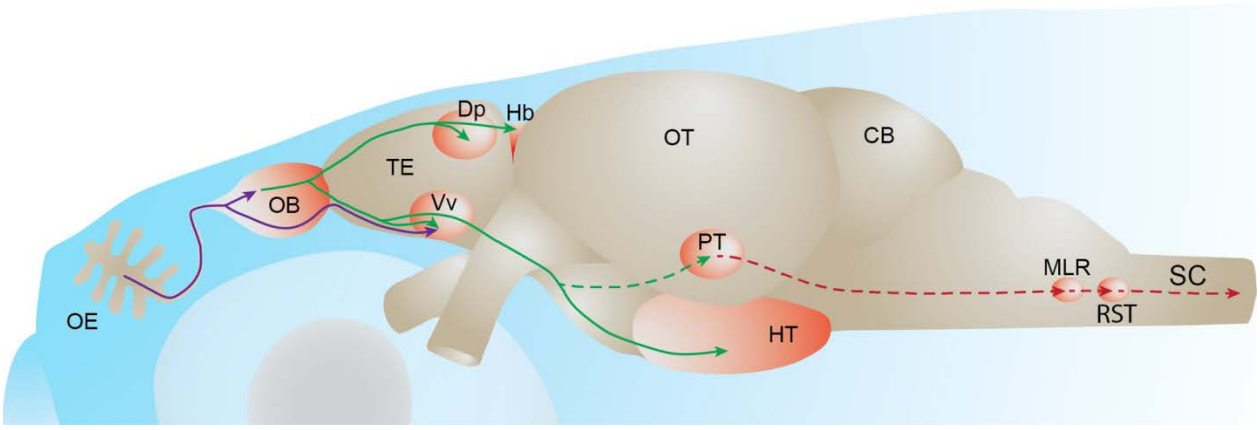

Figure 1.6: Axonal projection targets of olfactory bulb neurons in the zebrafish brain

(TE = telencephalon, Dp = dorsal-posterior telencephalon, Vv = ventral nucleus of the ventral telencephalon, Hb = habenula, OT = optic tectum, PT = posterior tubercle, HT = hypothalamus, CB = cerebellum, MLR = mesencephalic locomotor region, RST = reticulo-spinal tract, SC = spinal cord; Figure adapted from (Kermen et al., 2013)

Axonal tracing of genetically labelled mitral cells in zebrafish larvae revealed, that the dorsal-posterior telencephalon (Dp) and the posterior tubercle (PT) receive a non-selective input from almost all glomerular clusters, while the ventral telencephalon is innervated more specifically by

only some glomerular clusters. Only the right habenula is innervated by mitral cells from the OB (Miyasaka et al., 2014).

Because of its location in the dorsal part of the brain, the rather small size and its involvement in the formation of many behaviors the habenula was subject of several functional studies. It has a unique asymmetrical innervation pattern and was shown to be involved in the mediation between attraction and aversion/fear, and associated learning behavior in zebrafish (Agetsuma et al., 2010, Okamoto et al., 2012, Krishnan et al., 2014, Nathan et al., 2015, Lupton et al., 2017). The medial habenula is also a regulator of anxiety, as has been shown in ablation experiments (Mathuru and Jesuthasan, 2013).

The hypothalamus regulates motivated behaviors, such as food foraging, hunt and reproduction (Zohar et al., 2010, Muto et al., 2017), but also responses to sensory stimuli (Reinig et al., 2017). The hypothalamus was found to be directly innervated by OB neurons (Miyasaka et al., 2009) and is reported to be involved in behaviors elicited by olfactory stimuli, i.e. kin recognition (Biechl et al., 2017).

1.7 CRISPR/Cas9-based genome editing in the zebrafish, *Danio rerio*

To understand the relevance of a particular olfactory receptor for neuronal olfactory processing, it is of interest to remove that olfactory receptor from the system. In recent years the bacterial immune system CRISPR/Cas has been re-fitted to allow straightforward and efficient genome editing in a broad variety of species.

In defense against invading viruses and plasmids bacteria and archaea have developed an immune system, which provides them with acquired resistance against those invaders. The system is based on genomic loci with clustered regularly interspaced short palindromic repeats (CRISPR) (Barrangou et al., 2007) and relies on a sequence specific, RNA-guided detection of the intruder´s nucleic acids (Wiedenheft et al., 2012). Virus-derived sequences are integrated into the bacterial CRISPR loci after/during the infection. In a subsequent infection they are transcribed into a small guide RNA (or tracrRNA) including the target sequence and a binding scaffold, which interacts with CRISPR-associated nucleases (Brouns et al., 2008). The CRISPR associated protein 9 (Cas9) is an endonuclease, which selectively introduces double strand breaks in target DNA at positions defined by the guide RNA and thereby depletes invading viral nucleic acids (Jinek et al., 2012, Gasiunas et al., 2012). Scientists around the world have used this programmable genome editing tool to introduce mutations, gene knock-outs, and knock-ins at specific sites in the genome of many different species and model systems using engineered versions of the bacterial guide RNAs. The possible applications have developed rapidly in the past years as this method by far outperforms other genome editing tools like transcription activator-like effector nucleases (TALENs) or zinc finger nucleases (ZFNs) in many aspects (Ramirez et al., 2008, Ding et al., 2013). The working principle of the CRISPR-Cas9 system is depicted in Figure 1.7.

The Cas9 nuclease forms a complex with the guide RNA, which leads the complex to a specific genomic location. This complex can be guided to almost any location in the genome only restricted by the requirement of a so-called protospacer adjacent motif (PAM) sequence (with the bases NGG) in vicinity to the target site. The Cas9 nuclease introduces a DNA double strand break (DSB) ca. three basepairs upstream of the PAM sequence, which can then be repaired by different mechanisms. Non-homologous end joining (NHEJ) repair is error prone and often leads to small insertions or deletions of bases at the DSB site, which in turn can result in a frame shift or premature stop codon and thus a functional knock-out of the gene.

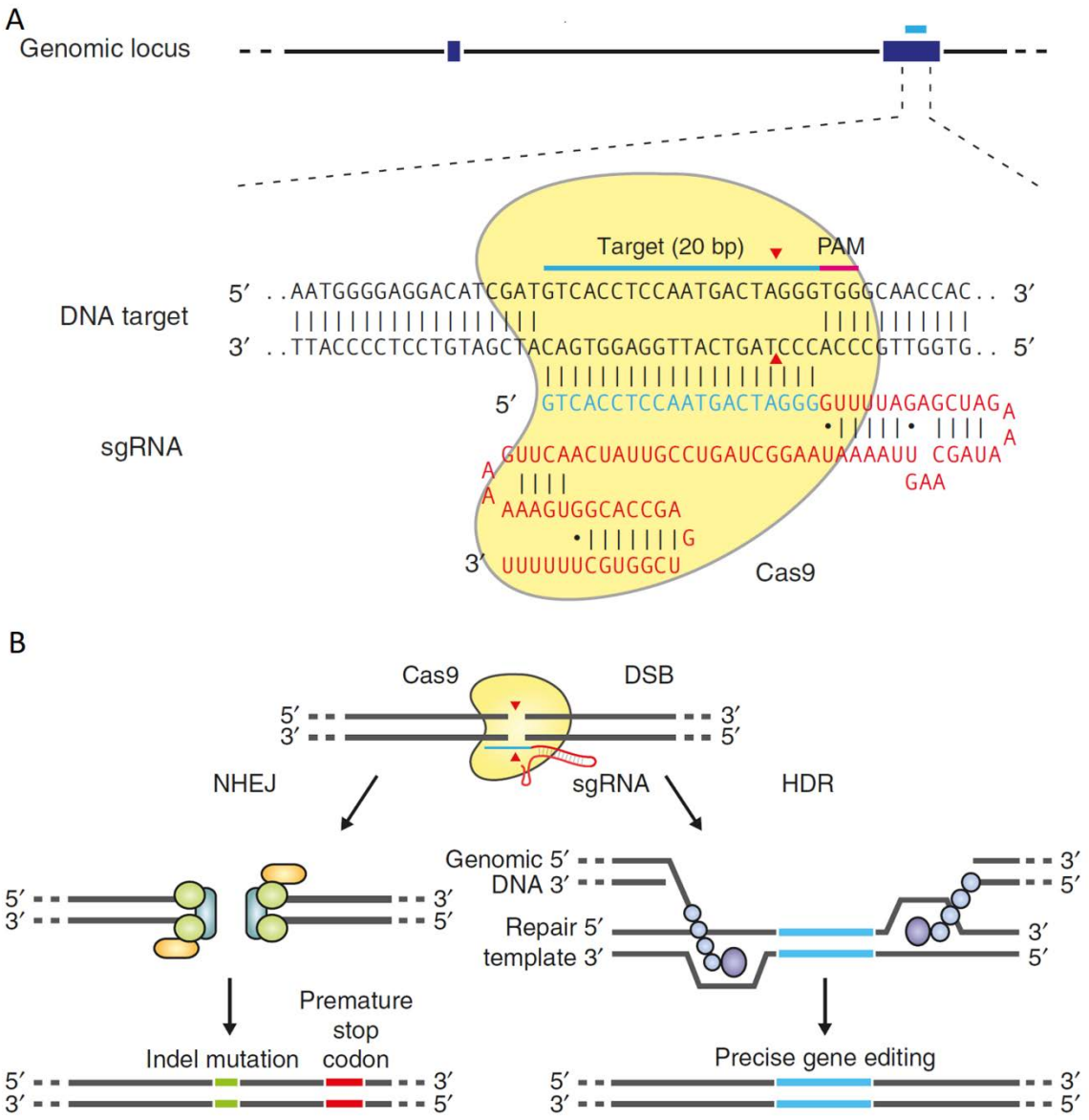

Figure 1.7: Genome editing with CRISPR-Cas9 A) The RNA-guided Cas9 nuclease binds to a specific genomic locus determined by a 20 bp target site sequence within the guide RNA and induces a double strand break about 3 bp upstream of the PAM sequence NGG. B) Double strand breaks created by Cas9 can be repaired either by the error prone non-homologous end joining (NHEJ), or, if a template with homologous arms is provided, by homology directed repair (HDR). (Ran et al., 2013)

If a DNA template with homology arms is provided externally, DNA sequences of interest can be inserted into the genome by homology directed repair (HDR) mechanisms (Ran et al., 2013).

CRISPR-Cas9 mediated genome editing applications were reported in zebrafish soon after the technique became available (Hwang et al., 2013) and the system was proven to generate gene

knock-outs with high precision and efficiency (Irion et al., 2014). Apart from local inversions or deletions, several groups have demonstrated that even larger genomic fragments can be cut out of the genome of zebrafish by use of CRISPR-Cas9 with more than one guide RNA followed by non-homologous DNA repair (Xiao et al., 2013, Ota et al., 2014).

A problem in the use of CRISPR-Cas9 system is the tendency to bind to off-target locations in the genome and introduce mutations at these unintended sites (Cho et al., 2014). In order to avoid off-targets various groups have developed bioinformatics tools to calculate off-target activities (Koo et al., 2015) and/or to develop and identify Cas9 variants with higher target specificity (Lin et al., 2017).

The CRISPR-Cas9 system holds large interest not only for basic research, there is an extraordinary interest in the technique from the field of clinical research as well. In fact first implementations that use CRISPR-Cas9 to create transgenic human immune cells, which can be used in the treatment of certain types of cancer or even HIV, are currently under investigation (Jensen and Riddell, 2015, Leibman and Riley, 2015, Liu et al., 2017b).

1.8 Aims

The study at hand uses the zebrafish, *Danio rerio,* as a model system to study genetic, structural and functional relationships of molecular and cellular components within the olfactory system, focusing on one receptor family, their ligands and subsequent neuronal information processing. The TAAR-family of GPCRs is conserved from early vertebrates to humans. TAARs have been shown to play an important role in amine detection and the generation of odor-induced behaviors in mammals as well as fish. As zebrafish possesses one of the largest TAAR receptor repertoires known in any species, the role of amines as olfactory cues is of special interest in this field.

This study uses a multi-disciplinary approach to target the following questions related to the sensation of amines in vertebrates.

What is the evolutionary origin of TAARs? It is not clear, whether TAARs evolved before or after the emergence of jawed vertebrates. Additionally ancestral TAAR-like genes may have evolved separately from the actual TAAR family. Now that many dozens of genomes have become available, a more profound analysis of the TAAR evolution can be performed.

What cell type in the fish olfactory epithelium is responsible for the detection of amines? The olfactory epithelium harbors a variety of OSN types, each with a different receptor repertoire, signal transduction and with different marker molecules. Here, we want to identify the amine sensing cell type using live-cell imaging and further characterize the cell type of those OSNs expressing the cadaverine receptor TAAR13c.

How are amine odors processed in the brain? In order to generate a behavior response, the olfactory information is transferred to the brain. Different odors activate different pathways in the brain. Here we contribute to the construction of an odor-map, by identifying specific amine-sensitive glomeruli and a cadaverine-specific glomerulus in the olfactory bulb.

Is the aversive behavior in response to cadaverine mediated by a single receptor, TAAR13c? We develop a CRISPR-Cas9 based strategy to knock out the cadaverine receptor TAAR13c.

Do zebrafish larvae already detect cadaverine and show an aversive behavior in response to cadaverine? We develop a behavior assay for 6 dpf larvae and use different techniques to look at neuronal activity in response to cadaverine in larvae stimulated with cadaverine.

2 MATERIAL AND METHODS

2.1 Organisms

2.1.1 Zebrafish strains and animal care

Fish were kept in groups of up to 30 animals in tanks with a day/night cycle of 14 h light and 10 h darkness at 28°C. Fish water supply consisted of a mixture from equal parts desalted water and tap water kept at pH 7,0 – 7,4. Fish were fed 2 times a day with living brine shrimp artemia (Sanders, USA) and flake food (Tetra, Germany). The zebrafish strains used in this study are listed in Table 2.1.

Table 2.1: Zebrafish strains

Strain	**Feature**	**Origin**
Wt/KS	wildtype	Cologne
Wt/Ab	wildtype	Tübingen
Tg(*OMP:lyn-mRFP-S*)	fluorescent marker in ciliated OSNs	Sato et al., 2005(Sato et al., 2005)
Tg(*TRPC2:gap-Venus*)	fluorescent marker in microvillous OSNs	Sato et al., 2005(Sato et al., 2005)
Casper(*elavl3*:GCaMP6s)	Calcium sensor in neurons	HHMI, Janelia Farms

On the evening before mating pairs of one female and one male fish were put into a mating tank with a plastic separator between them. In the morning of the next day the separator is removed. The eggs fall through a grid and are collected at the bottom of the tank. Eggs were then washed and kept in egg water (distilled water supplemented with 0,03% sea salt (Instant ocean, USA) until further use. Egg water was supplemented with 2 ml 0,1% w/v methylene blue per liter to prevent growth of fungi. Until 5 dpf fish larvae are kept in Petri dishes. From 5 – 15 dpf fish are

kept in nursery tanks with about 1 l of volume without waterflow. From day 5 onwards fish are fed powdered food (Tetra, Germany) twice a day. From day 12 - 15 onwards fish are fed brine shrimp artemia in addition. After about 3 weeks the tanks are connected to the water flow.

The animal handling was approved by the governmental animal care and use office (Landesamt für Natur, Umwelt und Verbraucherschutz Nordrhein-Westfalen, Protocol No. 8.87-51.05.20.10.217) and was in accordance with the German Animal Welfare Act as well as with the General Administrative Directive for the Execution of the Protection of Animals Act.

2.1.2 Bacterial strains

For transformations and cloning of plasmids the electroporation-competent strain *E.coli* XL1blue (Agilent Genomics, USA) was used.

2.2 Technical equipment, chemicals and disposables

2.2.1 Technical equipment

Type	Model	Manufacturer
Cryostat	CM1900	Leica
Electrophoresis Chamber		Bio-Rad
Electrophoresis Powersupply	Power Pac 300	Bio-Rad
Fluorescence Microscope	BZ-9000	Keyence
Gel Documentation System	GelDoc XR	Bio-Rad
Halogen Lamp	iLux 150NL	Visitool
Heating Plate	MEDAX	StörkTronic
Incubator (dry)		Memmert
Incubator (wet)	GFL	KMF
Laser Scanning Microscope	LSM 510	Zeiss
Laser Scanning Microscope	SP8	Leica
Microcentrifuge	Micro Star 17	VWR
Microcentrifuge (cooling)	Z233 MK-2	Hermle
Micropipette Puller	P-97	Sutter Instruments
Microwave	900 & Grill	Severin
Peristaltic Pump		Pharmacia Fine Chemicals
pH-Meter	Calimatic 766	Knick
Pipets (10/20/200/1000 µl)	Research Plus	Eppendorf
Pneumatic Pico Pump	PV 830	World Precision Instruments
Precision scale	LA 120 S	Sartorius
Rotary Mixer	R1	Pelco
Scale	universal	Sartorius
Shaker	Bio Shaker 3D	BIOSAN
SLR Camera	D5100	Nikon
Spectrophotometer	NanoDrop One	Thermo Fisher
Stereomicroscope	Stemi 2000	Zeiss
Thermal mixer	Thermomixer comfort	Eppendorf
Thermcycler	LifeEco	BIOER
Vortex	Vortex Genie 2	Bender & Hobein AG

2.2.2 Chemicals, reagents and pre-mixed solutions

If not stated otherwise all chemicals were obtained from VWR at molecular biology grade. All chemicals from other sources are listed below.

Description	Manufacturer/Supplier
Acetic anhydride	Sigma
BCIP (5-bromo-4-chloro-3-indolyl-phosphate)	Roche
Blocking Reagent	Roche
BSA (Bovine Serum Albumin) ≥ 96%	Sigma
Cadaverine	Sigma-Aldrich
D-Fructose	Applichem
Diethyl pyrocarbonate (DEPC)	Sigma-Aldrich
Dimethyl sulfoxide	Sigma
di-Sodium hydrogene phosphate	Merck
EDTA	Sigma
Heparin	Sigma-Aldrich
Instant Ocean Sea Salt	Instant Ocean
Low-melting point agarose	Sigma
Methylene Blue	Sigma
MS-222	Sigma-Aldrich
NBT (4-Nitro blue tetrazolium chloride)	Roche
Nuclease free water	Gibco
Phenol Red	Fluka
Phenol-Chloroform-Isoamyl alcohol mixture (25:24:1)	Sigma
Phenylthiocarbamide	Sigma
Sheep Serum	Sigma
TAE buffer 50x (Rotiphorese)	Roth
TissueTek cryo-embedding medium	Sakura
Triethanolamine	Merck
Triton X-100	Merck
Tween20	Sigma
Vecta mount permanent mounting medium	Vector Labs
Vecta mount permanent mounting medium (w/ DAPI)	Vector Labs
yeast tRNA	Thermo Fischer Scientific

2.2.3 Disposables

For sterile work plastic ware was autoclaved prior to use.

Disposables	Specifications	Manufacturer/Supplier
Borosilicate Capillary	GB100F-10	Science Products
Conical Tubes	15 ml, 50 ml	Falcon
Coverslips	24x60 mm	VWR
Hypodermic Needles	Sterican	Braun
Laboratory Film		PARAFILM
Latex Gloves	powderfree	VWR
Microcentrifuge Tubes	1.5 ml, 2 ml	Axygen
Microloader Tips	20 µl	Eppendorf
Microscope Slides	Superfrost	VWR
Microscope Slides	Standard	VWR
Pasteur Pipet		VWR
PCR-Tubes		VWR
Petri Dish	Ø 60mm, 100 mm	VWR
Pipet Tips	10/200/1000 µl	VWR
Pipet Tips with Filter	SurPhob	Biozym
Syringes	2/5/10/50 ml	Braun

2.3 Enzymes and premixed enzymes

Proteinase K	Roche, CH
GoTaq Green Mastermix	Promega, GER
T3-RNA Polymerase	Roche, CH
T4-DNA Ligase	New England Biolabs
BsaI	New England Biolabs
DraI	New England Biolabs
DNAseI	New England Biolabs
Cas9-NLS	New England Biolabs

2.4 Antibodies

Antibody	**Source**	**Catalogue number**
α-TAAR13c rabbit IgG, polyclonal	Hussain et al., 2013(Hussain et al., 2013)	-
α-pERK rabbit IgG, polyclonal	Cell Signaling Technology, USA	#9101
α-pERK mouse IgG, monoclonal	Cell Signaling Technology, USA	#9106
α -SV 2 mouse IgG, monoclonal	Developmental Studies Hybridoma Bank, Iowa, USA	-
α-tubulin mouse IgG, monoclonal	Promega, Germany	#G7121
α-S100 rabbit IgG	Agilent, former Dako, USA	#Z0311
α-G_{olf} mouse IgG, monoclonal	Santa Cruz Biotechnology, USA	#sc-55546
Alexa Fluor 488 goat α-rabbit IgG	Invitrogen, GER	#A21206
Alexa Fluor 488 donkey α-mouse IgG	Invitrogen, GER	#A21202
Alexa Fluor 594 goat α-rabbit IgG	Invitrogen, GER	# A11012
Alexa Fluor 594 goat α-mouse IgG	Invitrogen, GER	#A11005
α-DIG-AP IgG from sheep, polyclonal	Sigma, GER	#11093274910

2.5 Oligonucleotides

All oligonucleotides were ordered from Invitrogen as desalted standard DNA oligos at the scale of 25 nmoles if not stated otherwise. Their 5´ to 3´ sequences are listed below. gRNA target sites are marked in red.

Primer	5´ to 3´ sequence
Guide-constant oligo (50 nmol)	AAAGCACCGACTCGGTGCCACTTTTTCAAGTTGATAACGGACTAGCCT TATTTTAACTTGCTATTT CTAGCTCTAAAAC
gRNA Primer 1	GCGTAATACGACTCACTATAG
gRNA primer 2	AAAGCACCGACTCGGTGCCAC
5´13c site 1	GCGTAATACGACTCACTATAGGTGTGGAACAGTGGCTCAGGTTTTAGA GCTAGAAATAGC
5´13c site 2	GCGTAATACGACTCACTATAGGTGGATAATAATTAAGTAAGTTTTAGA GCTAGAAATAGC
5´13c site 3	GCGTAATACGACTCACTATAGGAGATTTCCTTTCAAATGAGTTTTAGA GCTAGAAATAGC
5´13c site 4	GCGTAATACGACTCACTATAGGTCTCATGCATGTTGTGGGGTTTTAGA GCTAGAAATAGC
tyrosinae target	GCGTAATACGACTCACTATAGGTCCAGTCTGGCCCGGCGAGTTTTAGA GCTAGAAATAGC
golden target	GCGTAATACGACTCACTATAGGAGTGACGACAGCAGCCTGGTTTTAGA GCTAGAAATAGC
exon13c site1_o1	TAGGGTCATGGTGATGATAAGT
exon13c site1_o2	AAACACTTATCATCACCATGAC
exon13c site2_o1	TAGGTGATGATAAGTTGGAGCA
exon13c site2_o2	AAACTGCTCCAACTTATCATCA
exon13c site3_o1	TAGGTGTACTCAAAAGCTAACT
exon13c site3_o2	AAACAGTTAGCTTTTGAGTACA
3´13c site1_o1	TAGGAAGAAACCCACACCAACA
3´13c site1_o2	AAACTGTTGGTGTGGGTTTCTT
3´13c site2_o1	TAGGTAACATCTAGTTTTTATG
3´13c site2_o2	AAACCATAAAAACTAGATGTTA
contr_3´13c_fw	TGAACAAATGTCAGGTGCTCG
contr_5´13c_rev1	GCCAAACATAGTGTGCTAGTGC
contr_5´13c_rev2	AGTTGATATTTAGCCGCACCG
actinb1_fw	CCCCATTGAGCACGGTATTG
actinb1_rev	TCACACCATCACCAGAGTCC
TARL1_fw1	TTCACGAGTCGCCCTCTATC
TARL1_rev1	ATAGGCCACCAACATGGTCA
TARL1_fw1_t3	AATTAACCCTCACTAAAGGTTCACGAGTCGCCCTCTATC
TARL1_rev1_t3	AATTAACCCTCACTAAAGGATAGGCCACCAACATGGTCA
TARL1_fw2	AGCCTCCATTTTCCACCTGA
TARL1_rev2	CCCATGATGATCCCTAGCGT
TARL1_fw2_t3	AATTAACCCTCACTAAAGGAGCCTCCATTTTCCACCTGA
TARL1_rev2_t3	AATTAACCCTCACTAAAGGCCCATGATGATCCCTAGCGT

2.6 Media

LB-medium 1 liter:	10 g	NaCl
	10 g	Tryptone
	5 g	yeast extract
	pH to 7.5	NaOH

	stock solution	**working concentration**
Ampicillin	100 mg/ml	100 µg/ml
Kanamycin	50 mg/ml	50 µg/ml

2.7 Buffers and solutions

1x PBS (Tween/Triton)	137 mM	NaCl
	2.7 mM	KCl
	10 mM	Na_2HPO_4
	1.8 mM	KH_2PO_4
	(0,1% v/v	Triton X100)
	(0,1% v/v	Tween20)
	pH 7.3	with NaOH
Paraformaldehyde	1x	PBS
	4% w/v	Paraformaldehyde
Primary antibody solution	1x	PBS-Triton
	1,5% w/v	BSA
	5% v/v	Sheep Serum
ACSF	119 mM	NaCl
	26.2 mM	$NaHCO_3$
	2.5 mM	KCl
	1 mM	NaH_2PO_4
	10 mM	Glucose
	2.5 mM	$CaCl_2$
	pH 7.2	with NaOH
	gas with	95% O2/5% CO2
DNA extraction buffer	100 mM	Tris-HCl
	100 mM	EDTA
	250 mM	NaCl
	1% w/v	SDS
	200 µg/ml	Proteinase K
"Quick" DNA extraction buffer	10 mM	Tris-HCl
	2 mM	EDTA
	0,2% w/v	Triton X100
	200 µg/ml	Proteinase K
20x SSC buffer	3 M	NaCl

	0.3 M	sodium citrate
Hybridization solution	50 % v/v 5x 0.1 % 50 µg/ml 500 µg/ml to pH 6.0 fill with	Formamide SSC Tween20 Heparin tRNA citric acid DEPC water
TN buffer	100 mM 150 mM (for blocking add 0.5 % (for washing add 0.05 %	Tris-HCL pH 7.5 NaCl Blocking reagent) Tween20)
Section ISH detection buffer	100 mM 100 mM 10 mM **for staining add:** 100 mg/ml 50 mg/ml	Tris-HCl pH 7.5 NaCl MgCl NBT BCIP
WM-ISH staining buffer	100 mM 50 mM 100 mM 0.1 % **for staining add:** 100 mg/ml 50 mg/ml	Tris-HCl pH 9.5 MgCl NaCl Tween20 NBT BCIP

2.8 Kits

The following Kits were used according to the manufacturer´s instructions.

Name	**Provider**
NucleoSpin® Plasmid	Macherey-Nagel, GER
NucleoSpin® Gel and PCR Clean-up	Macherey-Nagel, GER
HiScribe T7	New England Biolabs, USA
RNeasy Mini Kit	Qiagen, GER
Superscript™III Reverse Transcriptase	Invitrogen, GER

2.9 Molecular biology techniques

2.9.1 DNA extraction from embryos or tissue by phenol/chloroform method

This method was used to obtain large amount of purified genomic DNA.

One zebrafish embryo (1-6 dpf) was lysed in 30 µl DNA extraction buffer freshly supplemented with 200 ng/µl Proteinase K. Lysis was achieved either mechanically by mashing the tissue with a pestle or by shaking in a thermomixer at 700 rpm and 56°C for up to 1 h. 70 µl of extraction buffer were added and the tube was inverted several times. 50 µl of phenol/chloroform/isoamylalcohol (25:24:1) were added to extract the DNA and, again, the tube was inverted several times. After spinning the tube for 5 min at 13,000 g the aqueous phase was collected and transferred into a new tube. After adding 25 µl 3M Na-acetate (pH 7) the DNA was precipitated with 100 µl 100% ethanol. The DNA was pelleted by spinning for 8 min at high speed. The supernatant was removed. The pellet was washed with 200 µl 80% ethanol and centrifuged again. Subsequently the pellet was dried and re-suspended in 20-50 µl 10 mM Tris-HCl pH 8. The DNA concentration was determined with a NanoDrop™ Photometer.

The procedure can be scaled up for more embryos or larger tissues. Typically 200-300 µl of DNA extraction buffer is enough for pools of 10-20 embryos or larger tissue pieces (e.g. brain, muscle). After DNA precipitation with ethanol and spinning there usually is a visible pellet, when using more than 5 embryos.

2.9.2 “Quick” genomic DNA preparation for PCR

This protocol was used as a quick method to screen larger amounts of embryos by PCR. Up to twenty embryos (2-3 dpf) are lysed by in 50 µl “Quick” DNA extraction buffer incubation at 56°C for 2-3 h on a thermomixer. To speed up the lysis process the tubes were vortexed occasionally. Samples were boiled at 95°C for 5-10 min to inactivate the Proteinase K. Then, the tube was centrifuged for 30 s at 11,000 g in order to pellet tissue remnants. 10 µl of the sample were used for PCR applications. DNA samples were stored at -20°C for further PCR runs.

2.9.3 DNA amplification by PCR and colony PCR

Polymerase chain reaction was used for different purposes like subcloning of specific DNA fragments, amplification of templates for *in vitro* transcription, and identification of genome editing events in animals. If not stated otherwise, primers were designed using the primer3 tool (http://primer3.ut.ee/) or the NCBI primer design tool (https://www.ncbi.nlm.nih.gov/tools/primer-blast). For standard PCR 10-100 ng of DNA template was used. For colony PCR a bacterial colony was picked from the plate with a pipette tip and smeared into the bottom of the PCR tube. The tip was then used to inoculate a 4 ml liquid bacterial culture.

The standard protocol is presented below:

initial denaturation	95°C	3 min	
denaturation	95°C	45 s	35x
primer annealing	51-58 °C	45 s	
extension	72°C	30-90 s	
final extension	72°C	5 min	
end	4°C	∞	

The estimated optimal annealing temperature was calculated with the Tm-calculator provided on the Thermo Fischer website. Typical values range between 51°C and 58°C, depending on length and composition of the oligonucleotide primers. The length of the elongation step at 72°C depends on the length of the fragment that is to be amplified. Taq-based polymerases typically process around 1 kb/min.

2.9.4 cDNA synthesis by reverse transcription

Tissue specific RNA molecules can be transcribed into complementary DNA (cDNA) by reverse transcription using the enzyme reverse transcriptase. This allows PCR based analysis of gene expression (RT-PCR) for those tissues.

The SuperScript III kit (Thermo Fisher) was used to produce cDNA from isolated zebrafish whole RNA samples from different organs according to the manufacturer's instructions. cDNA concentration was determined with a NanoDrop™ photometer and samples stored at -20°C.

2.9.5 DNA Sequencing

DNA sequencing was used to check cloned plasmids amplified in bacteria as well as genomic alterations in zebrafish genomic DNA. DNA Sequencing was conducted either by GATC Biotech (Germany) or Eurofins Genomics (Germany) sequencing services. Samples were prepared as required by the sequencer and usually contained 10-50 ng/µl template DNA (purified PCR product, plasmid or genomic DNA) as well as 2,5 µM primer in a volume of 10-20 µl. Results were analyzed using the GATC viewer and/or NCBI blast, where sequence alignments were assessed.

2.10 Odor stimulation of zebrafish for use of α-pERK as neuronal activity marker

Phosphorylation of the extracellular-signal regulated kinase (ERK) has been described as a neuronal activity marker in the nose as well as the brain(Miwa and Storm, 2005, Hussain et al., 2013, Randlett et al., 2015).

For α -pERK immunohistochemistry experiments adult fish between 4 and 9 month of age were used. One night prior to the experiment fish were separated and kept in an individual freshwater-supplied tank. On the next morning fish were brought to a behavior room and allowed to acclimatize for 45 min in salt supplemented reverse osmosis water (0,03% w/v Instant Ocean Sea Salt), before putting them into smaller stimulation tanks and letting them rest for another 45 min. Odors were prepared freshly in fresh system water. Cadaverine was purchased from Sigma (#D22606). Amine mix was produced as reported previously (Gliem et al., 2013). System water served as a negative control stimulus. Stimuli were given through a flexible pipe to a final concentration between 1 µ M and 100 µ M. It was made sure, that the fish were in a calm state at the time point of stimulation and that the experimenter was not visible to the fish. 3 min after stimulation the fish were swiftly immobilized by immersion in ice water and killed by decapitation.

2.11 Histological methods

2.11.1 Tissue preparation for immunohistochemistry and *in situ* hybridization on cryosections

After decapitation, zebrafish heads were fixed in 4% PFA for 1 h. Zebrafish tissues were dissected in cold PBS. After several washings in PBS the olfactory epithelia were embedded in TissueTek (Sakura) and frozen. The heads were fixed in 2% PFA for another 4 h and put in 30% sucrose in PBS overnight. After dissection, brains were embedded in TissueTek and frozen. 17–20 µm cryosections of the olfactory bulb and 10 µm cryosections of the OE were produced with a cryostat (Leica CM1900) and dried.

2.11.2 2.5.2 Immunohistochemistry on cryosections

After rehydration in PBS and blocking in 3% BSA-PBST, sections were incubated over night with a dilution of primary antibody in blocking solution. Primary antibody dilution was 1:250 for all antibodies, except anti-acetylated tubulin (1:1000). On the next day, sections were washed three times in PBS for 10 min each, followed by incubation with secondary antibody (1:250 dilutions in PBST) for 3 h at room temperature. Sections were washed and then mounted with VECTASHIELD® mounting medium (Vector Laboratories) containing DAPI. Images were obtained using a Keyence BZ-9000 wide field fluorescence microscope (Keyence, Japan) with 20x and 40x air objectives and a 100x oil-immersion objective (Nikon, Japan).

2.11.3 Quantitative evaluation of OSNs and glomeruli from cryosections

To count co-labelled OSNs in the OE we took high magnification images of corresponding lamellae using at least a 40x objective and looked for fluorescent signal of the OSN-type markers (OMP, TRPC2, S100) in OSNs labelled by α -TAAR13c antibody.

Counts of activated glomeruli were performed on sections to obtain a higher accuracy. Images of serial OB sections were analyzed by counting the pERK-positive glomeruli. Glomeruli were identified by their typical shape, absence of nuclei (DAPI) and/or co-labeling with axons expressing fluorescent proteins in OBs of the transgenic reporter lines used. Particular care was

taken to avoid double counting of glomeruli in adjacent sections. In rare cases the distinction of adjacent active glomeruli was not unambiguously possible for the highest concentration of stimuli investigated. The position of an activated glomerulus was determined by measuring length (anterior-to-posterior, a↔p) and height (ventral-to-dorsal, v↔d) coordinates for its center. These values were then normalized to the overall length and height of the respective bulb section.

2.11.4 Whole mount immunohistochemistry on adult brains

After decapitation, the dorsal cranium was removed and heads were fixed in 4% PFA overnight. Brains were washed several times in PBST and transferred to − 20 °C methanol for ≥ 4 h or overnight. Brains were then rehydrated in a dilution series of 75%, 50%, 25% methanol in PBST (5 min each) and washed again in PBST. Blocking was performed with blocking solution containing 10% calf serum/1% DMSO in PBST for 1 h. Samples were incubated with primary antibody α -pERK (1:50 in blocking solution) at 4 °C for 5–7 days on a vertical rotator (~12 rpm). After washing several times with PBST, brains were incubated with secondary antibody (1:200 in blocking solution) at 4 °C for ≥ 3 days. Brains were washed several times in PBST and subjected to tissue clearing using a fructose-gradient (modified from Ke et al. (2013)). In short, brains were successively incubated in 20%, 40%, 60%, 80%, and 100% fructose in PBS (w/v) on a vertical rotator at RT for 4 h or at 4 °C overnight for each step. Images were obtained using a LSM 510Meta confocal microscope (Zeiss, Germany).

2.11.5 Whole mount immunohistochemistry on 3-8 dpf zebrafish larvae

For α-pERK experiments larvae were stimulated in the same way as the adult fish. Larvae were killed by immersion into ice water and fixed in 4% PFA for 1h at RT. After washing 4x 20 min in PBS-Triton larvae were stored in 100% Methanol at -20°C for at least 3 h until further use. Larvae were rehydrated in a PBS-T dilution series in methanol 75/50/25%, 3-4 min each, and washed 3x 20 min in PBS-Triton. Blocking was performed for 1.5 h at RT in PBS-Triton supplemented with 5% sheep serum, 1,5% BSA, and 1% DMSO. Larvae were then incubated in primary antibody solution (1:250) in blocking buffer for 1-3 days. After washing 3x 20 min in PBS-Triton larvae were incubated in secondary antibody solution (Alexa 488, 1:200) in PBS-Triton for 1-3 days. After extensive washing in PBS-Triton larvae were embedded in 0.8% low

melting agarose in PBS. Imaging was conducted with a Leica SP8 confocal microscope (Leica, Germany).

After the imaging larvae can be oriented in TissueTek and frozen to obtain images of cryosections in addition to the whole mount images. This facilitates the determination/identification of weak signals or single fluorescence-labelled cells.

2.11.6 *In situ* hybridization on cryosections

OE sections were obtained as described above. Slides were fixed in 4 % PFA in PBS for 10 min at RT. Fixation was followed by: 5 min incubation in 1x PBS 10 min incubation in 0.2 M HCl, 5 min incubation in 1x PBS, 10 min incubation in 5 mM acetic anhydride/0.1% triethanolamine/HCL. Sections were hybridized with 100-200 ng/ml RNA probes in hybridization solution supplemented with 5x Denhardt´s reagent for 16 h at 60°C in a wet chamber.

The next day, slides were shortly rinsed in 5x SSC and subsequently incubated in 50 % formamide/2x SSC, 2x SSC, 0.2x SSC each for 30 min at 65°C. This was followed by 15 min incubation in 0.2x SSC at RT, 5 min in 1x PBS at RT and a blocking step in TN buffer + 0.5 % blocking reagent, before the sections were incubated with a 1:500 dilution of α-DIG antibody conjugated to alkaline phosphatase in TN buffer + 0.5 % blocking reagent for 2-6 h at RT or overnight at 4°C.

The next day sections were washed 3x 10 min in TNT buffer and 2x 10 min in detection buffer, before they were incubated with NBT/BCIP in detection buffer to start the color reaction. Slides were checked for dark blue signal regularly. If no signal appeared within the first 2 h at RT, slides were incubated with staining buffer overnight at 4°C.

The color reaction was stopped by immersion into 1x PBS for 5 min. Slides were mounted with VectaMount and observed under a microscope.

2.11.7 Whole mount *in situ* hybridization on zebrafish larvae

Larvae were raised in 45 mg/l N-Phenylthiourea in order to bleach them. At the desired age larvae were killed, fixed in 4% PFA at 4°C overnight and then transferred into -20°C methanol until further use.

Larvae were rehydrated stepwise in methanol/PBS (75/50/25 % methanol in PBS) for 5 min at RT each. After extensive washing larvae were treated with proteinase K (10 µg/ml) in PBS for 30 min and then re-fixed in 4% PFA in PBS for 20 min at RT. After several 5 min washes in PBS-Tween larvae were pre-hybridized in hybridization solution for 60 min at 65°C. Hybridization was carried out with100-200 ng/ml RNA probe in hybridization solution overnight at 65°C.

The next day larvae were rinsed in 50% formamide/5x SSC and then stepwise transferred to 2x SSC (25/50/75/100% 2x SSC) 15 min at 65°C each step. Slides were washed 2x 30 min in 0.2x SSC at 65°C to quench unspecific signals and then stepwise transferred to PBS-Tween (25/50/75/100% PBS-Tween) 10 min at RT for each step.

Larvae were blocked in 2% sheep serum/ 0.2% BSA/ 0.5 mg/ml levamisole in PBS-Tween for 60 min at RT and then incubated in a 1:1000 dilution of α-DIG antibody conjugated to alkaline phosphatase in blocking solution overnight at 4°C.

The next day larvae were washed extensively in PBS-Tween and 3x 5 min in WM-ISH staining buffer, before incubating them with NBT/BCIP in staining buffer to start the color reaction. Larvae were checked regularly in the first 2 h after starting the reaction. If no staining appeared, larvae were further incubated at 4°C. Color reaction was stopped by immersion into PBS. Larvae were stored in PBS-Tween until imaging with an appropriate microscope.

2.12 Calcium imaging

2.12.1 Calcium imaging in adult OE explants

Fish were killed by an overdose of MS-222 and decapitated. In a bath of ACSF the skull bone-plate was opened, the olfactory nerve was cut and the OE was taken out of the nasal cavity. Then, the tissue was embedded in warm 2 - 2.5 % low melting agarose in ACSF. A water bath or incubator was used to keep the agarose in a fluid state prior to embedding. The temperature should not exceed 40-45°C in order not to damage the tissue. The hardened agarose block was mounted onto a vibratome stage using glue. The OE was cut horizontally (usually in the upper half, as most OSNs are located here) to produce a plain epithelial surface enabling assessment via a microscope objective. In that way two tissue specimens are obtained per OE and can then be further processed.

Agarose slices were transferred into a petri dish and incubated with the calcium-sensitive dye Fluo4-AM (50 µg/ml in ACSF) in the dark for 30 min at RT as was described earlier for *Xenopus* tissues by the Manzini group (Hassenklover et al., 2009). Properly prepared tissue should show intense cilia movement.

Tissue preparations were placed in an imaging chamber under a confocal microscope (Zeiss LSM 510, Argon Laser; Excitation at 488 nm/Emission at <495 nm). A constant flow of ACSF was applied. Stimuli were added to the flow at concentrations of 10 - 100 µM. Images were taken at 1 Hz with an image size of 512x512 pixels and about 10 images taken as control before onset of the stimulus. Optical slice thickness includes only one layer of cells.

Image analysis was performed using custom scripts written in MATLAB (MathWorks, USA) as described previously (Junek et al., 2009). In short, a pixel correlation map was created to facilitate the selection of regions of interest (ROIs). Fluorescence changes for individual ROIs were then plotted as $\Delta F/F_0$ with F_0 being the average fluorescence from the first 10 images. Averaged data from multiple ROIs were plotted as mean $\Delta F/F_0 \pm$ SEM.

The laminar height of Ca^{2+}-imaging ROIs or fluorescently labelled OSNs from transgenic reporter lines were measured by forming the ratio of the laminar height of the ROI or cell (h_1, distance from basal lamina to center of the ROI or cell) and the total laminar height h_0 at that position (distance from basal lamina to apical border of the lamella). Results were plotted as ECDFs.

2.12.2 Calcium imaging in the larval brain using the *elavl3*:GCaMP6s line

The transparent Casper background zebrafish line with pan-neuronal expression of GCaMP6s was kindly shared by Misha B. Ahrens from the Janelia Research Campus (Ashburn, VA, USA).

Larvae were checked for GCaMP6s expression at 2-3 dpf. Larvae with brightest fluorescence signal were selected, raised till 6 dpf and then used for Ca^{2+}-imaging experiments. Larvae were raised in reverse osmosis water supplemented with 0.3 % w/v sea salt. The same water was used to prepare all solutions used in this protocol.

Larvae were anesthetized in MS-222 and embedded in warm 1 - 1.5 % low-melting point agarose in sea salt water in an imaging chamber or petri dish such that the brain could be microscopically assessed from above. Heartbeat of the larvae was constantly monitored. Excess agarose was carefully removed from the rostrum. The olfactory epithelia have to be freed from agarose entirely. The chamber was filled with fresh water.

Subsequently larvae were placed under a confocal microscope (Leica SP8 with an argon laser; excitation 488 nm; emission >495 nm). Images from an optical plane were taken at 2-4 Hz and for at least 10 seconds before the onset of stimulus application. Stimuli were delivered via a syringe onto the rostral area of the larvae. Excess fluid was pumped out of the chamber by a peristaltic pump. Images were acquired for at least 90 s to allow multiple stimulus pulses.

ROIs were selected using ImageJ and fluorescence intensity values were plotted against the number of frames.

2.13 Creation of CRISPR/Cas9 mediated gene knock-outs in zebrafish

2.13.1 CRISPR/Cas9 target site design

Two open-source online tools for CRISPR/Cas9 target site design were used in this study.

In 2013 the Zhang Lab from Massachusetts Institute of Technology launched a website with a target site design tool for 16 different species. The algorithm predicts the efficiency for a specific target site and lists potential target sites according to their score, while also offering a potential off-target analysis (http://crispr.mit.edu/). Some of the target sites used for initial tests were designed using this tool.

However, during the years several CRISPR/Cas9 target site design tool became available online, offering a much faster and more convenient prediction of target sites and off-targets. One of them, CHOPCHOP (Labun et al., 2016), was used to design the target sites used in this study.

In CHOPCHOP a genomic location of interest was defined for the zebrafish genome assembly GRCz10. The results lists all possible target sites found in that region, also giving information about potential off-targets and target site efficiency. Off-targets are listed with their respective genomic location, the number of mismatches and the position of the mismatches in the sequence. For TAAR13c flanking regions only target sites with no predicted off-targets or no off-targets in gene-coding sequences were chosen. The efficiency is provided as a score value between 0 and 1. Target sites with scores above 0.50 usually should provide a sufficiently high genome editing rate, as has been observed in this study.

Because TAAR13 gene family members show high degrees of sequence identity, target sites for TAAR13c were chosen in the 5´and 3´flanking regions of the gene. This would enable the removal of the entire gene, as the two cut ends can join by non-homologous end joining (NHEJ), as has been shown before for zebrafish DNA fragments of up to 7.1 kb (Ota et al., 2014).

2.13.2 Plasmid-based guide RNA template synthesis

pDR274 (Addgene #42250) was obtained from Addgene and used as a gRNA transcription plasmid. Target sites were designed with as stated above and target site oligos with BsaI restriction site overhangs were ordered as in the example below.

Table 2.2: Example of target site oligonucleotides used to insert the target site into the pDR274 plasmid. The underlined bases were added to create BsaI restriction site overhangs at the ends of the annealed oligonucleotides.

name:	3´taar13c site 4
selected target site:	GGTGATGATAAGTTGGAGCA
insert-oligo 1:	TAGGTGATGATAAGTTGGAGCA
insert-oligo 2:	AAACTGCTCCAACTTATCATCA

For each target site insert oligos 1 and 2 were annealed by heating a mixture of equimolar volumes of both oligos to 95°C and letting them cool down gradually in a thermoblock. The insert-oligo pair was diluted to 0.1 µM and stored at -20°C.

10 µg of pDR274 were linearized by incubation with 10 U of BsaI for min. 3 h at 37°C. The linearized plasmid was run on a 1% agarose gel in an electrophoresis chamber, and purified using the gel extraction kit (Macherey Nagel). A ligation containing 1 µl linearized pDR274, 1 µl T4 Ligase, 2 µl 10x T4 ligase buffer, 2 µl 0.1 µM insert-oligo pair, and 14 µl nuclease free water was set up and incubated at 14°C for 4 h to overnight. 3 µl of the ligation were transformed into E.coli XL1 blue. The bacteria were dispersed on LB kanamycin plates and incubated overnight at 37°C. Clones were picked and insertion of the target site was checked by a colony PCR with the M13 forward primer and insert-oligo 2 as a reverse primer. Also, 4 ml cultures in LB kanamycin were inoculated for all clones picked. After 16 h at 37°C plasmids from positively tested clones were isolated from the bacterial culture using the NucleoSpin® Plasmid kit (Macherey Nagel). All plasmids were send to sequencing using the M13 fw primer and checked for correct target site insertion, intact T7 promoter and intact gRNA sequence.

To prepare the target-site plasmids for gRNA synthesis 5 µg of plasmid were digested with 4 µl DraI in a total volume of 50 µl for min. 3 h at 37°C. Digests were run on a 1 % agarose gel. The 286 bp band, containing the fragment with the T7 promoter and gRNA sequence, was cut out and

purified using the NucleoSpin® Gel and PCR Clean-up kit. The purified template for *in vitro* transcription was stored at -20°C until further use.

2.13.3 Short-oligo based guide RNA template synthesis

To speed up the process from target site design to injection, cloning free methods to obtain gRNA have been described (Gagnon et al., 2014, Talbot and Amacher, 2014). Here, a 119 bp IVT template containing the T7 promoter sequence, the target-site sequence and the gRNA scaffold sequence is produced by PCR using the four oligonucleotides listed below.

oligo name	**sequence (5´- 3´)**
short guide oligo	GCGTAATACGACTCACTATAGGNNNNNNNNNNNNNNNNNNGTTTTAGAGCTAGAAATAGC
guide-constant oligo	AAAGCACCGACTCGGTGCCACTTTTTCAAGTTGATAACGGACTAGCCTTATTTTAACTTGCTATTTCTAGCTCTAAAAC
gRNA primer 1	GCGTAATACGACTCACTATAG
gRNA primer 2	AAAGCACCGACTCGGTGCCAC

Table 2.3 Oligonucleotides required for the cloning free amplification of target specific gRNA. The short guide oligo is variable and contains the T7 promoter sequence (red), the desired target site sequence (yellow) and an overlap with the guide-constant oligo, that codes for the gRNA scaffold (purple). gRNA primers 1 and 2 anneal to the ends of the construct and allow amplification.

A 100 µl PCR reaction was set up as follows:

PCR reaction		**thermocycler protocol**		
2.5 µl	10 µM gRNA primer 1	95°C	1 min	
2.5 µl	10 µM gRNA primer 2	95°C	15 s	40x
2 µl	1 µM short-guide oligo	60°C	30 s	
2 µl	1 µM guide-constant oligo	72°C	20 s	
3 µl	DMSO	72°C	5 min	
50 µl	2x GoTaq Mix	4°C	end	
38 µl	sterile water			

2 µl were run on a 3 % agarose gel at 140 V. If a single fragment of ca. 119 bp length was visible, the remaining PCR product was purified with the NucleoSpin® Gel and PCR Clean-up kit and eluted in 20 µl elution buffer.

2.13.4 Guide RNA *in vitro* transcription and purification

Templates from either the plasmid-based or the cloning-free method of gRNA production were used for in vitro transcription with the HiScribe T7 kit (New England Biolabs). 1-2 µl of template DNA were used along with the kit components according to the manufacturer´s instructions. Transcription mixes were placed at 37°C in a thermoblock and incubated for 4-5 h. Then, template DNA was digested by incubation with DNaseI for 20 min at 37°C. RNA was precipitated by adding 2 µl 8 M LiCl and 75 µl of pre-chilled ethanol. Tubes were placed at -80°C for 1 h up to overnight. RNA was pelleted by spinning for 15 min at 15,000 g at 4°C. Pellets were washed with 80% pre-chilled ethanol and centrifuged again for 5 min. The supernatant was removed. RNA-pellets were dried and re-suspended in 30 µl nuclease free water. RNA concentrations were quantified with a NanoDrop™ photometer.

2.13.5 CRISPR/Cas9 microinjections

Borosilicate glass capillaries (0.78 x 1.00 x 100 mm; GB100TF-10 from Science Products) were pulled with a Flaming/Brown micropipette puller (Sutter Instruments). The tip of the pipette was broken off with a sharp pair of forceps to allow small injection doses to pass.

The injection mix of 10 µl was prepared as follows:

Injection mix	100-200 ng/µl	gRNA
	150 ng/µl	Cas9-NLS
	200 mM	KCl
	0.025%	Phenol Red
	x µl	H_2O to 10 µl

Shortly after mating fertilized one cell stage zebrafish embryos were collected, placed in agarose molds, and injected with the CRISPR/Cas9-NLS injection mix via a pneumatic pico pump (PV830, World Precision instruments) into the yolk, close to the cytosol whenever applicable. The drop volume was adjusted such that the injected volume filled around 1/8 off the egg, corresponding to 1-2 nl.

After injections embryos were raised in egg water supplemented with methylene blue in petri dishes. 4-8 h after the injections dead embryos were discarded. The egg water was changed daily until 6 dpf, when embryos were transferred to nursery tanks. At 2-3 dpf a part of the embryos was

used for DNA extraction and PCR-based screening of mutation frequencies. The remaining embryos were raised as described in the chapter ´animal care`. Note that the injection mixes, if not used up completely, can be shock-frozen in liquid nitrogen and used for injections again after thawing on ice.

2.14 Data mining in NCBI fish genomes and phylogenetic analysis

All fish genomes available in the NCBI genome database (as of February 2017) were examined, except *Latimeria chalumnae*, which is subject of a separate study in the lab. Some genomes displayed only a partial genomic coverage, which lead to the exclusion of 2 species. The tetrapod (lobe-finned) lineage was also not included into the search.

The zebrafish TAAR13 amino acid sequence and, if required, also the TAAR12h amino acid sequence were used as query in a tBLASTn search for class II TAAR sequences in all genomes examined. *E*-values of 10^{-20} and a minimal sequence length of 200 amino acids were used as cutoffs to select potential candidate genes.

In a first step amino acid sequences of candidate genes from 5 species were aligned with the known zebrafish TAAR sequences using MAFFT version 7 (http://mafft.cbrc.jp/alignment/software/). A selection of ORs and Aminergic Receptors served as outgroup (Hussain et al., 2009). Aligned sequences were gap-stripped with a 90% tolerance using Gap Strip/Squeeze version 2.1.0 (https://www.hiv.lanl.gov/content/sequence/GAPSTREEZE/gap.html). A preliminary phylogenetic tree was constructed using maximum likelihood method (PhyML) (Guindon et al., 2010).

In this tree class II TAARs were identified by their position among the known class II members from zebrafish. Initially TARLs were identified by their unique position in the tree between class I TAARs and a family of serotonin receptors that was used as outgroup. Later on zebrafish TARL1 was used as query for a tBLASTn search in all genomes examined. TARL genes from jawed fish are highly conserved and were easily identifiable by their high sequence similarity, usually ~95% identity among closely related species, but at least ~85% even among remotely related species.

Genomic sequences of all candidate genes were then extended up to 2 kb in the 5´and 3´direction to identify start and stop codons and obtain the complete amino acid sequence prediction. GeneWise (www.ebi.ac.uk/Tools/psa/genewise/) was used to complete fragmented or multi-exonic sequences. Expasy translate tool (http://web.expasy.org/translate/) was used to identify start and stop codons. Few amino acid sequences could not be completed because of incomplete genomic sequence.

For the final phylogenetic tree we used all derived sequences (205 class II TAARs, 84 jawless TARLs, and 86 jawed fish TARLs) together with a selection of reference TAARs (classes I, II, and III) and a total of 102 aminergic receptors as outgroup. These 510 sequences were aligned using MAFFT version 7, gap-stripped (90% tolerance), and used for the construction of the final PhyML tree. A complete list of all genes and sequences is provided on the supplementary CD.

Sequence logos of TM7 and its flanking amino acids were created for TAARs in general, class II TAARs, jawed fish TARLs, jawless TARLs and aminergic receptors using an online tool provided by the University of Berkeley, CA (Crooks et al., 2004).

3 RESULTS

3.1 Sensation of amines and diamines in the olfactory epithelium

Amines and diamines are important odors for aquatic organisms and thought to be processed mainly by TAAR receptors. Zebrafish TAAR13c has been shown to be activated by the death-associated odor cadaverine and is one of few deorphanized zebrafish TAARs (Hussain et al., 2013). A thorough characterization of the receptor neurons has not been reported yet and would represent a first step in the elucidation of neuronal circuits activated by this odor class.

3.1.1 TAAR13c is expressed in a sparse population of OSNs in the olfactory epithelium

Olfactory receptors are usually expressed in small subsets of OSNs. The olfactory epithelium of zebrafish is an almost globose organ, formed by olfactory lamellae (see Figure 3.1 A). These lamellae consist mainly of OSNs interspersed with supporting cells. At the base of the lamellae various types of stem cells, i.e. OSN precursors, can be found.

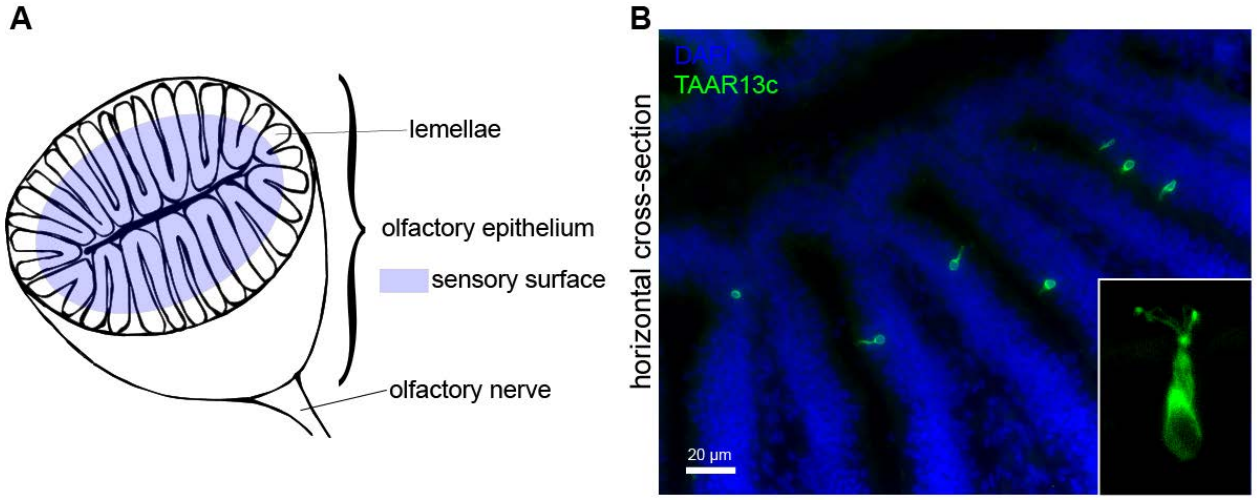

Figure 3.1: TAAR13c is expressed in OSNs in the zebrafish OE A) schematic of the zebrafish olfactory epithelium depicting the lamellar arrangement of the sensory surface. B) TAAR13c antibody (green) labels a sparse population of OSNs, with mainly elongated shape and sensory cilia. Nuclei were visualized by DAPI staining (blue).

In order to study receptor neurons they have to be visualized for microscopic assessment. Here, TAAR13c expressing OSNs were labelled in 10 µm sections of the OE by an antibody against the receptor (Figure 3.1 B). The antibody was visualized under a fluorescence microscope after

treatment with a fluorescent secondary antibody against immunoglobulins of the species of origin of the primary antibody. Usually, only few TAAR13c expressing cells were detected per lamellae, as has been reported before (Hussain et al., 2013). OSNs mainly had an elongated shape with a dendrite stretching out to the apical border of the respective lamella. In higher magnification micrographs even the sensory cilia were visualized (see inlet in Figure 3.1 B).

3.1.2 TAAR13c neurons are ciliated OSNs and do not co-localize with markers for other OSN types

The olfactory epithelium harbors a variety of different OSN types. In order to determine which OSN type TAAR13c expressing neurons belong to, these neurons were co-labelled with accepted markers for ciliated, microvillous and crypt neurons either in reporter gene-expressing zebrafish lines or via co-labelling with two antibodies (see Figure 3.2). Furthermore, TAAR13c expressing OSNs were co-labelled with antibodies against G_{olf}, the olfactory specific Gα subunit, and acetylated tubulin, a structural element of sensory cilia. All of these antibody stainings were conducted on 10 µm horizontal cross sections of the zebrafish nose. Nuclei were counterstained with DAPI.

Ciliated OSNs were visualized with a fluorescence microscope in OEs of a transgenic zebrafish line expressing red fluorescent protein (RFP) under control of the promoter for olfactory marker protein (OMP) (Sato et al., 2005). A very robust co-localization of OMP fluorescence and TAAR13c antibody could be observed. In fact, when quantifying the co-localization, more than 93% of all counted TAAR13c neurons also expressed RFP under the control of the OMP promoter (compare Figures 3.2 A and 3.3). Consistent with this observation no co-localization with markers for other OSN-populations could be found (Figure 3.2 D and 3.2 E). Only very rarely, in less than 3% of the counted cells, TAAR13c-labelled cells appeared to be Venus-positive in the TRPC2:gap-Venus expressing zebrafish line or S100 positive in an co-immunostaining (see Figure 3.3). These rare occurrences may reflect close neighborhood and therefore a false positive overlay of two adjacent cells, as the epithelium is densely packed with neurons.

To further confirm the ciliated nature of OSNs labelled by the TAAR13c antibody the cells were co-labelled with an antibody against G_{olf}, which is a key component of the olfactory signaling

cascade. As expected G_{olf} antibody labels a densely packed layer of cilia at the apical border of the sensory epithelium, which co-localizes with the tip of the apical dendrite of OSNs labelled by the TAAR13c antibody (compare Figure 3.2 B). G_{olf} is known to be the stimulatory Gα-protein involved in the signaling of OR and TAAR expressing OSNs (Zhang et al., 2013, Ihara et al., 2013).

Acetylated tubulin is a cytoskeletal element of sensory cilia (Arikawa and Williams, 1993). To confirm the previous findings, a co-labelling with TAAR13c antibody and an antibody against acetylated tubulin was conducted. α-acetylated tubulin labels apical dendrites of a large number of OSNs in the zebrafish OE. Among these are also the apical dendrites of α-TAAR13c labelled OSNs (see fig. 3.2 C)

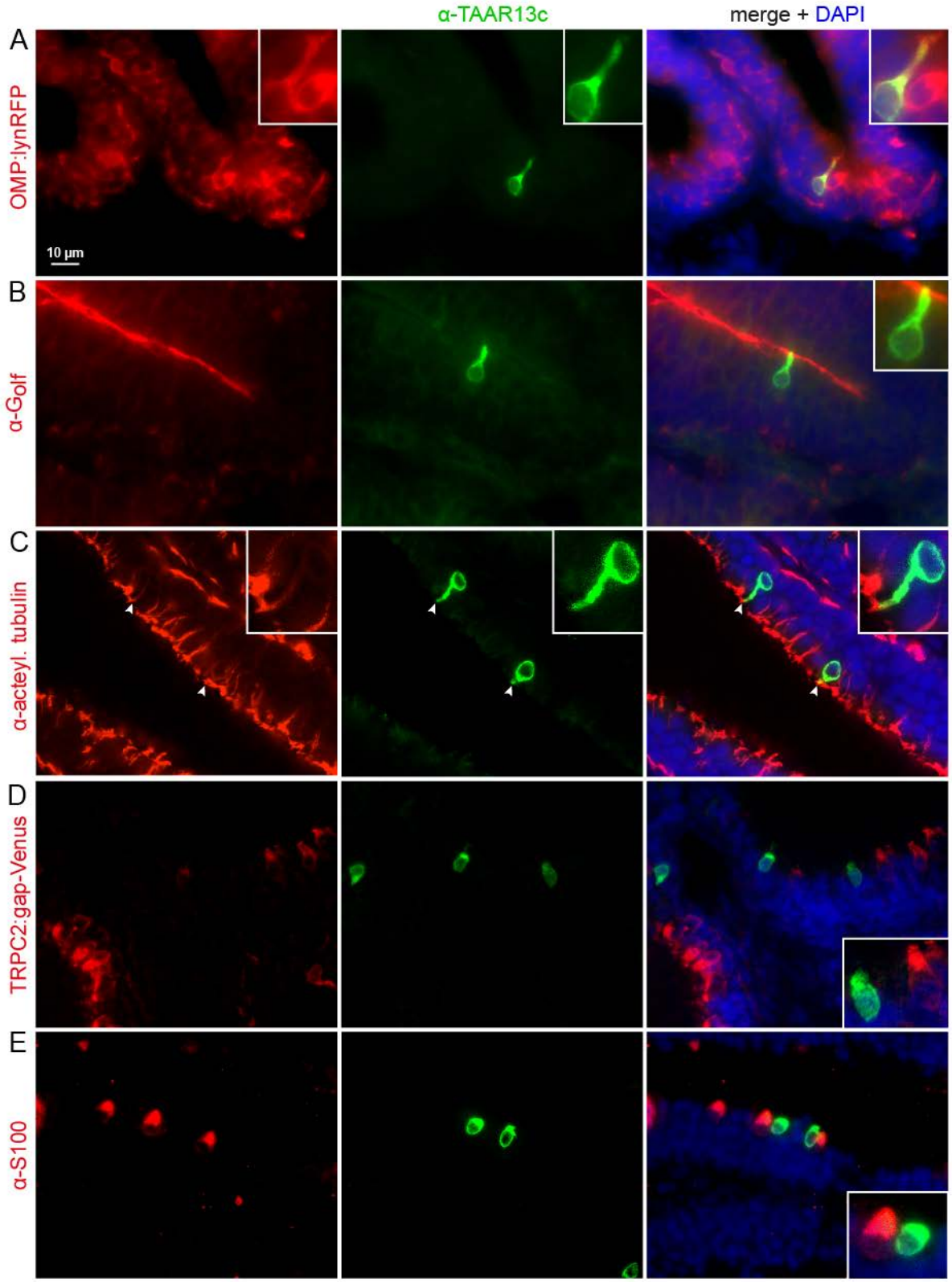

Figure 3.2: Characterization of TAAR13c expressing OSNs TAAR13c expressing OSNs (green) were co-labelled with A) the ciliated neuron marker OMP, B) the olfactory specific Gα-protein G_{olf}, C) the cilia marker acetylated tubulin, D) the microvillous OSN marker TRPC2, and E) the crypt OSN marker S100.

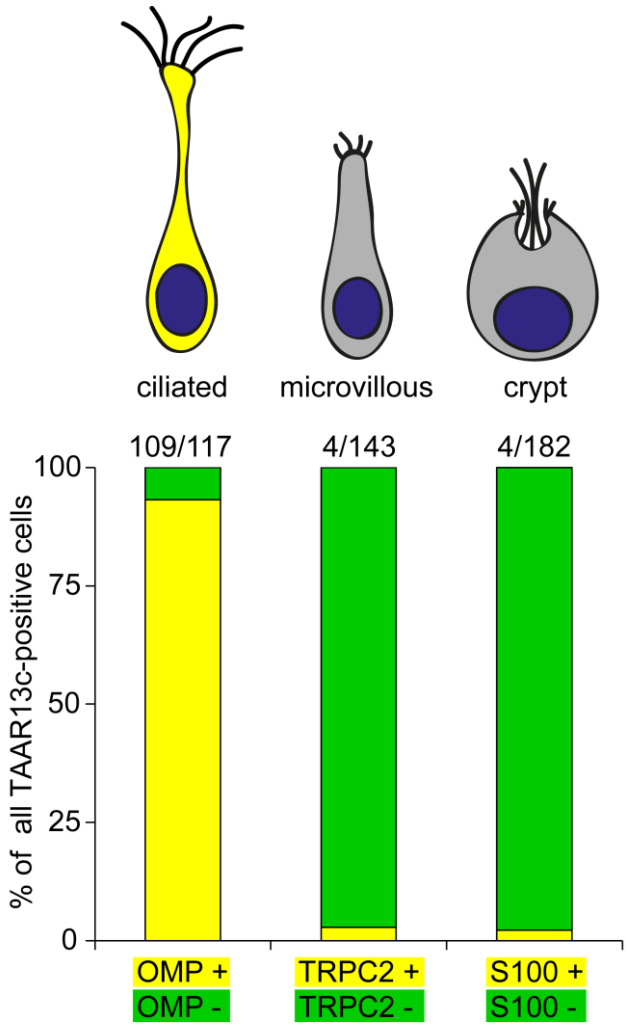

Figure 3.3: Quantitative evaluation of co-localization of TAAR13c-positive neurons with OSN cell type
Over one hundred TAAR13c-labelled cells were evaluated for co-localization with several cell type markers. Results are shown as bar graph below the schematic representation of the three cell types examined. Co-localization is indicated by yellow, non-co-localization by green segments. Nearly all TAAR13c-positive cells were also positive for OMP, a ciliated neuron marker. In contrast, almost no co-localization with TAAR13c staining was observed for TRPC2 and S100, markers for microvillous and crypt neurons, respectively.

3.1.3 Development of a calcium imaging technique in the zebrafish OE

Immunohistochemical techniques allow the statical assessment of molecular parameters in a cell or tissue at a given time point. Here, we established a calcium imaging technique to measure OSN activity over time in response to odors in live tissue using the Ca^{2+}-sensitive fluorescent dye FLUO4-AM. This dye easily crosses membranes due to the bound acetoxymethyl(AM)-ester groups and can be taken up by living cells. The dye was loaded onto horizontally sliced olfactory epithelial tissue, which was carefully embedded into an agarose block before slicing. Neuronal activity in response to applied odors was than imaged with a confocal microscope on the tissue surface, which includes a layer of dye loaded OSNs. We observed a reliable dye penetration into the superficial tissue layer, which was exposed to the dye, after 30 min of incubation at room temperature (see Figure 3.4). Upon application of different odor stimuli changes in intracellular calcium of cells in the OE were detected within few seconds after odor onset.

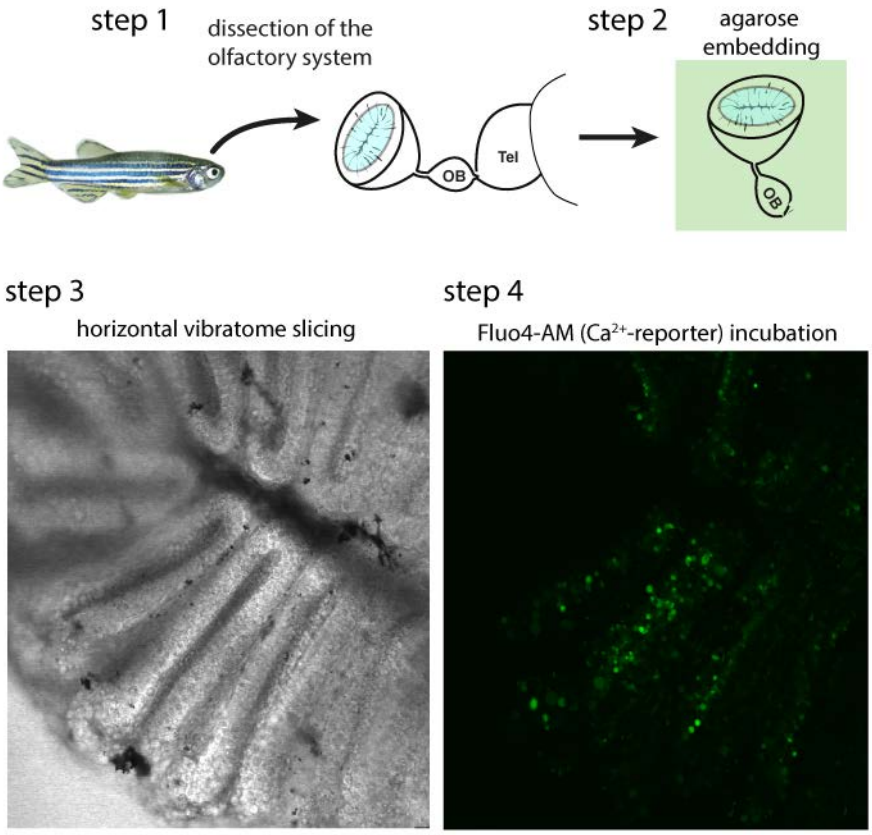

Figure 3.4: Calcium imaging preparation of the zebrafish olfactory epithelium; the olfactory epithelium and bulb were dissected from MS222 euthanized fish (step 1). The OE was embedded in low melting agarose and mounted to a microtome (step 2). The OE was horizontally sliced in the sensory region (step 3). The tissue surface was loaded with FLUO4-AM, a calcium sensitive fluorescent dye.

3.1.4 Amines and ATP activate distinct cellular populations in the OE

Using the protocol depicted in Figure 3.4 the tissue could be maintained in a functional state. Strong cilia movement could be observed in the non-sensory region of the OE (see supplementary videos). These non-sensory cilia create a water circulation in the lumen of the nose, allowing the ligands to reach the sensory cilia in the sensory region of the epithelium. Under the microscope tissue preparations were kept in a constant flow of artificial cerebrospinal fluid (ACSF). Fluorescence on the OE surface was measured at 1 hz. Odors were given at defined time points. The recording was started 10 seconds prior to the stimulus and continued for 60 seconds. Signals were plotted as average change in fluorescence over time for defined regions of interest (ROIs). The cells were allowed to recover for at least 3 minutes between measurements.

Several different odorant classes were applied to the bath, with different outcome. Monoamines and ATP evoked the strongest and most abundant signals in cell of the sectioned OE surface. Usually these signals could be replicated at least twice for the same section, although the changes in fluorescence appeared to become weaker after multiple stimulations. Also, signal reproduction can be hindered by movements in the tissue, which we tried to avoid by holding it in place with a fine thread scaffold. It can be noticed, that, although the whole epithelium was horizontally sliced, changes in fluorescence could only be detected in few lamellae per session. This is due to minor distortions in the tissue surface, that might have occurred during vibratome slicing, and the slim focal plane visualized by the confocal microscope, usually only around 10 µm, depending on the pinhole size. As a result stimulus dependent changes in fluorescence could usually only be measured in about 2-3 lamellae at a time.

Amino acids, aldehydes, ketones, bile acid, and diamines did not evoke any reliable and reproducible response. Thus, we focused on the cellular responses to amines and ATP, which both are of interest for this study, because amines are thought to be the main ligand class for TAARs and ATP is most likely sensed by another receptor class, that could serve as a reference.

To gain an overview of the cells activated by a particular stimulus, a pixel correlation map was created, using a published MatLab script (Junek et al., 2009). In this correlation map pixels with a change in fluorescence over time are color coded from blue, equaling no change in fluorescence, to red, equaling strong change in fluorescence.

Application of a mix of twelve different primary, secondary, and tertiary amines resulted in a change in fluorescence intensity in a large number of cells per lamella, often more than 100 cells per section imaged (see Figure 3.5 A). These cells often resembled elongated OSNs with respect to their shape and location within the olfactory lamella. In contrast, stimulation with ATP mainly evoked changes in fluorescence in horizontal cells positioned at the base of the lamella (see Figure 3.5B). The lower two lamella seem to be in the focal plane of the microscope during the measurement, as they contain the main spots of cellular activity in this particular experiment (Figure 3.5). Note that the dark red spots in panel B do not correspond to maximum activity, but were created by a particle moving in front of the objective and are in fact an artefact. All other signals, from light blue to bright red, can be interpreted as changes in intracellular calcium levels.

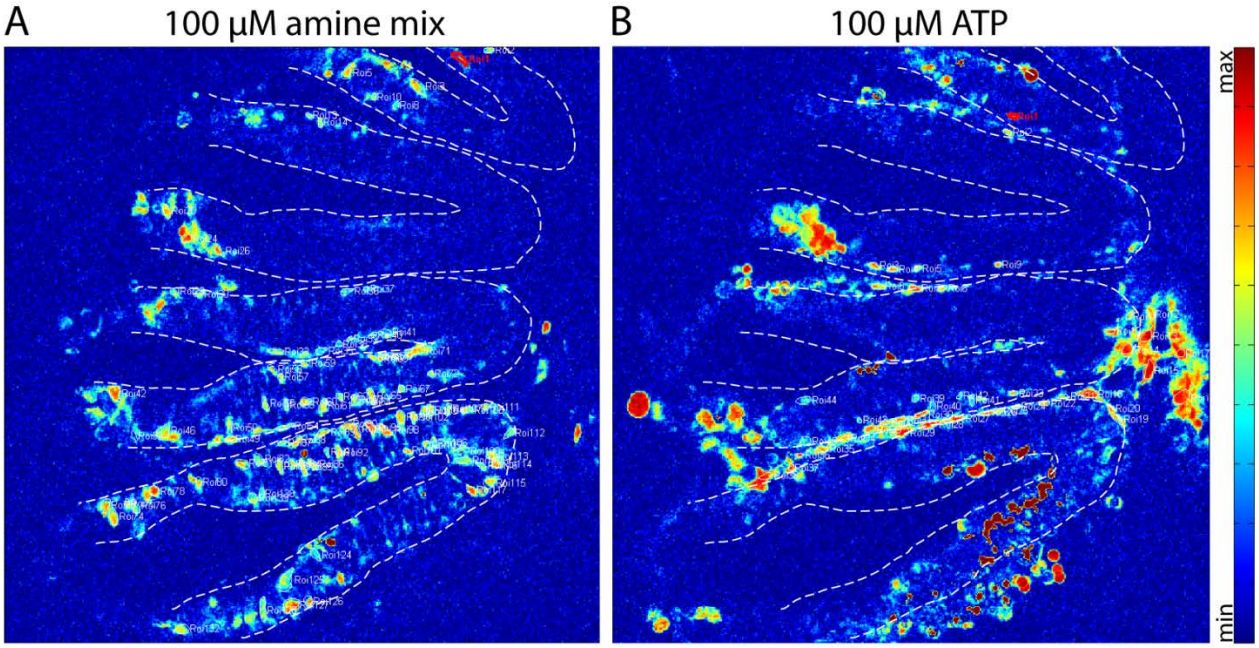

Figure 3.5: Pixel correlation map of odor-induced activity in the olfactory epithelium Blue pixels correspond to no change in fluorescence over time. Red pixels correspond to high change in fluorescence over time (see scale bar). Dashed lines indicate borders of lamellae in this section. Pixel correlation maps after A) stimulation with 100 µM amine mixture and B) stimulation with 100 µM ATP. Amines and ATP activate different subsets of cells in the olfactory epithelium.

Spots of activity with cellular shapes and positioning were defined as regions of interest and subjected to a further analysis. The fluorescence signals from a given region of interest were averaged, baseline subtracted, and visualized as $\Delta F/F_0$ over time in different plots (Figure 3.6). Active spots that were too small to represent a cell were omitted from analysis as well as spots so densely packed with activity, that an unambiguous shape could not be identified.

Application of an amine mix mainly activates OSN-shaped regions in the OE. The calculated changes in fluorescence compared to the baseline of a ROI for a particular time point ($\Delta F/F_0$) are depicted as heat map plots in Figure 3.6 (left column). Dark blue represents no or even negative $\Delta F/F_0$ for a given time point. Red represents a strong change in $\Delta F/F_0$. Color codes are shown in scale bars next to the respective heat map. The stimulus given and the time point of stimulation are indicated by a black bar above the heat map.

From a single measurement 62 ROIs in the sensory area of the epithelium showed a significant odorant dependent increase in calcium levels in response to stimulation with 100 µM amine mix (Figure 3.6 A). The average maximal response for amine mix in this measurement was 183.2 ± 64.7 % ΔF/F0. The onset of the response can be delayed. The delay varies from cell to cell and can amount to up to 10 seconds. It is unlikely that this delay represents a technical artefact, because it is absent in the ATP stimulated ROIs.

Upon stimulation with 10 µM ATP 88 ROIs, that displayed a significant change in fluorescence in the same sample preparation, were selected for analysis (Figure 3.6 B). Selection was done because there was an abundant number of responding ROIs. Most of these ROIs were located at the basal lamina from the sensory lamellae and seemed to be oriented in a horizontal line along the basal lamina. Few of the ROIs resembled OSNs according to their shape and position in the lamellae. The selected ROIs were randomly picked from lamellae in the imaged focal plane of the sensory area of the epithelium. There was also a densely packed area of activity in the middle raphe, where single cells could hardly be identified (compare Figure 3.5). Thus, this region was not included in the analysis. ATP evoked signals in this measurement had an average maximal response peak of 210.4 ± 64.4 % ΔF/F0. In the ATP responses no delay could be observed. After onset of the response, the peak intensity was also reached faster than in the responses to amines (compare chapter XX). In general the ATP responses were very reliable, robust and strong. While it was sometimes difficult to get the neurons respond to amines a second or third time, ATP responses were always reproducible. This may be due to the fact that ATP seemed to be mostly activating a population of basal cells rather than OSNs, which may use a faster signal transduction mechanism for ATP.

ACSF was added to the flow as a negative control stimulus. It did not evoke any changes in fluorescence in ROIs that were previously shown to respond to amines or ATP (Figure 3.6 C).

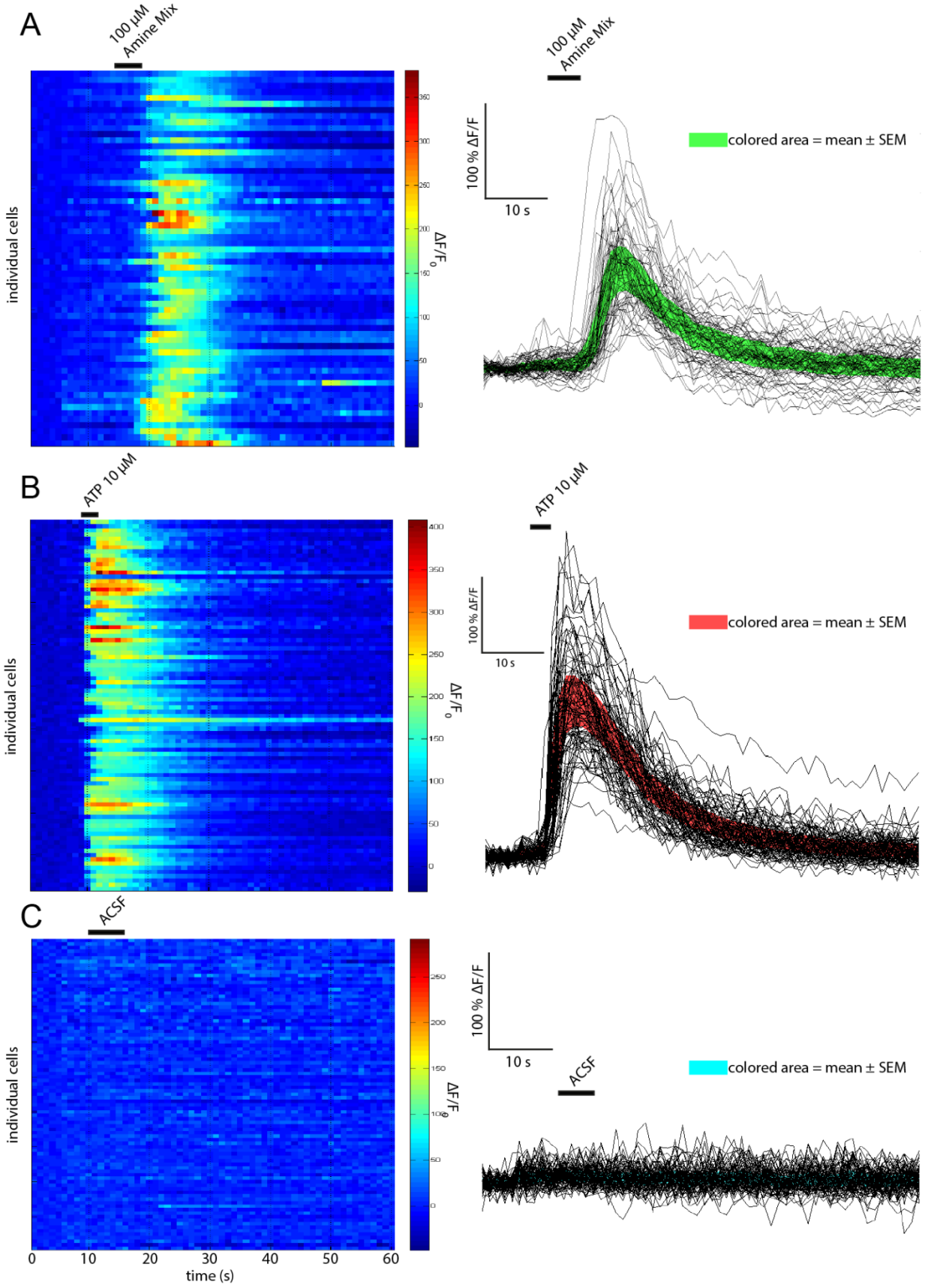

Figure 3.6: Calcium dynamics in amine and ATP sensitive cells of the olfactory epithelium (legend on next page).

Figure 4.6: Calcium dynamics in amine and ATP sensitive cells of the olfactory epithelium. Heat maps show a color-coded representation of the changes in fluorescence over time in response to an odor (left column). Single cell (black curves) and averaged (colored area) calcium response profiles (right column). A) Amine-responsive ROIs; B) ATP-responsive ROIs; C) ACSF (negative control); Number of ROIs analyzed in that measurement: Amine mix n = 62, ATP n = 88, ACSF n = 89.

3.1.5 Horizontal basal cells are labelled by proliferating cell nuclear antigen (PCNA) antibody

The olfactory epithelium has an enormous regenerative potential. OSNs are regenerated continuously throughout lifetime and olfactory function can be restored within weeks after chemical or mechanical ablation of the sensory epithelium. The OE comprises at least two different types of basal stem cells, globose basal cells and horizontal basal cells. Globose basal cells continuously renew OSNs in the OE, while horizontal basal cells are only activated to multipotency and proliferation when the OE is injured (for review see (Schwob et al., 2017)). An ablation of horizontal basal cell function impedes regeneration of the OE following injury (Suzuki et al., 2015).

In the calcium imaging experiments mostly horizontally arranged cells at the basal lamina were shown to respond to ATP. Only some of the ATP-responsive cells resembled OSNs in terms of shape and position in the lamellae. Immunohistochemical stainings was performed to clarify, if the ATP-responsive horizontal ROIs in deed correspond to the horizontal basal cells.

An antibody against proliferating cell nuclear antigen (α-PCNA) labels proliferative cells and, as shown in Figure 3.7, can be used as a marker for horizontal basal cells. In addition it labels a very sparse population of OSN-like cells that have a long apical dendrite, but appear to be OMP-negative. Therefore they do not belong to the ciliated OSNs. These cells may either belong to another OSN-type or represent immature ciliated cells that do not express OMP yet. However, the cells labelled by the antibody overall seem to resemble the population activated by ATP. Therefore, the distributions of the laminar height position of cells labelled with both approaches were compared.

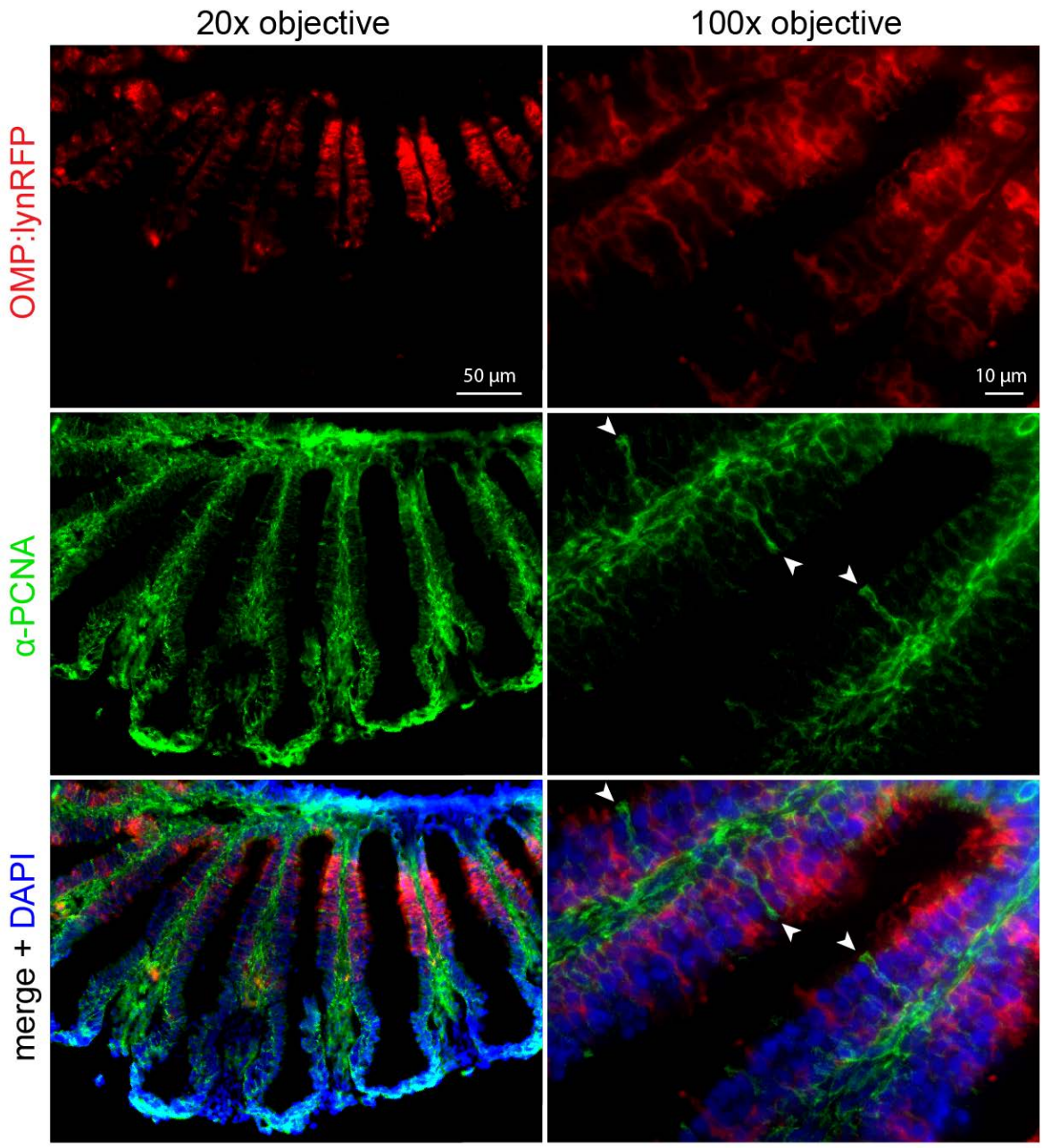

Figure 3.7: α-PCNA labels horizontal basal cells in the OE and a small population of OSN-like cells. Low (left column) and high (right column) magnification images of olfactory lamellae showing genetically RFP-labelled ciliated neurons (red), cells labelled by PCNA antibody (green) and a merge image showing both markers together with DAPI as nuclear counterstain (blue). PCNA labels horizontal basal cells at the base of each lamella and a very sparse population of OMP-negative, OSN-like cells (white arrowheads).

3.1.6 Laminar height properties of amine vs. ATP sensitive cells in comparison to other cell type markers

The known types of olfactory sensory neurons not only differ in their receptor repertoire, they also exhibit different morphological characteristics. The average height position in the olfactory lamella and the cumulative distribution for instance is different for ciliated (basal), microvillous (rather medial), and crypt neurons (apical). The laminar height distribution of OSN populations in the OE can be a reproducible parameter to differentiate between populations (Ahuja et al., 2014). We figured that horizontal basal cells can be included into this paradigm, as they also display a unique laminar height position (even more basal than ciliated neurons) and morphology (horizontally stretched).

Average laminar height and the laminar height cumulative distribution were determined for ciliated as well as microvillous OSNs. The OMP:lynRFP line expresses RFP in ciliated OSNs (Figure 3.8.A left). The TRPC2:gapVenus line expresses the green fluorescent protein Venus in microvillous neurons (Figure 3.8.A right). Laminar height of these two reference populations were compared to the laminar height of ROIs responding to amine mix and ATP obtained in calcium imaging experiments and to the laminar height of α-PCNA labelled cells (Figure 3.8.C + D).

To determine the laminar height the position of single cell body centers was measured from the basal lamina (h_i) and set in relation to the total height of the lamella at the same position (h_0), which is schematically depicted in Figure 3.8.B. This results in a value between 0, corresponding to a basal position, and 1, corresponding to an apical position.

Laminar height was determined for ciliated (OMP), microvillous (TRPC2), amine sensitive, ATP sensitive and α-PCNA labelled cells. As expected, microvillous OSNs, which are labelled by TRPC2, exhibited the most apical position from all cell populations analyzed in the olfactory lamellae. Their average laminar height amounts to $h_i/h_0 = 0.53 \pm 0.01$ (mean ± SEM of n = 292 cells; compare Figure 3.8.C) and is significantly different from all other populations ($p < 0.0001$; Mann-Whitney-U test for unpaired datasets).

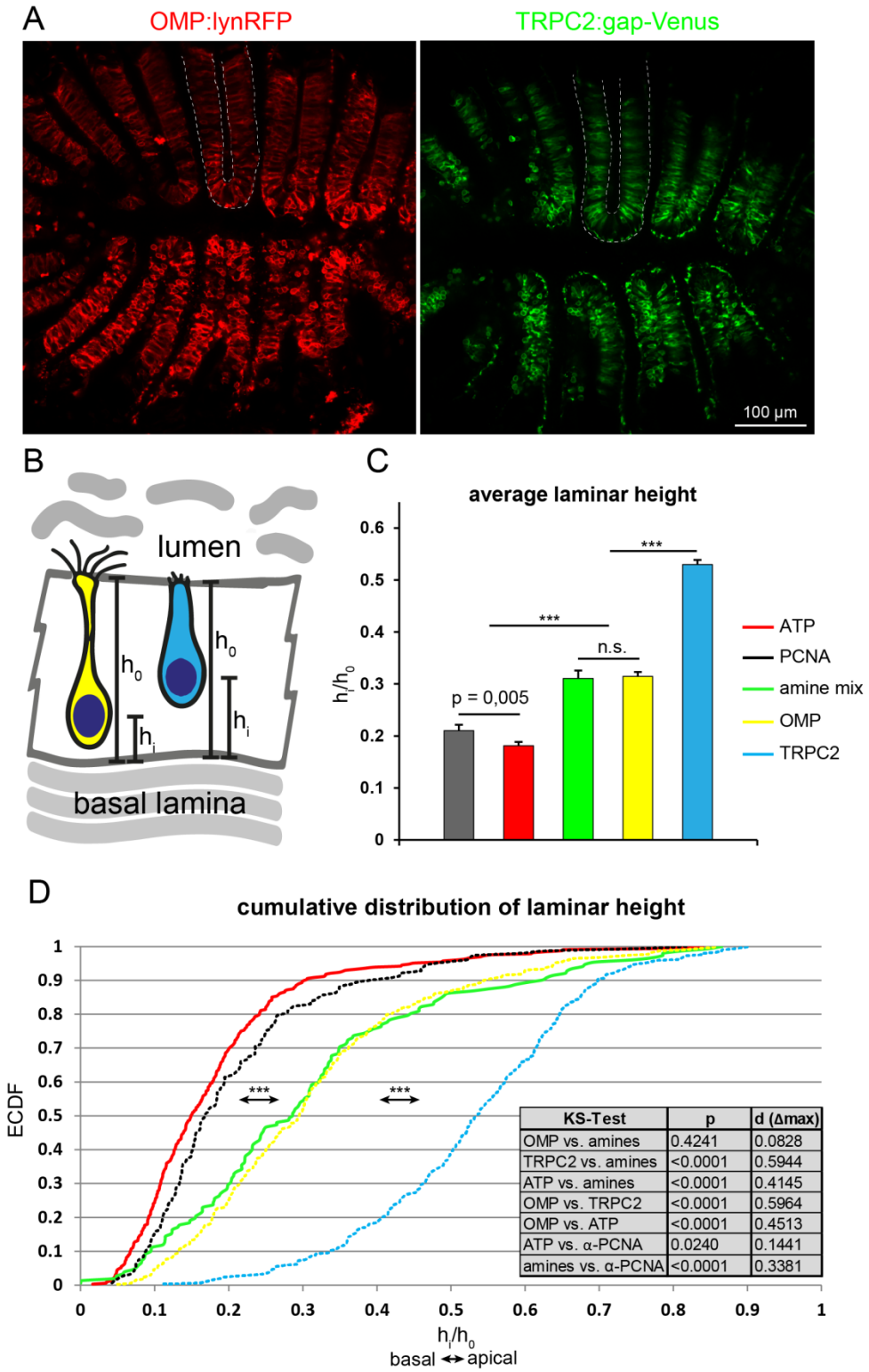

Figure 3.8: average laminar height and cumulative distribution of laminar height for different olfactory epithelial cell populations. A) Exemplary image of OE sections with ciliated (left) and microvillous (right) OSN transgenic reporter lines. B) Schematic laminar height measurement of cells in olfactory lamellae. C) Average laminar height of five different cell populations analyzed. D) Cumulative distribution plots of the same five populations as in C). Error bars represent SEM.

The laminar height characteristics of microvillous cells are also represented in the cumulative distribution plot, which shows a majority of the microvillous cells having a laminar height hi/h0 between 0.4 and 0.8 (blue dotted line, Figure 3.8.D). None of the cell populations activated by amines or ATP in calcium imaging experiments had a similar laminar height, neither on average, nor in the cumulative distribution plot.

OMP-labelled, ciliated OSNs are generally located more towards the basis of the lamella, with an average laminar height of hi/h0 = 0.315 ± 0.01 (mean ± SEM of n = 392 cells; compare Figure 3.8.C). Strikingly, this is almost exactly the same average laminar height as the one obtained from amine sensitive ROIs from calcium imaging experiments, which was 0.31 ± 0.02 (mean ± SEM of n = 152 cells). Accordingly there was no significant difference between OMP-positive and amine sensitive cells, neither on average, nor in the cumulative distribution plot. This leads to the conclusion that amine responses in the OE might be mediated by ciliated OSNs.

ATP sensitive ROIs exhibit a laminar height distribution, which does not comply with any of the known OSN-types. The average laminar height is 0.18 ± 0.01 (mean ± SEM), which is very basal. The average height as well as the cumulative distribution are significantly different from those of amine sensitive ROIs, ciliated neurons and microvillous neurons. In fact, 90 % of the ATP sensitive cell body centers are located in the lower third of the lamella, reflecting the observations made in the pixel correlation maps for ATP (Figure 3.5.B) and supporting the hypothesis that the ATP sensitive ROIs correspond to horizontal basal cells. To further validate this hypothesis the average laminar height and cumulative laminar height distribution of α-PCNA labelled horizontal basal cells was analyzed. The calculated average laminar height of α-PCNA labelled cells is 0.21 ± 0.01 similar (mean ± SEM), which is similar but still different from the ATP-sensitive cells ($p = 0.005$; Mann-Whitney-U test for unpaired datasets). However, when the cumulative distribution is considered, laminar heights of α-PCNA and ATP-sensitive cells display a very similar distribution and are not significantly different ($p = 0.024$; Kolmogorov-Smirnoff Test with significance level 0,01 as published before (Ahuja et al., 2014)). The cumulative distribution of laminar height of α-PCNA labelled cells is significantly different from amine sensitive, ciliated and microvillous populations.

3.2 Amine and diamine odor processing in the olfactory bulb

Phosphorylation of the extracellular signal-regulated kinase (ERK) has been established as a robust marker for neuronal activity both in the olfactory epithelium and in the olfactory bulb (Hussain et al., 2013, Miwa and Storm, 2005, Wakisaka et al., 2017). All OSNs expressing the same receptor project to distinct glomeruli in the OB. The glomeruli form an odor map with distinct, but fixed activation patterns created by stimulation with different odors or odor mixes. Here, an antibody against phosphorylated ERK (α-pERK) was used to decipher the glomerular activation patterns in response to the death-associated odor cadaverine and amines in general providing insights about the next step in the neuronal circuit processing amine and diamine stimuli.

3.2.1 Cadaverine dose dependently activates dorso-lateral glomeruli in the olfactory bulb

Before odor stimulation animals were acclimatized to the stimulation tank for 45 min. Odors were given though a tube to a final concentration of between 3 µM and 100 µM and stimulation was done for 3 minutes, before the animals were swiftly killed on ice and dissected (Figure 3.9.A). The stimulation in a static tank was chosen over a flow tank because we observed highly increased background pERK levels in flow stimulated animals (data not shown). Tissues were subjected to immunostaining with α-pERK and imaged with either a fluorescence microscope (OE sections) or a confocal microscope (whole mount olfactory bulbs)

To make sure our assay works we reproduced the activation of TAAR13c-expressing OSNs by low concentrations of cadaverine shown in an earlier publication (Hussain et al., 2013). The authors observed a specific activation of TAAR13c-expressing ONSs by 10 µM cadaverine. We could reproduce this data as could be shown by co-labelling OSNs with α-TAAR13c and α-pERK on sections of the olfactory epithelium (Figure 3.9.B), although the labelling was less specific than published before. We supposed that even lower concentrations are sufficient to specifically activate TAAR13c.

This was confirmed when we looked at the activity patterns in response to cadaverine in the olfactory bulb.

In some cases, when stimulated with low cadaverine concentrations of 10 µM or lower, a single glomerulus in the dorso-lateral cluster (dlG) was shown to be activated in the OB (Figure 3.9.D;

10 µM cadaverine). When using higher concentrations >10 µM to up to 100 µM we saw activation of many more glomeruli in the same cluster.

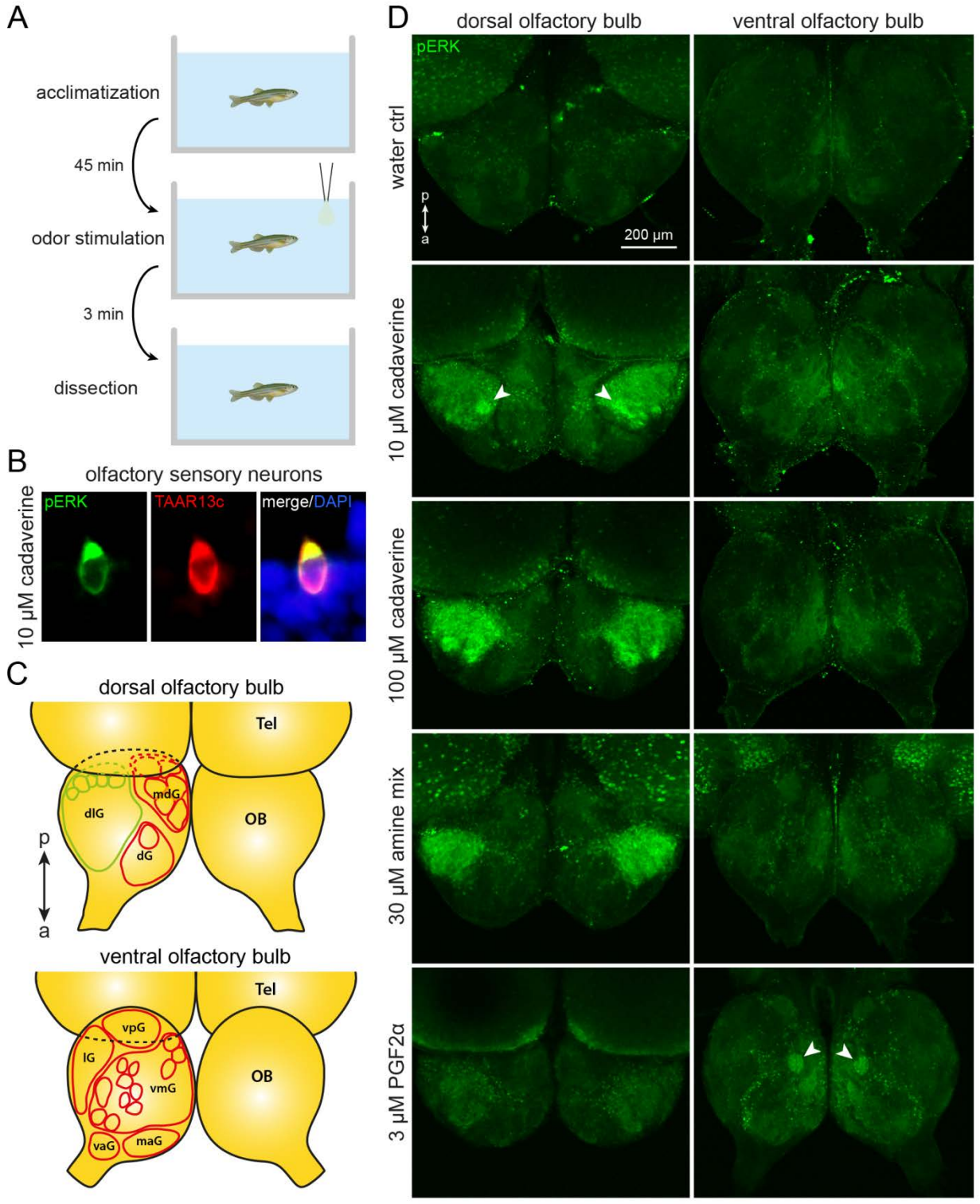

Figure 3.9: Odor-induced neuronal activation shown by pERK labelling in the zebrafish olfactory bulb. A) Schematic of the time course of the experiments. B) Exposure to 10 µM cadaverine elicits

specific pERK labelling of TAAR13c-expressing OSNs consistent with previous observations (Hussain et al., 2013). C) Schematic of glomerular clusters in the dorsal and ventral olfactory bulb (dlG, dorso-lateral cluster; dG, dorsal cluster; mdG, medio-dorsal cluster; lG, lateral chain; vpG, ventro-posterior glomerulus; vmG, ventro-medial glomeruli; vaG, ventro-anterior glomerulus; maG, medio-anterior cluster). D) Maximum projections from confocal z-stacks of pERK-labelled olfactory bulbs stimulated with different odors. Top row, no activated glomeruli were seen in the negative control (water as stimulus). Second row, 10 µM cadaverine activates few glomeruli, one of them strongly (arrowhead). Third row, 100 µM cadaverine activates many glomeruli within the dorso-lateral cluster. Fourth row, a mix of amines results in a strong activation restricted to the dorso-lateral cluster. Bottom row, 3 µ M PGF2α activates a single glomerulus (arrowhead) in the ventral olfactory bulb.

In fact, almost the whole cluster seemed to be activated at 100 µM cadaverine concentration (Figure 3.9.D; 100 µM cadaverine). A detailed schematic map of the zebrafish olfactory bulb with all glomerular clusters is provided in Figure 3.9.C.

These findings could also be reproduced in sections of the olfactory bulb (compare Figure 3.10).

3.2.2 The dorso-lateral cluster is dedicated to processing of amine odors in general

When using a mix of 13 different amines at intermediate concentrations (30 µM) the same cluster of glomeruli was activated as when using 100 µM of cadaverine (Figure 3.9.D), indicating that this cluster is likely responsible for the processing of amine stimuli. At high cadaverine concentrations additional glomeruli might be activated through unspecific binding of cadaverine to similar receptors, supposedly other diamine or amine receptors from the TAAR family, that project to the same cluster.

Neither with amines, nor with cadaverine, we observed an activation of ventral glomeruli. There was usually some weak background activity, but no specific labelling of bilateral pairs of glomeruli (Figure 3.9.D; right column).

As a positive control odor the fish were stimulated with the reproductive pheromone prostaglandin F2α (PGF2α) at 3 µM concentration. In our experiments this odor reliably activates a large ventromedial glomerulus on both left and right olfactory bulb (Figure 3.9.D; bottom row), which was already known from previous observations (Friedrich and Korsching, 1998).

These findings could also be reproduced in sections of the olfactory bulb (compare Figure 3.10).

3.2.3 Low concentrations of cadaverine activate a single, OMP-positive glomerulus

Knowing that cadaverine activates one or few glomeruli in the dorso-lateral cluster, we next wanted to further specify these results with respect to the location of the glomerular pERK signals in the OB.

Therefore, OBs from stimulated animals were obtained in the same way as explained in Figure 3.9.A, embedded into cryo-medium and afterwards cut into sections of 17-20 µm thickness. Serial sections from wildtype animals as well as transgenic reporter lines for ciliated (OMP:lynRFP) and microvillous (TRPC2:gap-Venus) OSNs were subjected to immunostaining with α-pERK and imaged with a fluorescence microscope. The sections with the maximal pERK signal for the respective odor are shown and compared to the same OB region sections from negative control stimulated animals (Figure 3.10).

When stimulated with a high cadaverine concentration (100 µM) a strong pERK signal was observed in the dorso-lateral and dorsal region of the olfactory bulb sections (Figure 3.10.A; first row), as was shown before in the whole mount OB. These glomeruli did not co-localize with glomeruli form microvillous neurons, that were labelled by the TRPC2:gap-Venus transgene and must therefore belong to another OSN type. We observed an increase in the number of pERK labelled cells, which presumably are mostly mitral cells, in the OB (arrows in Figure 3.10.A) and moderately elevated pERK levels in the neuropil adjacent to active glomerular clusters (row of triangles in Figure 3.10.A) when compared to the negative control OBs.

Stimulation with a low concentration of cadaverine, here 3 µM, often resulted in the pERK labelling of a single glomerulus in the dorso-lateral region of the OB (Figure 3.10.A; second row). This glomerulus was formed by axons of ciliated neurons that were visualized by the OMP:lynRFP transgene. When using water as a negative control stimulus neither the single dorso-lateral glomerulus nor the dorso-lateral region as a whole showed any glomerular pERK signal (Figure 3.10.B). Stimulation with PGF2α, which was again used as a positive control odor, induced a pERK signal in a large elongated ventral glomerulus (dotted line in Figure 3.10.B).

Stimulation with amines was confirmed to elicit neuronal activity shown by α-pERK in glomeruli in the dorsal and dorso-lateral olfactory bulb. Co-labelling with glomeruli from ciliated neurons (OMP:lynRFP) showed, that this region is mostly innervated by axons from this OSN type. Note,

that there were also some OMP-negative glomeruli in the dorsal OB region that were activated by amine odors mix.

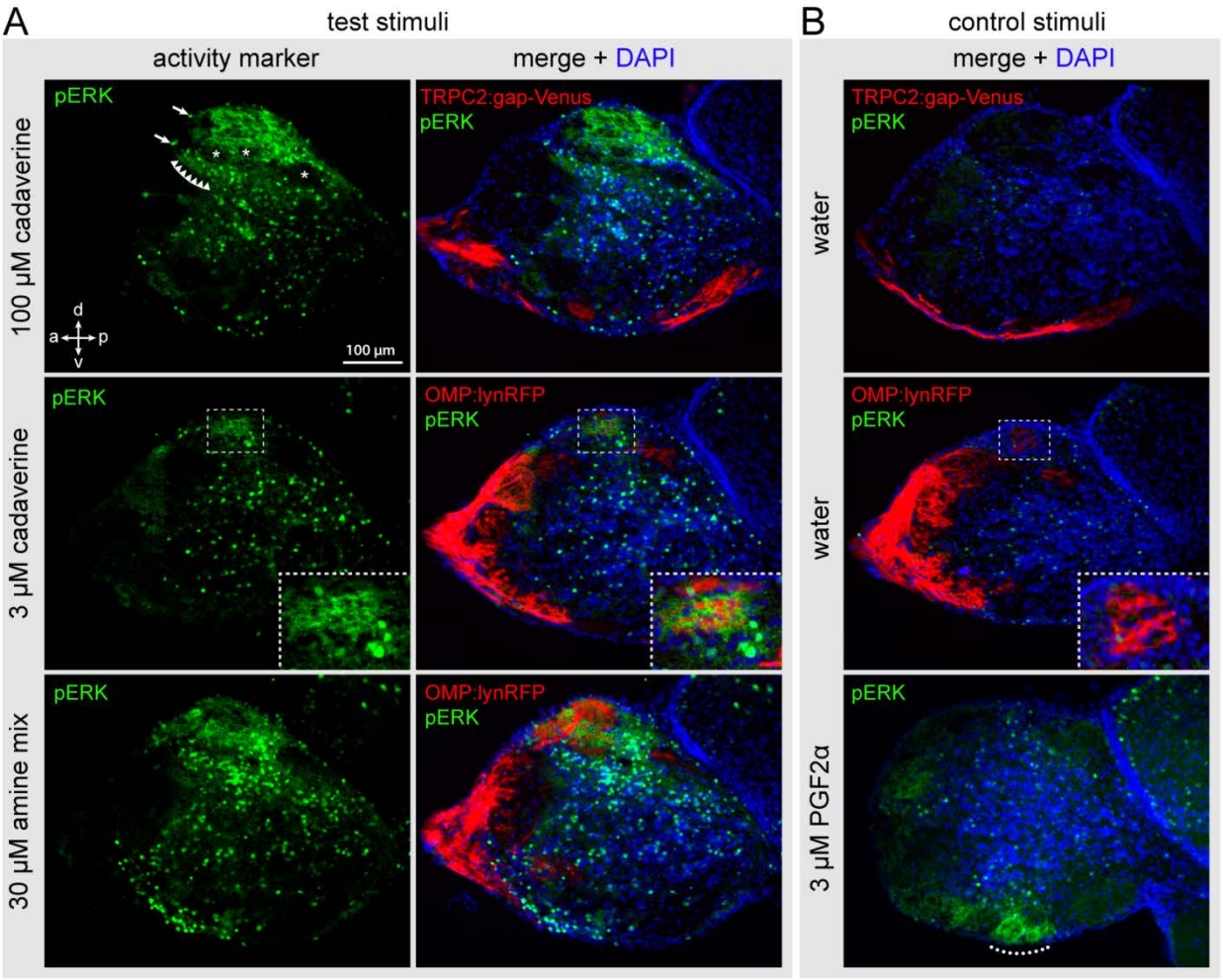

Figure 3.10: Odor-induced neuronal activation shown by pERK immunohistochemistry on sections of zebrafish olfactory bulb. Sections with maximal pERK signal for the respective odor are shown. A) Top row, exposure to high level of cadaverine (100 µ M); middle row, exposure to low level of cadaverine (3 µ M); bottom row, exposure to a mix of 13 different amines (30 µ M). Left column of panel A) shows the pERK signal, right column shows the pERK signal merged with DAPI and the cell type markers TRPC2 and OMP as indicated on the panels. High cadaverine and the amine mix evoked a strong signal in the dorsal glomeruli. Low cadaverine concentration evoked a much more restricted dorsal signal. B) Stimulation with water served as negative and with PGF2α as positive control. No pERK labelling is visible in the water control in both the TRPC2:gap-Venus and OMP:lynRFP transgenic lines. PGF2α activates a ventral glomerulus (dotted line). Arrows indicate exemplary pERK-labelled cell bodies in the OB. The row of triangles shows a weak labelling of the neuropil in the vicinity of the dlG. Asterisks point out pERK-negative glomeruli interspersed with the active glomeruli in the dlG. Dashed boxes in the middle row show enlarged views of the single-cadaverine-responsive glomerulus, which is pERK-positive after stimulation with 3 µ M cadaverine and pERK-negative in the negative control.

Our next objective was to quantify the number of active glomeruli in response to different cadaverine concentrations. Glomeruli do not contain any cell bodies as they are exclusively formed by the descending axon terminals from OSNs and by dendrites from innercating mitral cells. Thus, they do not harbor any nuclei, which makes them easy to identify in sections by absence of the nuclear counterstain DAPI (see for example Figure 3.10.B; absence of nuclei in areas of the dorsal OB). In addition, glomeruli were identified by either the characteristic glomerular shape of pERK-labelled spots and/or by co-labelling of a glomerular shaped area by a fluorescent reporter protein (RFP for ciliated neurons and Venus for microvillous neurons). Using these parameters glomeruli could be unambiguously identified and counted from serial sections of one olfactory bulb at a time (see Figure 3.11.A).

The number of glomeruli activated upon stimulation with a certain cadaverine concentration varied between experiments. Stimulation with 100 µM cadaverine lead to strong pERK labelling in 10.3 ± 0.7 dorso-lateral glomeruli (mean ± SEM; n = 6) on average.

Upon stimulation with 10 µM cadaverine this number was decreased to an average of 3.7 ± 0.7 pERK-labelled glomeruli (mean ± SEM; n = 6), indicating a much more specific activation of a smaller number of olfactory receptors. This is consistent with the higher pERK-labelling specificity in low cadaverine stimulated OSNs reported earlier (Hussain et al., 2013).

When using 3 µM cadaverine as a stimulus we observed pERK labelling of a single glomerulus in the dorso-lateral cluster in 3 out of 6 specimens. The average number of glomeruli labelled in response this low cadaverine concentration was 1.8 ± 0.4 (mean ± SEM; n = 6). The activity dependent labelling of a single glomerulus would correspond to activation of a single olfactory receptor in the nose. This cadaverine-responsive glomerulus always seemed to appear in the same position within the olfactory bulb and we therefore termed it dlG_{cad}.

In the negative control animals, which were stimulated with water, no pERK labelled glomeruli were observed in all but one cases (11/12 OBs). The average number of active glomeruli in response to mock-stimulation with water was 0.1 ± 0.1 (mean ± SEM; n = 12).

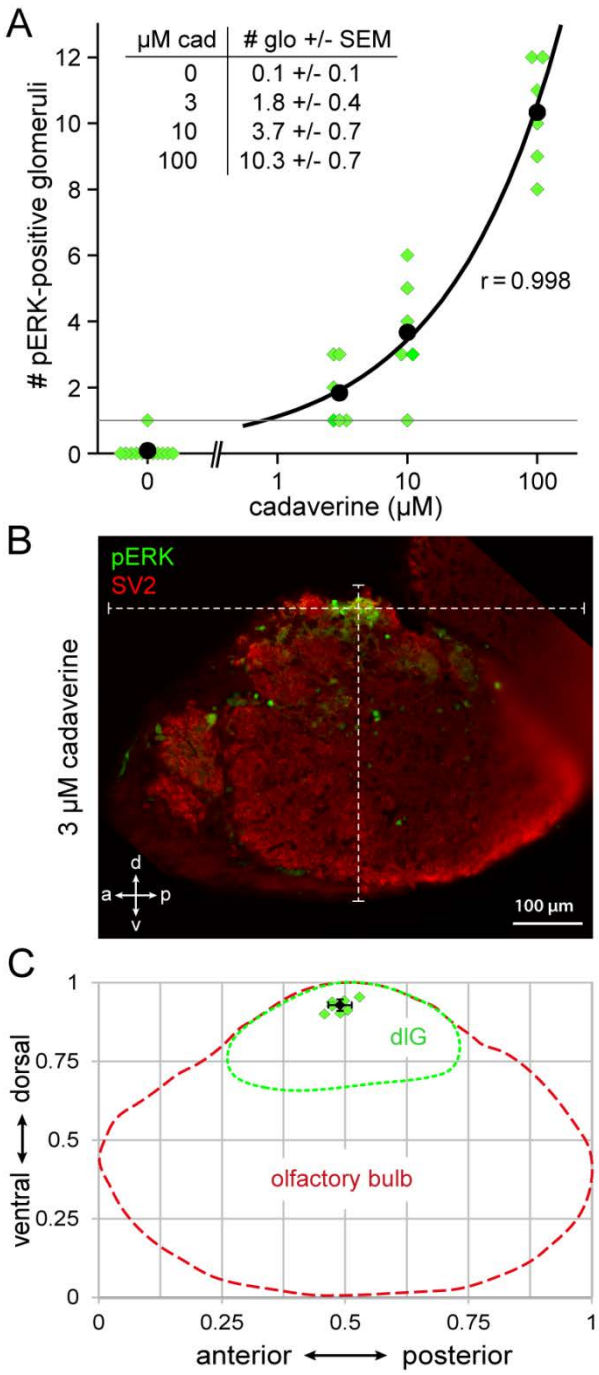

Figure 3.11: A single invariant glomerulus is activated by exposure to low concentrations of cadaverine. A) Number of glomeruli activated in response to different doses of cadaverine was counted from sections. Water did not evoke any pERK signal in the dorso-lateral cluster in all but one cases (n = 12). At 3 and 10 µM cadaverine one to few glomeruli were labelled (see table inset). At 100 µM cadaverine about 10 glomeruli were labelled (n = 6 for each cadaverine concentration used). (b) Exemplary image of a single glomerulus labelled by pERK, double labeling with SV2 to visualize all glomeruli in this section. White dashed lines intersect in the glomerulus center and show overall a↔p and v↔d length of the olfactory bulb section used for calculating the normalized glomerulus position. (c) Schematic representation of the dlG_{cad} coordinates measured in the olfactory bulb. Red and green dashed lines represent olfactory bulb and dorso-lateral cluster contours, respectively. Green squares represent single measurements from 7 different bulbi. Black square and error bars represent mean value ± SD.

3.2.4 The single cadaverine-responsive glomerulus has a stereotyped position

The glomerular map in the zebrafish bulb is not flexible but is formed by consistent glomerular clusters and with a number of large glomeruli with characteristic positions, which are identifiable across animals (Braubach et al., 2012). The remaining, mostly smaller glomeruli are often densely packed in their respective clusters and are not easily identifiable across animals by morphological parameters. As another way of confirming the invariance and consistency of the glomerular map we determined the position of the cadaverine-responsive glomerulus dlG_{cad} in relation to the in 8 different olfactory bulbs of fish that were stimulated with low cadaverine concentrations. Therefore it´s position relative to the total size of the OB was measured in different dimensions (a↔p = anterior to posterior; v↔d = ventral to dorsal; see Figure 3.11.B). The position was strikingly invariant in 8 samples (Figure 3.11.C), with average coordinates a↔p = 0.49 ± 0.02 and v↔d = 0.93 ± 0.02 (mean ± SD; n = 7). In the third dimension, medial to lateral (m↔l), we determined the glomerulus position from whole mount samples treated with low cadaverine concentrations (for example see Figure 3.9.D second row) and found it to be located at m↔l coordinate 0,57 ± 0,03 (mean ± SD; n = 5).

We conclude that the sensitive, cadaverine-responsive glomerulus dlG_{cad} has a fixed and stereotyped position in the dorso-lateral cluster of glomeruli.

3.2.5 Processing of amine and diamine odors in the olfactory bulb of a neoteleost fish, the three-spined stickleback

The lineages of the “old” teleost zebrafish, *Danio rerio*, and the neoteleost three-spined stickleback, *Gasterosteus aculeatus*, are separated by around 250 million years of evolution (Betancur et al., 2013). Evolutionary studies on TAAR family of olfactory receptors demonstrated dramatic changes in the TAAR repertoire (Hussain et al., 2009), which could very well also have occurred in other receptor families. Here, we were interested to see how the general glomerular architecture of the glomerular clusters in the OB changed and if odor representations in the olfactory bulb are still organized in a similar pattern. Because we already have a good knowledge about the odor representations of amines and diamines (this study, chapter 3.2) and also amino acids, i.e. food odor ((Friedrich and Korsching, 1997) we chose these odors to serve as references in the stickleback olfactory bulb.

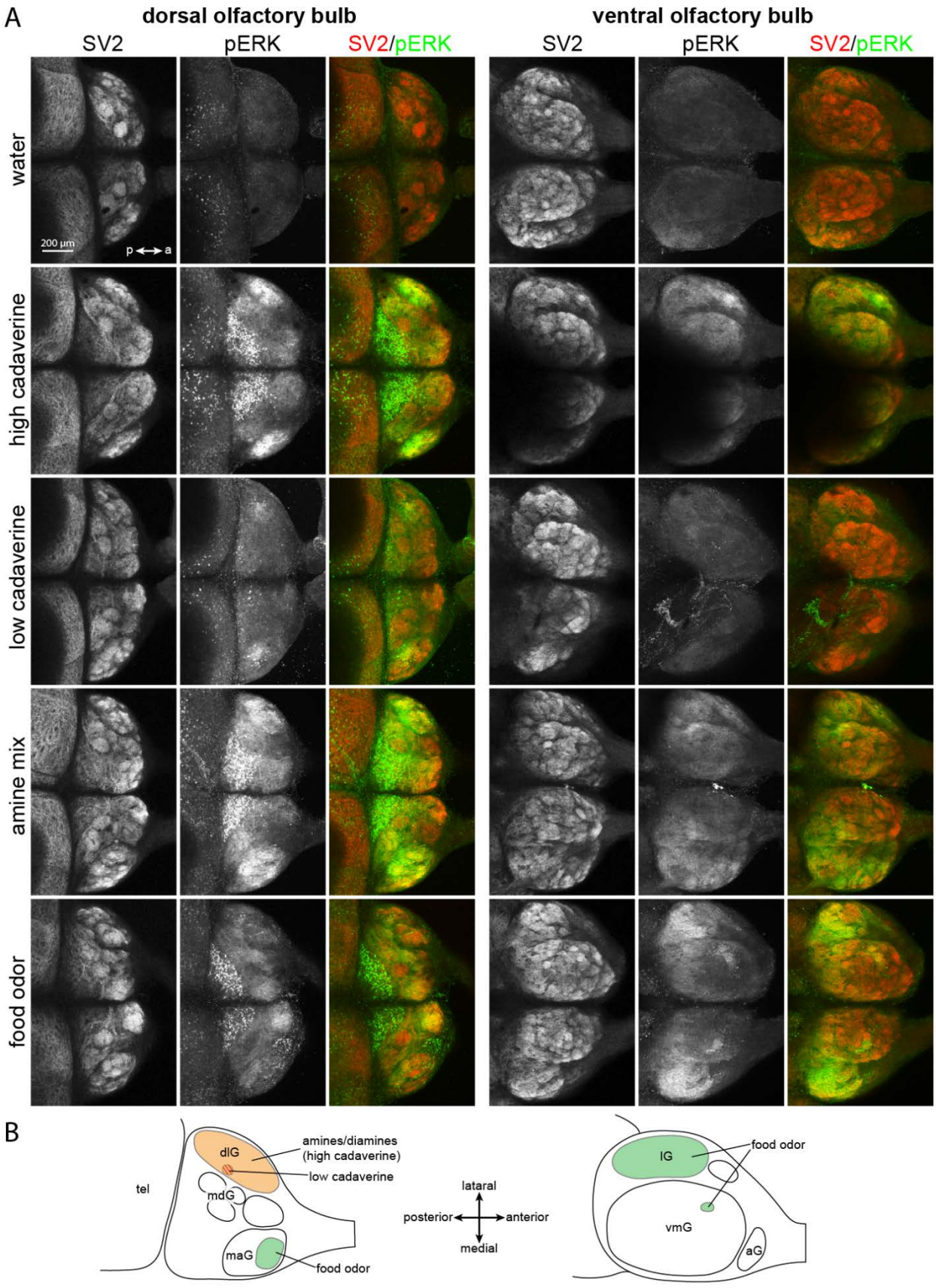

Figure 3.12: Glomerular activity patterns in response to different odors in the OB of the three-spined stickleback (legend on next page).

Figure 3.12: Glomerular activity patterns in response to different odors in the OB of the three-spined stickleback Fish were stimulated with the respective odor for 3 minutes, dissected and subjected to immunohistochemical staining with α-pERK and α-SV2 as described earlier for zebrafish. A) α-SV2 served as a glomerular marker (left column of dorsal and ventral OB panels, respectively), α-pERK served as neuronal activity marker (middle column). The merge picture (right column) allows identification of activated glomerular clusters or single glomeruli. B) Schematic drawing of the glomerular architecture in the dorsal (left) and ventral (right) olfactory bulb with indications for regions activated by specific odors. A) + B) High cadaverine and amines activate a dorso-lateral cluster (dlG) of glomeruli. Low cadaverine concentrations activate presumably only a single glomerulus in the dlG. Food odor activates a large medio-anterior glomerulus in the dorsal OB as well as most of the lateral chain glomeruli (lG) and one or two small ventro-medial glomeruli (vmG) in the ventral OB. Tel = telencephalon, dlG = dorso-lateral glomeruli, mdG = medio-dorsal glomeruli, maG = medio-anterior glomeruli, lG = lateral glomeruli, vmG = ventro-medial glomeruli, aG = anterior glomeruli.

Sticklebacks were stimulated with high (100 µM) and low (3 µM) concentrations of cadaverine, intermediate amine mix concentrations (30 µM) and a 1% (w/v) preparation of food odor for three minutes, decapitated, dissected and fixed in 4% PFA, as has been described for zebrafish tissues earlier (see chapter 3.2.). Neuronal activity in the OB was visualized by immunohistochemistry with α-pERK. Glomeruli were stained with α-synaptic vesicle protein 2 (SV2).

The glomerular architecture of the stickleback OB is schematically pictured in Figure 3.12.B. SV2 immunoreactivity from 11 animals served as a template for the glomerular clusters depicted.

In general the stickleback OB glomerular architecture appeared to be similar to the zebrafish OB, but less complex. In the dorsal OB (Figure 3.12.B, left) a dorso-lateral cluster, hence termed dlG (in line with the zebrafish OB terminology from Braubach et al. 2012) can be identified unambiguously. There are several large glomeruli in the center of the dorsal OB, hence termed dG. At least two of them are identifiable across animals in our specimens. There is also a medio-anterior cluster harboring several glomeruli. Interestingly the medio-posterior portion of the OB, where in zebrafish the mdG cluster is located, appears to be completely void of glomeruli. Instead this part of the OB harbors neurons, which get strongly activated upon odor stimulation (see Figure 3.12.A, pERK signal in odor stimulated OBs)

When looking at the ventral side (Figure 3.12.B, right), there are essentially two large identifiable glomerular clusters, a lateral cluster (lG) and a ventro-medial cluster (vmG), which makes up the largest part of the ventral OB surface. Anterior to the vmG there is a small cluster of few glomeruli, hence termed anterior glomeruli (aG).

As in zebrafish, pERK seemed to be a reliable marker for neuronal activity in the OB of stickleback. When mock-stimulated with water no pERK signal was evident, neither in the dorsal nor in the ventral OB (Figure 3.12.A, 1st row). Glomeruli as well as OB neurons remained inactive.

Upon stimulation with a high concentration of cadaverine (100 µM) the dorso-lateral cluster of glomeruli was strongly activated. In addition a large number of neurons in the posterior medio-dorsal OB were activated (Figure 3.12.A, 2nd row). There could correspond to clustered mitral cells. When stimulating with a low concentration of cadaverine (3 µM) a single glomerular area in the dlG seemed to get activated in the stickleback OB (Figure 3.12.A, 3rd row). The two major ventral OB clusters were not activated by cadaverine stimuli. The active zone in the ventral view of the high cadaverine stimulated OB presumably corresponds to the dlG, as imaging was performed over a z-range of several 100 µm.

Stimulation with 30 µM amine mix evoked a strong pERK signal in the same region as high cadaverine concentrations, i.e. the dlG cluster. It also resulted in very strong activation of the same group of neurons in the posterior medio-dorsal OB (Figure 3.12.A, 4th row).

Finally, stimulation with food odor, thought to activate another population of OSNs than amines and diamines, indeed induced pERK labeling in the majority of the lateral chain glomeruli of the ventral OB (lG), one or two small glomeruli in the vmG, and a large glomerulus in the maG of the dorsal OB. This indicates that amines and food odor are processed by different OSN populations, similar to the situation in zebrafish.

3.3 Cadaverine processing in the larval brain and larval behavior

Processing of sensory stimuli in the animal brain is very complex. In order to simplify the analysis of neuronal networks involved in sensory processing it is useful to study larval zebrafish brains. The larval brain is much smaller and therefore more easily accessible with live-imaging techniques than the adult zebrafish brain. Neuronal circuits are compressed in a much smaller space, which simplifies analysis of axonal projection targets.

Zebrafish larvae already display behaviors mediated by chemosensation (Sumbre and Depolavieja, 2014). Projections of olfactory sensory neurons and secondary olfactory neurons have been analyzed in larval zebrafish (Sato et al., 2007, Miyasaka et al., 2014). The neuronal circuits mediating olfactory sensory processing might therefore already be established in the larvae, although the exact ontogenetic development has not been dissected yet.

Therefore, the zebrafish larva could serve as a suitable model to study olfactory behaviors and associated neuronal circuits and mechanisms. Here we use zebrafish larvae to study the processing of the death-associated odor cadaverine.

3.3.1 Onset of TAAR13c expression in the larval olfactory epithelium

To be able to investigate the neuronal mechanisms underlying olfactory processing and behaviors in response to cadaverine the onset of receptor expression in the OE has to be determined.

Therefore 1-7 dpf zebrafish larvae were collected every 24 h after fertilization, sectioned (Figure 3.13.A), and subjected to immunohistochemical staining with α-TAAR13c (example of labelled OSNs in Figure 3.13 B). TAAR13c expressing neurons generally had a typical OSN morphology with elongated shape and presence of an apical dendrite. As the OE does not exhibit the typical lamellar structure, a laminar height analysis is not applicable for the larval zebrafish nose.

The number of labelled OSNs was quantified from serial sections for each time point and plotted in Figure 3.13.C as mean ± SEM. No TAAR13c-expressing OSNs were labelled by the antibody 24 hours after fertilization (n = 7, not shown in graph). The earliest occurrence of a labelled neuron was 48 hours post fertilization, in 1/9 animals. Reliable expression was observed 72 hours post fertilization, in 9/10 animals with an average of 1.6 ± 0.43 (mean ± SEM) neurons per larvae. The average number of neurons expressing TAAR13c increases, possibly exponentially

with OE growth, over the next days until day seven with an average of 10.14 ± 0.96 neurons per larva.

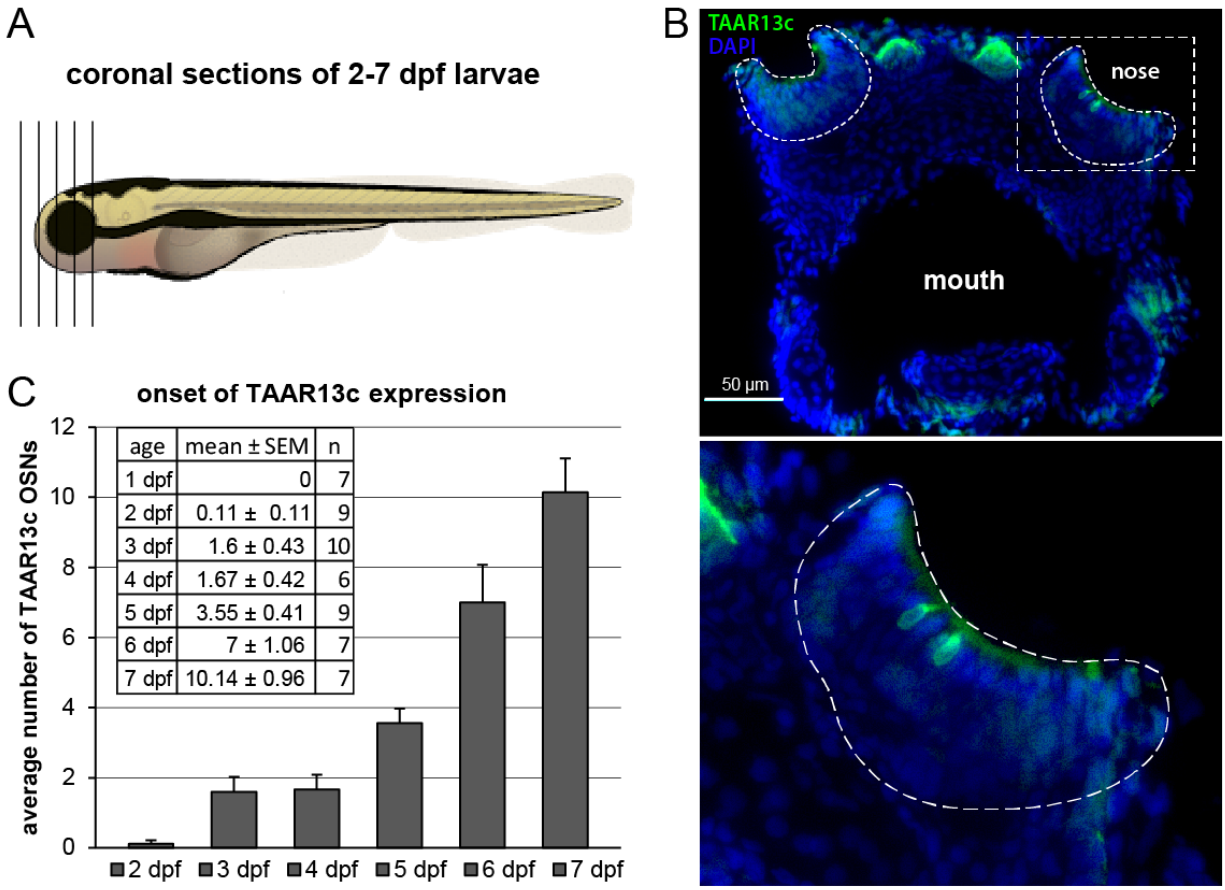

Figure 3.13: Onset of TAAR13c expression in zebrafish larvae 2-7 day old zebrafish larvae were subjected to cryostat sectioning and α-TAAR13c immunohistochemistry. A) Schematic of the zebrafish larvae and orientation for sectioning. B) A section of a 6 dpf zebrafish head including the nose, stained with α-TAAR13c (full view of the head and higher magnification of the nose). The antibody labels specific OSNs in the OE. C) Quantification of TAAR13c-expressing OSNs in 2-7 dpf larvae shown as mean ± SEM for each day. Onset of TAAR13c expression is between day 2 and 3 after fertilization and with a growing OE the number of TAAR13c OSNs increases. For each day cells from between 6 and 10 animals were counted.

3.3.2 Cadaverine-induced neuronal activity in the larval olfactory bulb and higher brain

Secondary olfactory circuits are already established in 7 dpf zebrafish larvae, as has been shown in studies of the projectome of olfactory bulb neurons (Miyasaka et al., 2009, Miyasaka et al., 2014). The neuronal identity of potential cadaverine-sensitive neurons is also already determined at these larval stages, as has been shown in the previous chapter. Thus, cadaverine could already represent a relevant olfactory stimulus to zebrafish at the larval stages.

To visualize neuronal activity in response to cadaverine (and control odors) fish were stimulated for 1 min, killed by immersion into ice cold water and fixed in 4% PFA. The larvae were then subjected to immunohistochemical staining with α-SV2 as glomerular and synaptic marker and α-pERK as a neuronal activity marker.

Figure 3.14.A shows a maximum projection of a confocal z-stack of a 7 dpf zebrafish larvae stained with α-pERK from the dorsal side. Landmark brain regions are encircled by dashed lines as indicated. The olfactory epithelia are easily identifiable between mouth and eye. With this confocal imaging approach the olfactory bulbs, telencephalon and habenula could also be portrayed as a whole, as they are located dorsally and are relatively small structures with less than 150 µm depth. Figure 3.13.B schematically shows the larval forebrain regions involved in olfactory processing. These regions were also subjected to a further analysis.

α-SV2 reliably labels glomeruli in the olfactory bulb of 7 dpf larvae. The glomerular staining is strong and individual “precursor” clusters or large glomeruli can be identified (compare Figure 3.14.C, left row). Although the OB glomeruli are not fully developed yet, the glomerular clusters, that are present in the zebrafish OB, can already be identified, as was shown in detail in another study (Miyasaka et al., 2014). We then wanted to test the suitability of pERK as a marker for neuronal activity in glomeruli as well as other components of the olfactory pathway in the larval forebrain, such as OE, OB, telencephalon, and habenula. α-pERK indeed labels glomeruli as well as neurons in these parts of the brain in response to odor stimulation (compare Figure 3.14.C, middle row and right row for co-labeling with glomeruli).

Changes in neuronal activity shown by pERK were analyzed and quantified in the OE, OB (glomeruli and neurons), telencephalon, and habenula as shown in Figure 3.15.

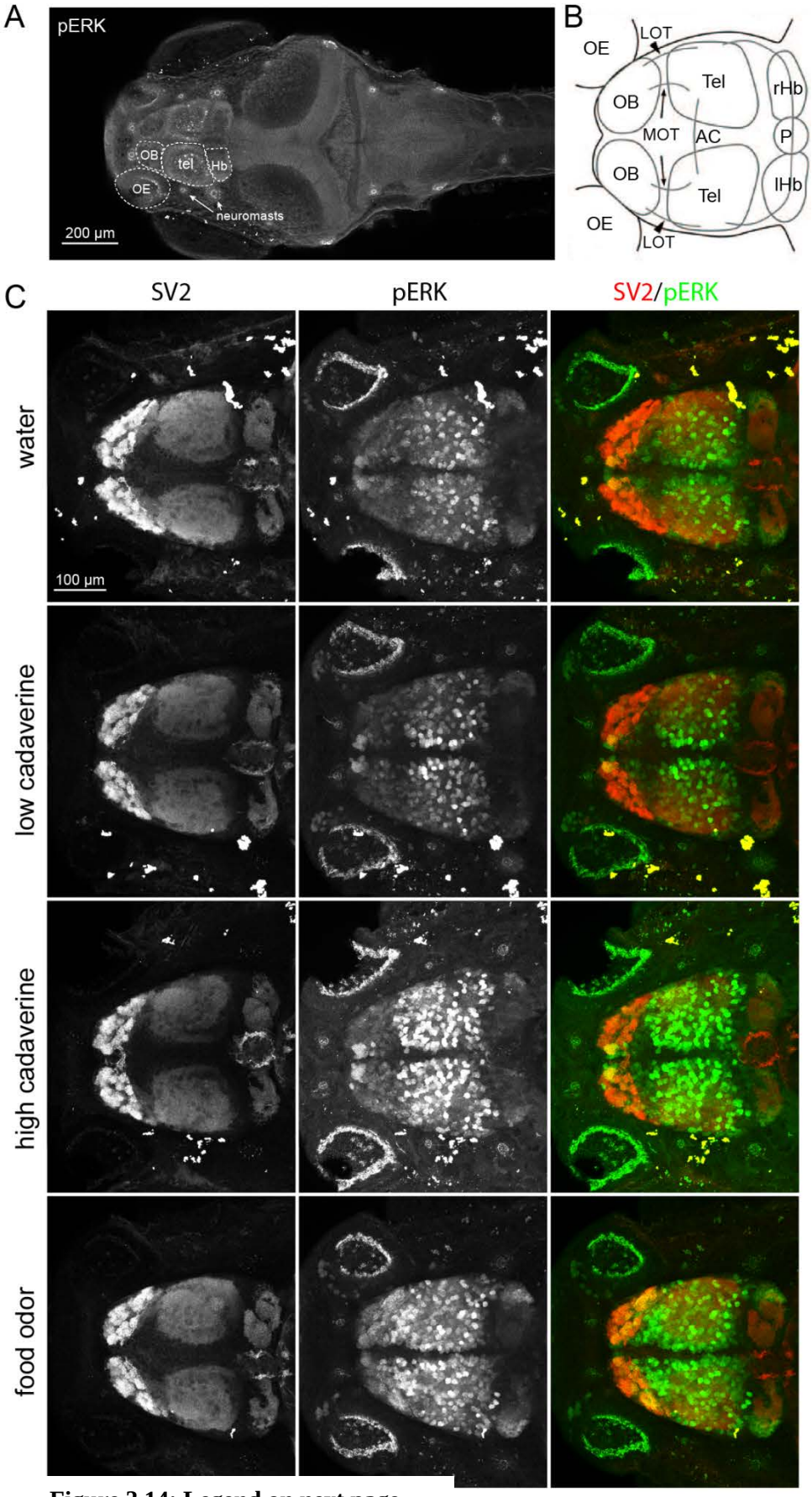

Figure 3.14: Legend on next page.

Figure 3.14: Neuronal activity in the larval zebrafish brain in response to cadaverine and food odor. Larvae were stimulated for 1 min, fixed, and subjected to immunohistochemistry. A) Maximum projection of a z-stack from a zebrafish brain stained with α-pERK, as a neuronal activity marker with relevant brain regions. B) Schematic of the larval zebrafish forebrain adapted from (Miyasaka et al., 2009). C) Higher magnification maximum projections of z-stacks from zebrafish forebrains stimulated with different odors and stained with α-SV2, as a synaptic marker densely labeling olfactory glomeruli, and α-pERK, as a neuronal activity marker. Colored image shows an overlay of both markers used.

The baseline activity of the brain can be determined by using water as a negative control stimulus. Activity that is observed under these conditions is not olfactory mediated and represents the default status of the larval brain activity under the given conditions (surroundings, lighting, salinity, etc.). Active cells in the indicated regions were counted with the ImageJ cell counting plugin. Only cells which exhibited fluorescence intensity values of at least double the surrounding background fluorescence were counted as active cells and plotted in Figure 3.15. Active glomeruli were identified by co-labeling with synaptic marker SV2. Cells and glomeruli were counted from 8 different hemispheres. Although asymmetry in the neuronal architecture has been described for several zebrafish brain areas, e.g. the habenula (Dreosti et al., 2014), no obvious differences in numbers of active cells or glomeruli could be observed between hemispheres of the same animal.

When compared to the water control the number of pERK-labelled cells in the OE and OB is significantly elevated upon stimulation with food odor as well as cadaverine. The stimulus-induced neuronal activity is particularly high for food odor, which results in the highest numbers of active cells in the OE and OB (compare Figure 3.15.A; highest significance in food odor responses in the OE and OB with $p < 0.01$ and $p < 0.001$, respectively). Same is true for the number of glomeruli activated by food odor, which is significantly elevated upon stimulation with that odor ($p < 0.001$), while cadaverine does not increase the number of active glomeruli in this experimental approach (compare Figure 3.15.B).

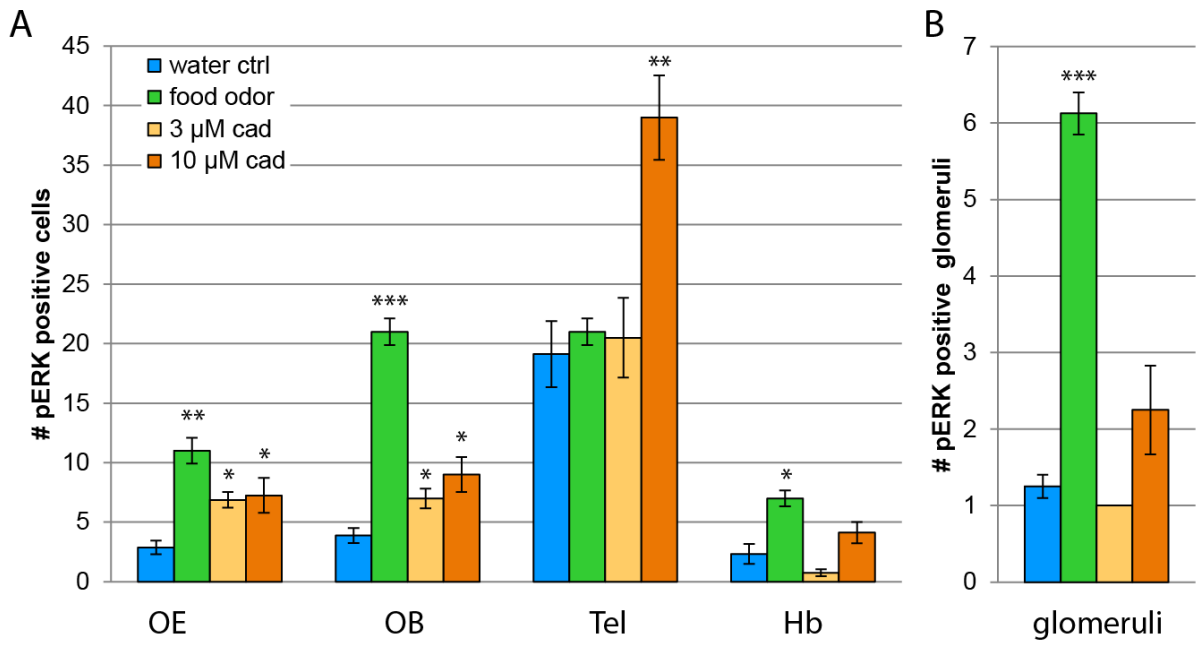

Figure 3.15: Quantification of olfaction mediated pERK signals in the larval forebrain Larvae were stimulated with an odor for one minute. pERK immunohistochemistry indicated active cells and glomeruli. Larvae were stimulated with water (blue), 3 µM (light orange) and 10 µM (dark orange) cadaverine and food odor (green). A) Quantification of pERK-positive cells in the OE, OB, telencephalon and habenula shown as bar graphs. Cells were counted positive if fluorescence signal intensity exceeded double the surrounding background fluorescence value. B) Quantification of pERK-positive glomeruli in the olfactory bulb shown as bar graphs. Significance was calculated with a studens t-test (*$p \leq 0.05$; **$p \leq 0.01$; ***$p \leq 0.001$).

The telencephalon is a major target of bulbar projections and thought to be highly involved in the processing of odor stimuli (Miyasaka et al., 2014). When stimulated with 10 µM cadaverine the number of pERK-labelled neurons in the telencephalon doubled. Interestingly this effect could not be observed upon stimulation with low cadaverine (3 µM) and food odor, although at least food odor was shown to have a high impact on the activity of OSNs, olfactory glomeruli and OB neurons (Figure 3.15).

The habenula is involved in the generation of behavioral responses to sensory stimuli (Dreosti et al., 2014). Here, the number of pERK-labelled cells in the lateral habenula was quantified in stimulated and mock-stimulated animals. In general the number of clearly pERK-positive cells was very low (max. 5 cells in the water control animals; mean ± SEM = 2.33 ± 0.84). The only significant increase in the number of pERK-labelled cells compared to the negative control was obtained with food odor (mean ± SEM = 5.5 ± 0.66; $p < 0.05$).

3.3.3 Suitability of the *elavl3*:GCaMP6 line to analyze odor-induced neuronal activity

Genetically encoded calcium indicators (GECIs) are widely used in biological research, because they allow the visualization of cellular activity as a calcium-dependent change in fluorescence *in vivo*. GCaMP is a GECI specifically designed for imaging of neuronal activity (Nakai et al., 2001). It consists of a circularly permuted green fluorescent protein (cpGFP) linked to the calcium binding protein calmodulin (CaM) by the CaM-interacting M13 peptide (Figure 3.16.A). The original GCaMP was subsequently engineered to obtain a higher calcium sensitivity and a better temporal resolution, ultimately resulting in the GCaMP6 proteins (Chen et al., 2013), which have been successfully and extensively used to study neuronal activity in various model organisms in the past years. One of the GCaMP6 versions, GCaMP6s, was used in this study.

Animals stably expressing GCaMP6s under the control of the *elavl3* promoter (formely called *HuC*) were obtained from the Janelia Farm Research Campus, Virginia, USA. The promoter drives expression in nearly all neurons as can be seen by fluorescence microscopy (Figure 3.16.B)

We wanted to find out, whether these animals are in general suitable to visualize neuronal activity in the larval brain with the Leica SP8 confocal microscope accessible imaging facility of the Biocenter Cologne. In an initial set of experiments the experimental setup was established and optimized. 6-7 dpf larvae were anesthetized, embedded in agarose and placed under the confocal microscope. The agarose embedding prevents the larvae from moving, thereby ensuring that the focal plane does not change during the imaging session. Solutions were delivered to the rostral area via an injection needle connected to a reservoir, allowing switching of the flow between odorless water and odorant solutions.

The zebrafish brains were accessed from the dorsal side, allowing the visualization of calcium signals from these parts of the brain. As the forebrain is a key target of projections from the olfactory bulb, these regions were of particular interest and were focused in the imaging experiments. The framerate was set to around 2-4 frames per second if possible, depending on the size of the illustrated brain area. Covering of large areas causes lower frame rates, limited by the detectors maximum speed. However, this framerate should allow the reliable detection of action potentials in the neurons (Chen et al., 2013). Calcium signals were recorded over a time period of up to 5 minutes, including up to 3 stimulation pulses.

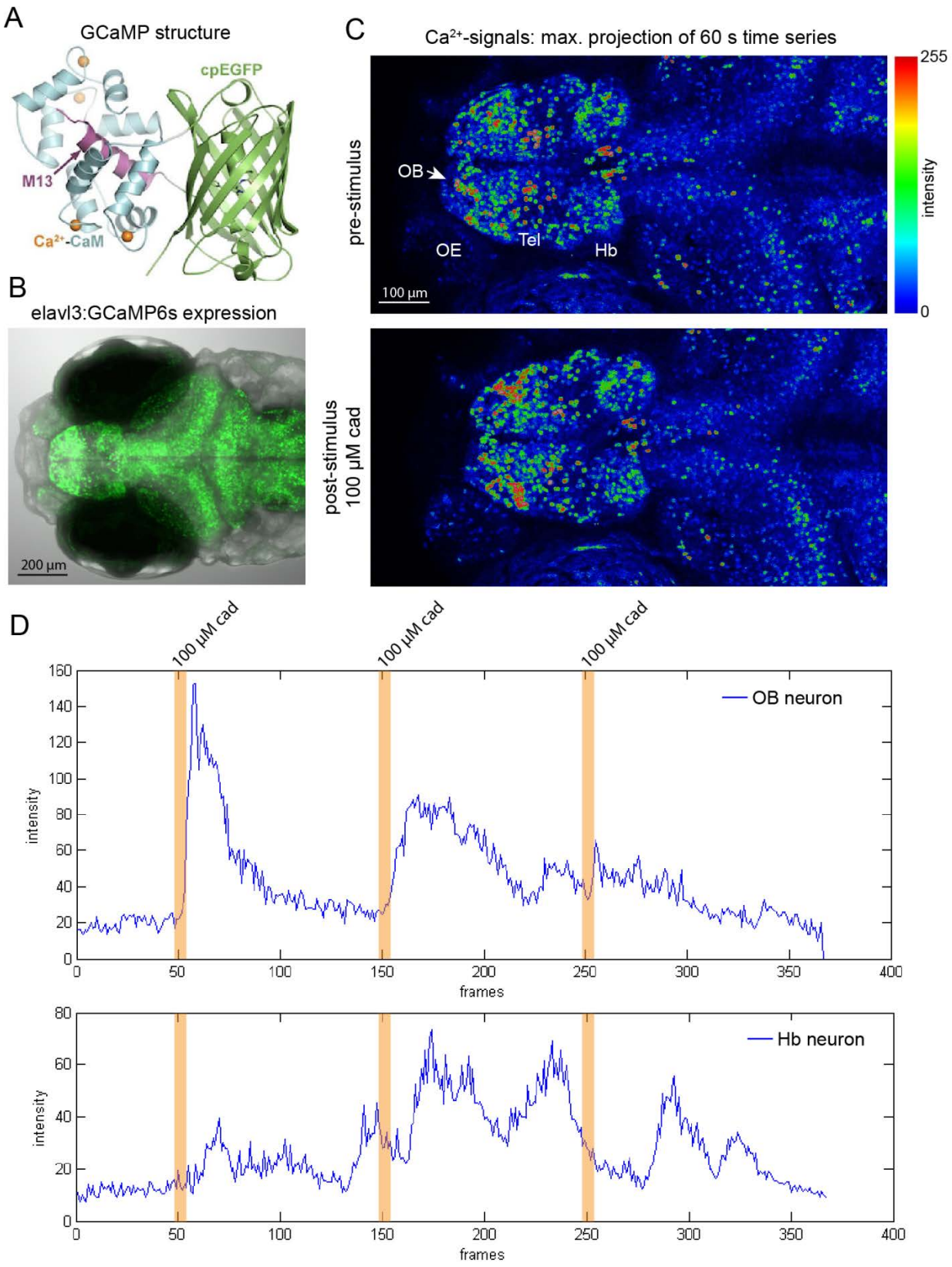

Figure 3.16: Legend on next page.

Figure 3.16: The *elavl3*:GCaMP6s line allows calcium-dependent activity imaging in the larval zebrafish brain A) Structure of GCaMP adapted from (Akerboom et al., 2009). B) Expression of GCaMP6s under the *elavl3* promoter in a 6 dpf zebrafish larvae. GCaMP 6 is shown as green fluorescence merged onto the brightfield picture. C) Heat-map color-coded maximum projections from 60 s time series before (pre) and after (post) stimulation with 100 µM cadaverine. Dark blue pseudo-color corresponds to no fluorescent signal. Red pseudo-color corresponds to maximum fluorescent signal. D) Example traces from bulbar and habenular neurons from the same optical section. Neuronal activity can be detected as changes in fluorescence intensity over time. Orange bars mark the stimulation periods. The olfactory bulb neuron clearly responds to stimulation with cadaverine. After multiple stimulations the response intensity is decreased, probably due to adaptation. The activity of the habenular neuron is not coupled to the stimulus but occurs spontaneously. (OE = olfactory epithelium; OB = olfactory bulb; Tel = telencephalon; Hb = habenula; cad = cadaverine)

In the pre-stimulation phase, when only water is applied to the larva, there is a certain pattern of neuronal activity in the forebrain, which represents the default state of the neuronal network under the given experimental conditions (Figure 3.16.C; upper panel). There is a moderate activity in several spots in the posterior olfactory bulb and also some active cells in the telencephalon and habenula. This default-state activity pattern changes upon stimulation with cadaverine. Especially in the olfactory bulb there are more cells with increased activity after cadaverine stimulation. Also, the fluorescent signal in the OB neurons is stronger (shift to red color in Figure 3.16.C; lower panel), than in most neurons of other brain regions.

Single cells were marked as regions of interest (ROIs) and the average fluorescence intensities of these ROIs at any given frame were plotted as a function of time (here 3.86 frames/second; Figure 3.16.D). Cadaverine pulses were given at Activity of an OB neuron and a habenular neuron were chosen as example traces. Changes in fluorescence intensity of the OB neuron are induced by stimulation with cadaverine, as the increase in fluorescence clearly follows the stimulation periods. Within around 50 frames (ca. 13 seconds) the fluorescence intensity levels return to baseline levels. Although the activity is still coupled to the stimulus, subsequent stimulations induce smaller changes in fluorescence intensity, possibly due to desensitization of the olfactory pathway. Meanwhile, the activity of the habenular neuron is not coupled to the stimulation with cadaverine. Spontaneous activity peaks can be observed, but the mode of action of this neuron remains unclear.

The results show that the *elavl3*:GCaMP6s zebrafish line is in general suitable to detect odor-induced activity in the larval forebrain, which includes important odor processing brain areas. Limitations are set by the technical properties of the confocal microscope (scanning speed, tissue

penetration depth). For example it was not possible to detect fluorescence changes in the hypothalamus, because of its ventral position in the brain.

3.3.4 A behavior setup to test larval attraction and aversion in response to olfactory stimuli

TAAR13c-expressing OSNs were detected as early as 3 day post fertilization in zebrafish embryos (as shown earlier in this chapter, compare Figure 3.13). In 6 - 7 dpf animals we could detect increased neuronal activity in the olfactory bulb in response to cadaverine by staining against pERK (Figure 3.14 + 3.15) as well as Ca^{2+}-imaging using GCaMP6s lines (Figure 3.16).

This now leads to the question, whether the cadaverine-induced behavioral response, which was shown to be present in adult fish (Hussain et al., 2013), is also present at that larval stage. As the larvae begin to forage for food at around 6 dpf, they display a characteristic swimming behavior. This permits the observation of stimulus-induced behavioral changes like attraction and aversion.

6 - 7 dpf larvae were placed in small elongated tanks, allowed for acclimatization to the new environment until they displayed normal swimming behavior, and then stimulated with the respective odor. 500 µl of stimulus solution were observed to spread over around 25-30% of the tank length (see Figure 3.17). Cadaverine was used in a concentration of 300 µM, which should result in an intermediate final cadaverine concentration in the testing tank, similar to the 10-100 µM, that were used in the pERK and Ca^{2+}-imaging experiments.

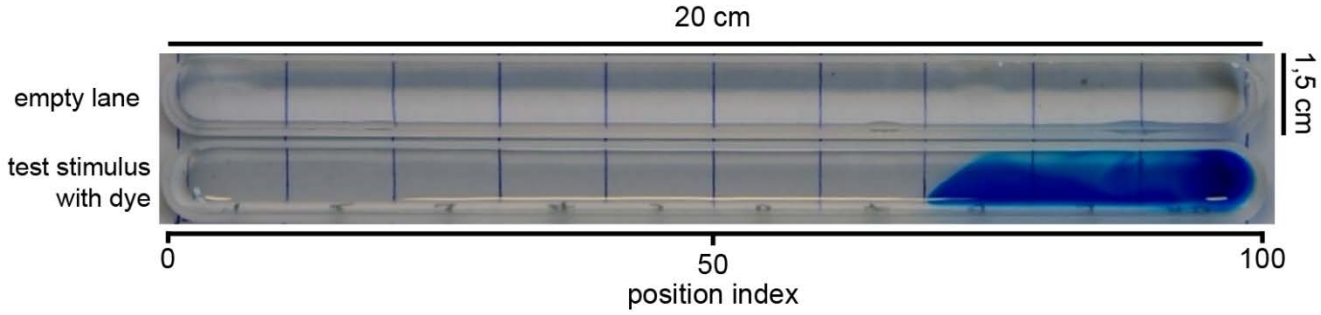

Figure 3.17: Behavioral setup for attraction/aversion in larval zebrafish. Elongated tanks (dimensions 20 cm length x 1.5 cm width) were filled with 10 ml of water before the larvae were placed inside. Stimulus range was tested by application of a dye. 500 µl of stimulus solution spread across 25-30 % of the tank (see example lane with dyed solution).

3.3.5 Larval zebrafish are not repelled by cadaverine

Animals were recorded for 20 min, with a 10 min pre-stimulus phase and a 10 min post-stimulus phase. To make observations about the animals place preference, the position of the animal was determined every 30 seconds (position index). The position index specifies the animals position as a value between 0, representing the remote end of the tank (away from the stimulus), and 100, where the stimulus was given. As the stimulus was observed to spread to around 30 % of the tank, an animal attracted to the stimulus would display high position indices between 70 and 100. An animal repelled by the stimulus would display position indices < 70 most of the time.

For each stimulus recordings of 10 random animals were used for analysis. The larval zebrafish cannot be tracked with our software (LoligoTrack 4) in this setup, as the contrast is not high enough for the software to continuously recognize the position of the fish, especially when the larvae swims close to the tank border. Thus, the fish position was measured manually every 30 seconds, resulting in 20 data points obtained both for the pre-stimulus phase and the post-stimulus phase. This data provides a random placement representation of the larvae throughout the experiment and was found to provide reliable information for the larval response to negative control stimuli, i.e. water, as well as positive control stimuli, i.e. food odor.

Figures 3.18, 3.19, and 3.20 show the behavioral data obtained from 10 individual larvae for water (negative control), cadaverine and food odor, respectively.

Larvae were numbered as indicated. Two figures are presented for each larva. The left figure shows the position indices (y-axis) obtained over the course of the experiment as a function of time (x-axis). In that way the general movements of the larvae within the tank can be reconstructed. As the larvae were starved for at least 3 hours before the experiment, they usually explored the tank swimming in turns from one end to the other in search for food. Most larvae covered at least half of the tank length, although this might not be visible in the individual data, because indices were only determined every 30 seconds. On the average of 10 animals though, this effect should disappear. The second figure shows the same data points (position indices) as an empirical cumulative distribution function (ECDF). The black line always represents the pre-stimulus position indices measured. The colored line always represents the post-stimulus position indices measured. If the position indices are very similar in the pre- and the post-stimulus phase

the ECDFs will also be very similar, i.e. the curves will have more or less the same course and will repeatedly cross each other.

This is the case for 9 out of 10 animals stimulated with water as a negative control stimulus (compare ECDFs in Figure 3.18). The pre-phase and post-phase ECDFs from all but one animal are essentially the same, with only minor differences. Animal 2 displayed slightly altered position indices after giving the stimulus, with a weak tendency to spend more time close to the odor source (Figure 3.18, animal 2). Note that no statistical test were done on the individual larvae, as the datasets are usually not big enough (only 20 values) to fulfill test criteria requirements. Overall, water seemed to be a reliable negative control stimulus in this setup. This also becomes evident, when the position indices from all 10 animals are pooled and plotted as ECDF for pre- and post-phase (Figure 3.21.A). Here, a Kolmogorov-Smirnoff test was done to test the pre- and post-phase position index distributions for significant differences. The larval positioning in the pre- and post-phase of water stimulated animals was essentially the same.

Another way to show the average larval position in the tank is to calculate the average time in specific regions of the tank (dwell time). Therefore the tank was divided into 10 sectors (binning) and the average dwell time in percent of the total duration of pre- and post-phase, respectively, was plotted as bar graphs (Figure 3.21.B). The average dwell time in pre- and post-phase was not significantly altered in any of the 10 sectors (Wilcoxon Rank Sum test for non-normally distributed data).

When looking at cadaverine stimulated animals, a change in behavior in response to the stimulus can be observed. Again, the behavior of 10 larvae in response to cadaverine was analyzed using the position indices collected every 30 seconds. For each larva the results were plotted as position index over time (left panel) and empirical cumulative distribution function (right panel; see Figure 3.19). The behavioral response to cadaverine can differ from animal to animal. In this experiment it ranged from a slight aversion in two animals (animals 1 and 5) to strong attraction in two different animals (animals 3 and 10). Other animals seemed to be indifferent to the cadaverine stimulus and their positioning did not change in response to the stimulus (animals 2, 8 and 9).

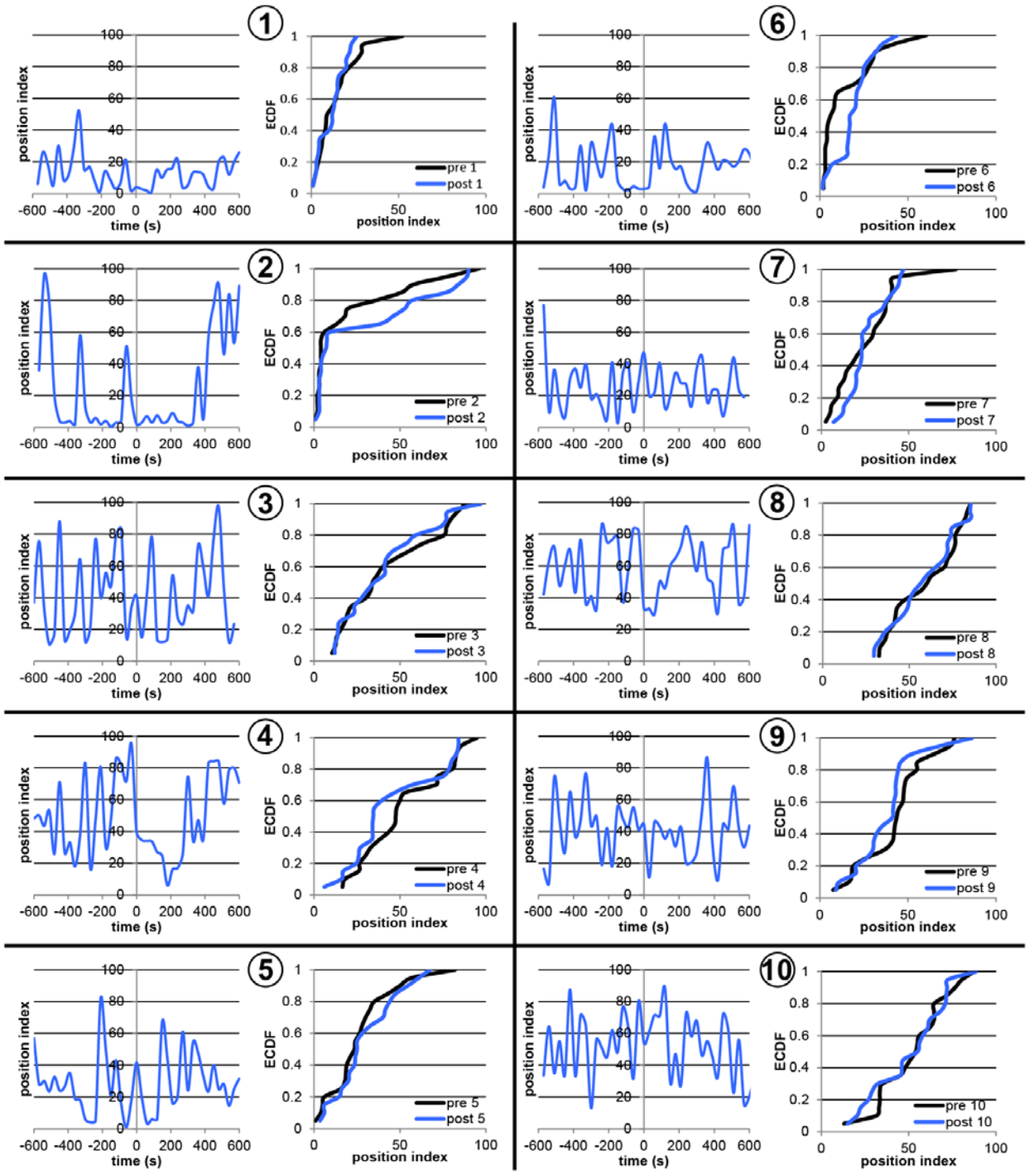

Figure 3.18: Individual larval behavior in response to water as a negative control stimulus The position of each larva (n = 10) was determined every 30 seconds over a period of 20 min (10 min pre-stimulus, 10 min post-stimulus). The position index values were plotted against the time (s) in the left panel, respectively. In that way the general movements of the larvae can be reconstructed. The right panel shows the position indices before (black) and after (blue) giving the odor stimulus as an empirical cumulative distribution plot (ECDF). As ECDFs from pre- and post-stimulus phase differ only marginally in all 10 animals, water represents a suitable negative control stimulus in this behavioral assay.

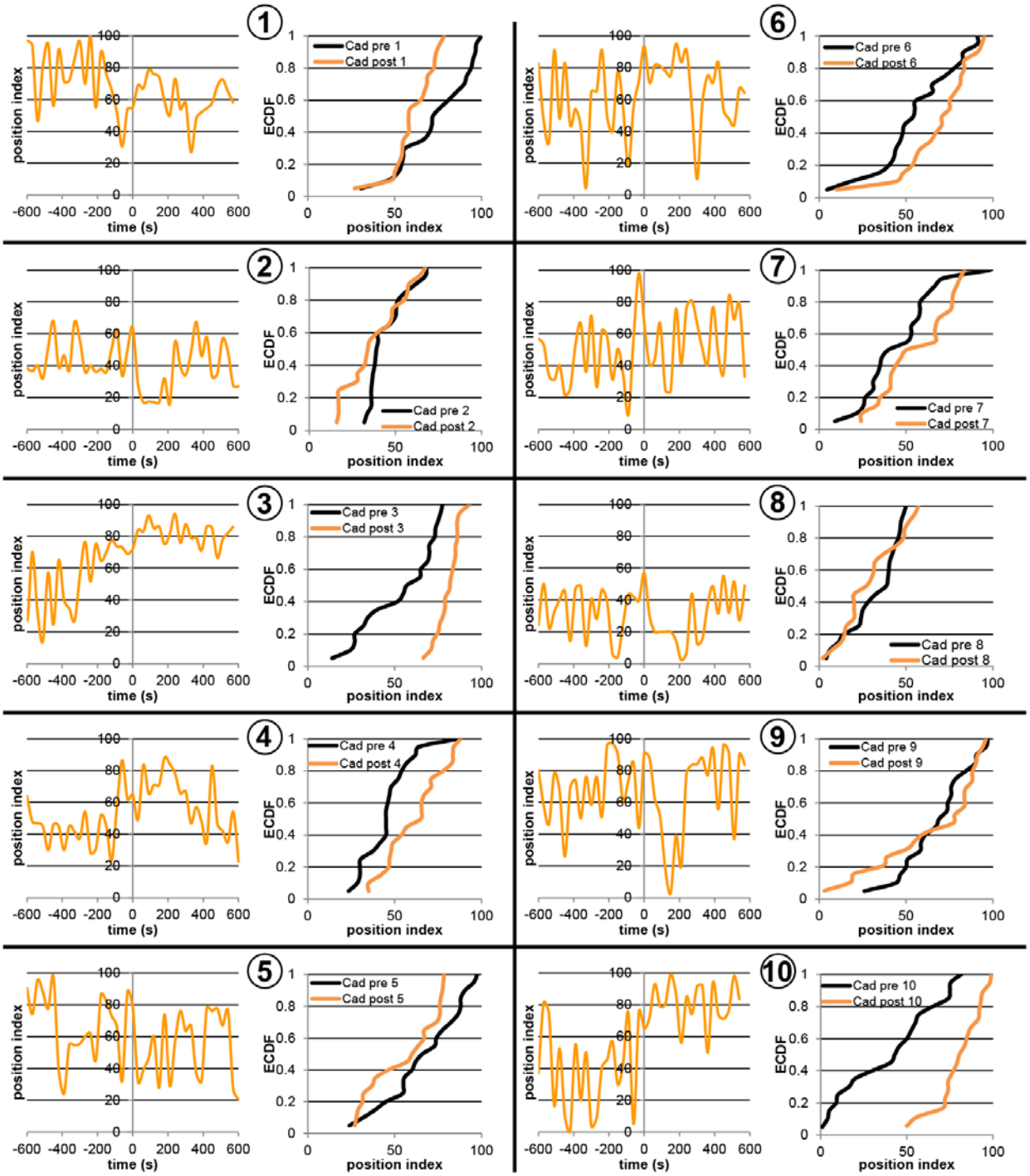

Figure 3.19: Individual larval behavior in response to cadaverine The position of each larva (n = 10) was determined every 30 seconds over a period of 20 min (10 min pre-stimulus, 10 min post-stimulus). The position index values were plotted against the time (s) in the left panel, respectively. In that way the general movements of the larvae can be reconstructed. The right panel shows the position indices as an empirical cumulative distribution plot before (black) and after (orange) giving the odor stimulus. Larvae 3 and 10 were attracted by cadaverine (clear shift of position towards the odor source). Larvae 4, 6, 7 showed a trend towards attraction (small shift towards the odor source). Larvae 1, 5 showed a trend towards aversion (small shift away from the odor source).

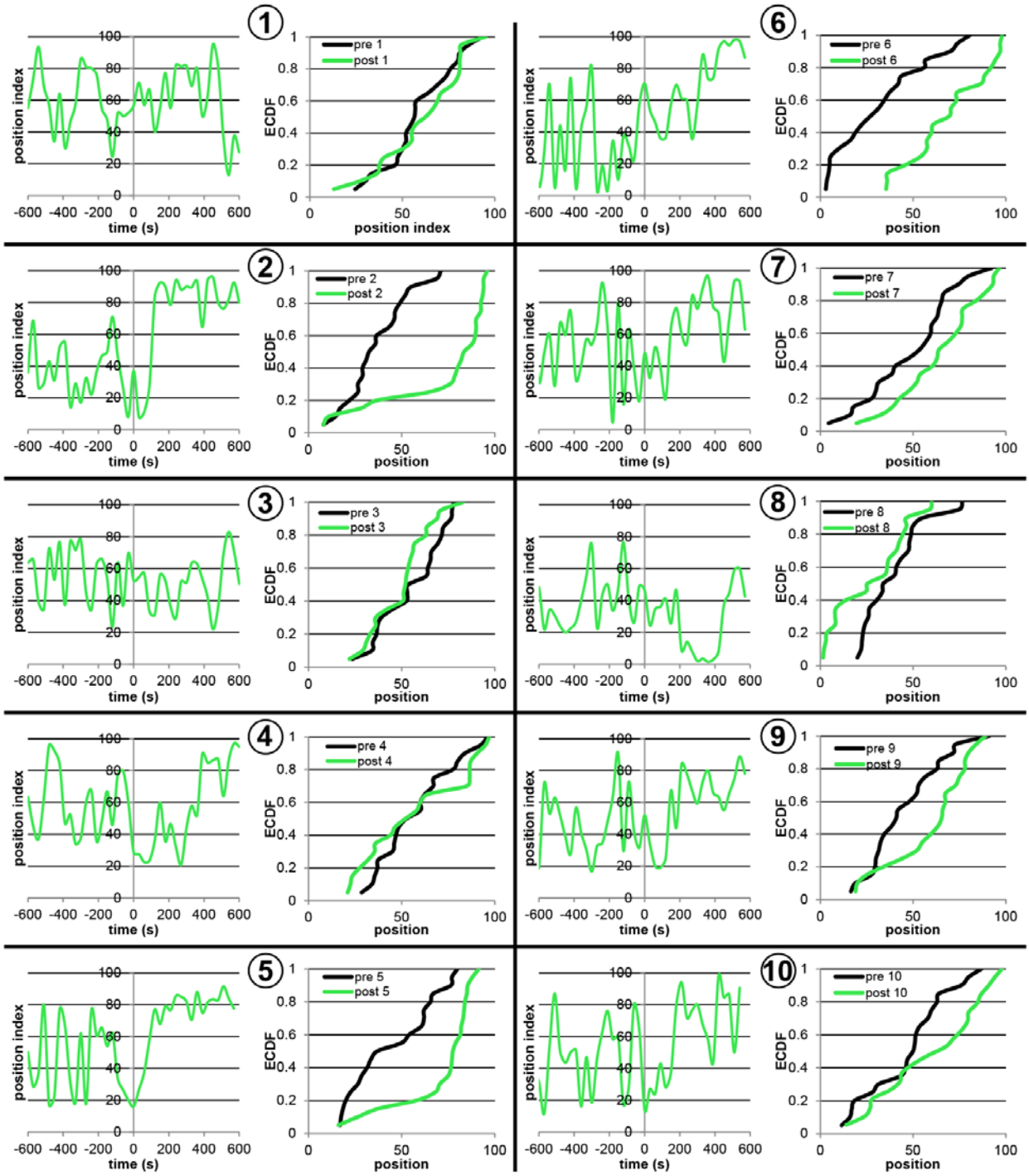

Figure 3.20: Individual larval behavior in response to food odor The position of each larva (n = 10) was determined every 30 seconds over a period of 20 min (10 min pre-stimulus, 10 min post-stimulus). The position index values were plotted against the time (s) in the left panel, respectively. In that way the general movements of the larvae can be reconstructed. The right panel shows the position indices as an empirical cumulative distribution plot before (black) and after (green) giving the odor stimulus. Larvae 2, 5, 6 showed strong attraction to the stimulus (clear shift of position towards the odor source). Larvae 7, 9, 10 showed a trend towards attraction (small shift towards the odor source). Larvae 8 did not encounter the odor.

In animals 3 and 10 the position over time already allows to notice a clear attraction towards the odor source. After giving the stimulus they obviously spend more time close to the stimulus (position indices close to 100) than in the pre phase. This is also reflected in the ECDFs for these two animals. The position index distribution is clearly shifted towards the odor source (shift of the orange curve to the right, i.e. higher position indices). Animals 4, 6 and 7 showed a trend towards attraction, as their position index distribution shifted slightly towards the odor source.

In general the behavioral response to cadaverine seemed to be ambiguous on the level of the individual. Therefore the pre- and post-phase position indices of all animals were pooled and plotted as ECDF as well as average dwell time per sector in a binned environment (Figure 3.21.C + D, respectively). In the pooled ECDF it becomes clear, that the distributions from the pre-phase is different from the one in the post-phase (KS test result $p = 0.001$). The overall position indices shift towards the odor source, when looked at this summarized data from 10 animals. Also in the average dwell time bar graph a trend towards dwelling in sectors close to the cadaverine source can be observed, which is however not significant at this sample size ($p = 0.07$, Wilcoxon Rank Sum test). This result is not consistent with the behavioral response of adult animals, which displayed aversive behavior in response to cadaverine in a similar experimental setup (Hussain et al., 2013).

Food odor served as a positive control. As the larvae were starved for at least three hours before the experiment we expected that they would forage for food. The data was analyzed as before and shown as position index over time as well as position index ECDF (Figure 3.20). In fact three out of 10 larvae showed a clear attraction to the food odor source (as evident in Figure 3.20; animals 2, 5, 6). Three more animals showed a slight attraction and still spent on average more time close to the food odor source than in the pre-phase (animals 7, 9, 10). One animal did not encounter the stimulus physically and trended towards aversion (animal 8). In three animals the position index distribution was not notably affected by the food odor stimulus (animals 1, 3, 4).

Altogether, food odor seemed to be a relatively reliable positive control odor for attractive behavior, as six out of 10 animals displayed attraction. This is even more clearly reflected in the ECDFs and average dwell time analysis of the pooled position indices (Figure 3.21.E + F, respectively). In the ECDF a significant change of the positioning distribution towards the food odor source could be observed ($p < 0.001$; KS-test).

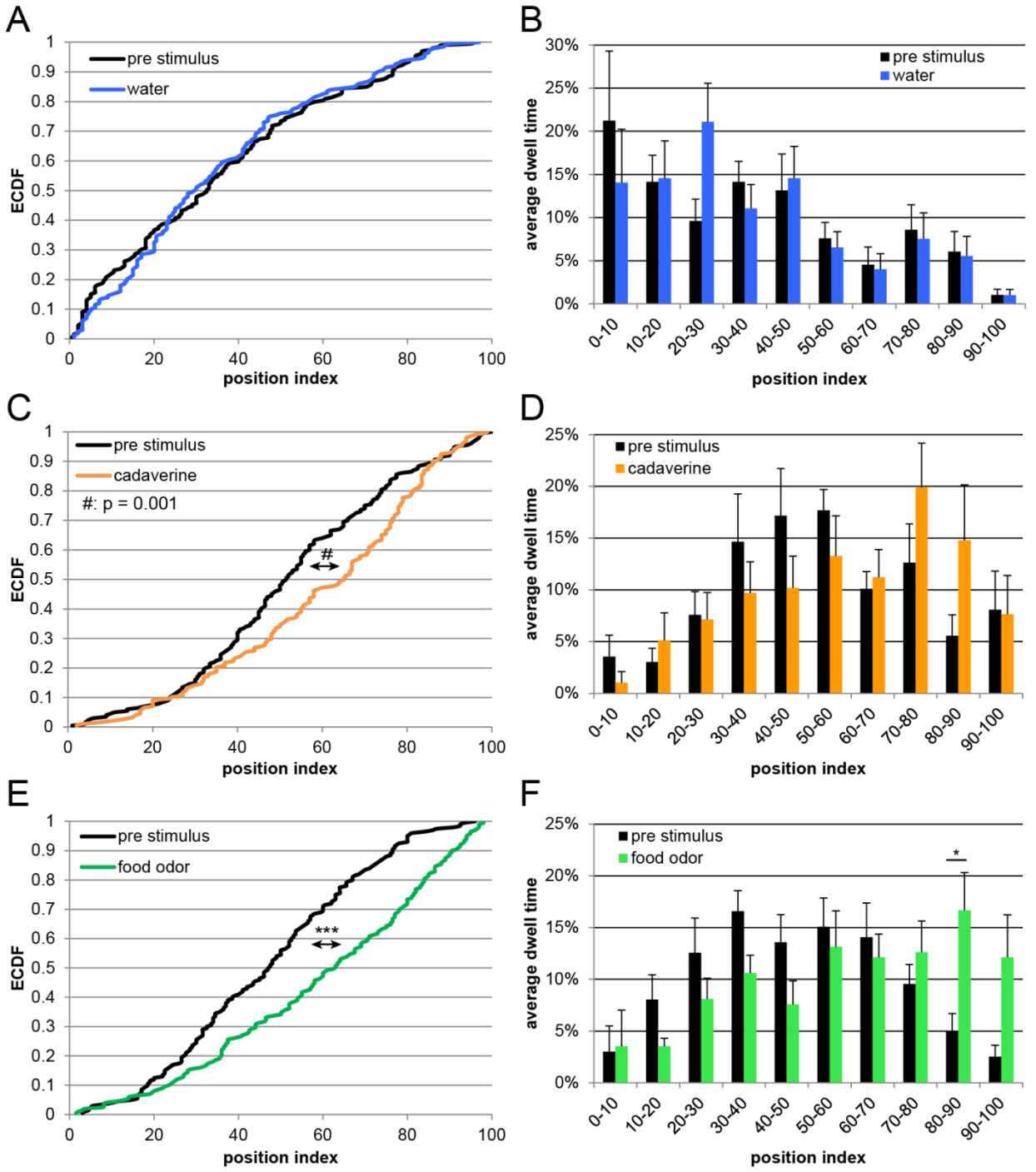

Figure 3.21: Summarized larval behavior response The position indices measured from 10 larvae were pooled in order to exploit the overall behavioral response to the tested odors. ECDFs of the measured position indices were plotted for water (A), cadaverine (C), and food odor (E) stimuli. At the level of the entire sample group both cadaverine and food odor-induced attraction in 6 dpf larvae ($p = 0.001$ and *** $p < 0.001$, respectively; KS-test). The average dwell time was calculated for binned position indices pre and post stimulation and plotted as bar graphs for water (B), cadaverine (D), and food odor (F). Larvae stimulated with food odor stayed significantly longer in an area close to the odor stimulus ($p < 0.05$; WRS-test). Larvae stimulated with cadaverine showed a trend towards attraction, which was not significant. Error bars represent SEM.

Looking at the average dwell time, the animals spent noticeably more time close to the food odor source, with a significantly increased time spent at position indices between 80 and 90 ($p < 0.05$, Wilcoxon Rank Sum test).

In summary, this experimental setup is suited to observe odor-induced attraction/aversion behaviors in the 6-7 dpf larval zebrafish. If the effects are rather small, data from multiple individuals should be pooled to gain statistical significance. Stimulation with water can serve as a reliable negative control, as it does not change the average larval positioning within the tank. Food odor represents a reliable attractant stimulus. Surprisingly, larvae were also attracted by cadaverine, which had the contrary effect in adult animals (Hussain et al., 2013).

3.4 CRISPR-Cas9 mediated knock-out of TAAR13c

Gene knock-outs are generated to gain insight on the physiological role of the gene of interest. The zebrafish olfactory receptor TAAR13c is activated by cadaverine, which induces aversive behavior in zebrafish. An earlier study attempted to knock out TAAR13c by using the CRISPR-Cas9 system (Dissertation Venkatesh Krishna, Köln 2017). In that study CRISPR-Cas9 target sites within the TAAR13c genomic sequence were chosen in order to introduce small insertions or deletions within the gene, leading to frameshifts and/or premature stop codons.

However, the number of suitable target sites within the TAAR13c gene is very limited due to high homology within the TAAR13 gene subfamily. Therefore, most target sites within the gene would target multiple genes within the TAAR family.

In order to avoid these and further off-target effects a different approach was chosen in this study. We designed CRISPR-Cas9 target sites in the 3´UTR and 5´UTR of TAAR13c, which do not share high homology with other loci in the genome. Co-injecting multiple gRNAs DNA fragments of several kb can be cut out from the genome (Ota et al., 2014). If Cas9 induces a double strand break at two locations within a certain range at the same time, the fragment in between the breaks can eventually be deleted as the loose ends of the DNA are joined together by non-homologous end joining (NHEJ).

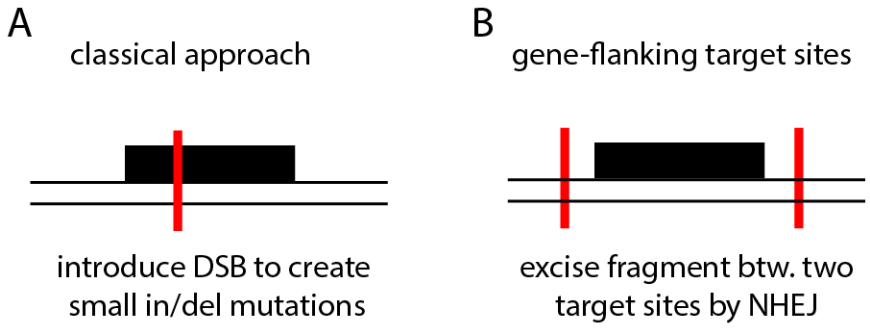

Figure 3.22: Different CRISPR-Cas9 gene knock-out strategies The CRISPR/Cas9 system induces double strand breaks (DSB) at target sites determined by guide RNAs. A) A DSB at a single target site can cause small insertion or deletion events, which lead to frame shifts and/or premature stop codons. B) Using two target sites at the same time, the DNA sequence between the target sites can be excised from the genome as the strands are repaired by non-homologous end joining (NHEJ). Exemplary target sites are marked in red. Black square represents the targeted exon.

3.4.1 Guide RNA synthesis

Target sites were designed as shown in chapter 2.5. The CHOPCHOP tool provided a more convenient output, than the “http://crispr.mit.edu/” platform. CHOPCHOP directly lists potential off targets in the GRCz10 version of the zebrafish genome and scores the target sites according to their predicted efficiency. The target sites are listed in material and methods section and schematically shown in Figure 3.26.A.

Two different methods for gRNA synthesis were used. For the plasmid-based gRNA synthesis annealed oligonucleotides defining the target site were ligated into a plasmid harboring a T7 promoter site (pDR274). A template for *in vitro* transcription was produced by restriction with DraI (gel data not shown). The *in vitro* transcription with T7 RNA polymerase results in full length guide RNAs. gRNAs obtained with this method are shown below (Figure 3.23.A).

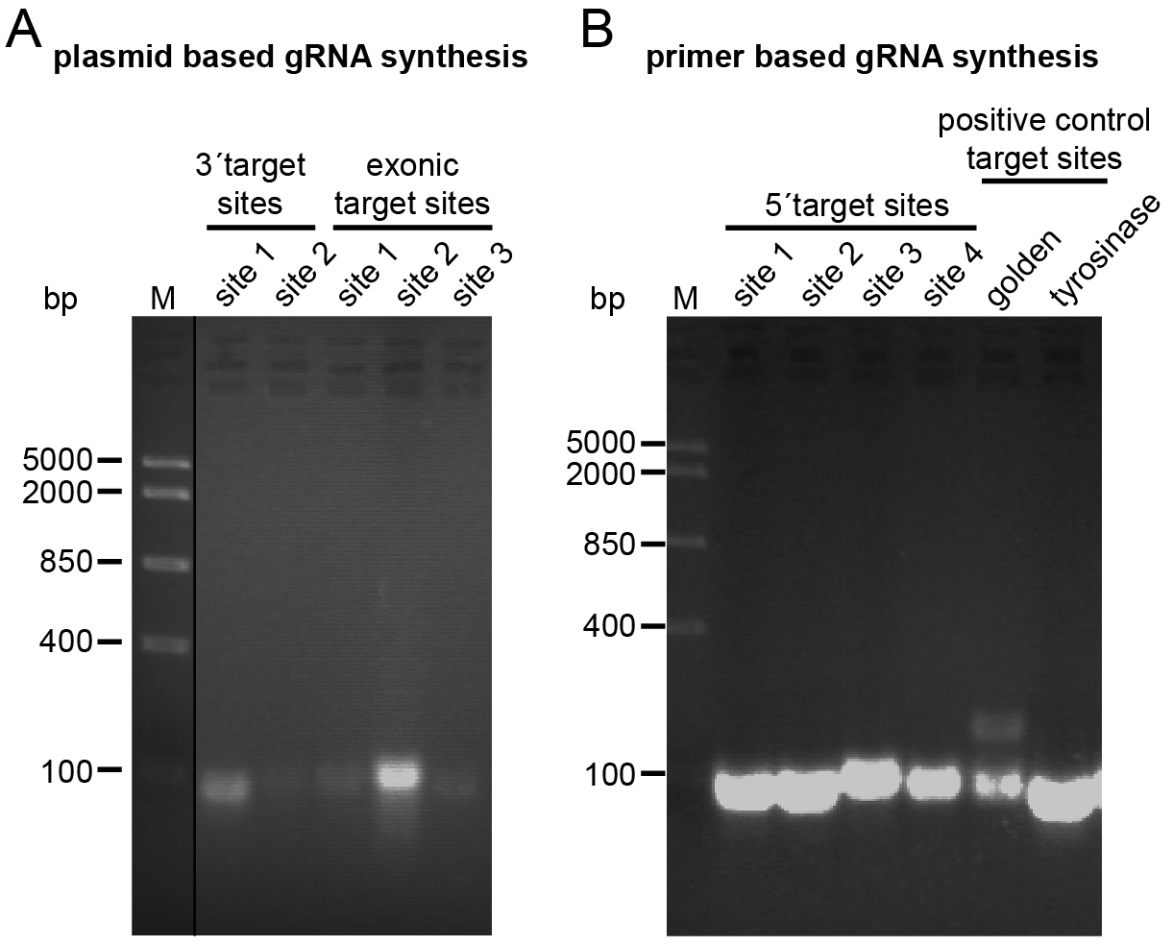

Figure 3.23: Comparison of two gRNA production methods A) Plasmid-based gRNA synthesis results in full length gRNA, but with relatively low yields. B) Primer based gRNA synthesis yields high levels of full length gRNA running at around 100 bp.

The primer based method for guide RNA synthesis was adapted from Talbot and Amacher (Talbot and Amacher, 2014). It is less time consuming and results in higher gRNA yields. Oligonucleotide primers containing a T7 promoter site, the target site sequence as well as the guide RNA scaffold are used to produce the *in vitro* transcription template via PCR (see methods). The *in vitro* transcription with T7 RNA polymerase then results in full length guide RNAs. Example gRNAs obtained with this method are shown above (Figure 3.23.B). The primer based method for gRNA synthesis usually resulted in higher gRNA yields than the plasmid-based method.

3.4.2 Survival rates following CRISPR-Cas9 injections

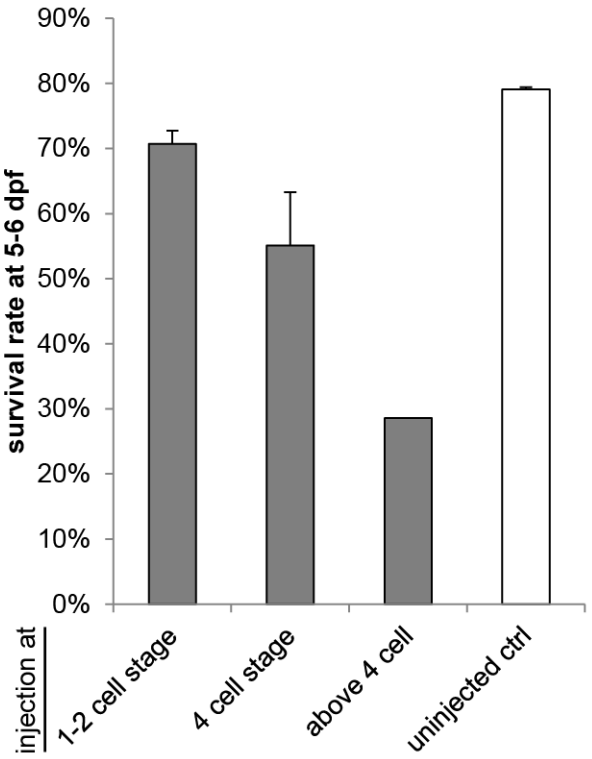

injection at	survival rate mean ± SEM	n
1-2 cell stage	0.71 ± 0.02	11
4 cell stage	0.55 ± 0.08	2
above 4 cell	0.29	1
uninjected ctrl	0.79 ± 0.003	3

Figure 3.24: Survival rates of CRISPR/Cas9 injected zebrafish larvae at 5-6 dpf. The bar graph shows the percentage of animals with no obvious health defects after injection of Cas9 and gRNAs at different stages after fertilization of the egg in comparison to the percentage of healthy uninjected wildtype embryos.

Injections of the Cas9 protein and the gRNAs were carried out as stated in material and methods using borosilicate glass pipettes and a pneumatic pico-pump (see chapter 2.5 for details). Embryos were raised in 0.03 % sea salt water supplemented with methylene blue, as this procedure reduces growth of fungi, which otherwise tend to infest the eggs. The number of dead and healthy larvae was noted regularly. Survival rates from 5-6 dpf animals are depicted in Figure 3.24. Non-injected wildtype larvae had a survival rate of 79 ± 0.3 % (mean ± SEM, n = 3). Eggs injected with gRNA and Cas9 had a 5-6 dpf survival rate of 71 ± 2 % (mean ± SEM, n = 11), which is not substantially lower than the survival rate of the non-injected wildtype embryos. Injections at later points of the embryonal development, here 4 cell stage and above, lead to higher death rates (see Fig. 24).

3.4.3 Knock-out efficiency of positive control injected larvae: loss of pigmentation

The CRISPR/Cas9 system is a genome editing technique with potentially high efficiency depending on various parameters, like the model organism, mode and timing of the delivery into the cell, etc. In the experiments presented in this work an engineered Cas9 protein, harboring a nuclear localization sequence (Cas9-NLS, New England Biolabs), and *in vitro* transcribed gRNAs were injected into freshly fertilized zebrafish eggs.

To determine the efficiency of the system gRNAs targeting the pigmentation related genes tyrosinase and golden were used as a positive control. The target sites were adopted from an earlier study (Ota et al., 2014) and are listed in material and methods chapter 2.5. While the non-injected wildtype embryos displayed a normal pigmentation pattern in the skin and eyes (Fig. 3.25.A), the injection of gRNAs against tyrosinase and golden resulted in complete loss of pigmentation in 86 ± 3 % of the surviving embryos injected with this mix (Fig. 3.25.B + C). 7.2 ± 0.2 % of the embryos showed an intermediate pigmentation and only 6.4 ± 3 % of the injected embryos showed a wildtype-like pigmentation.

Taken together, almost 90 % of the injected embryos underwent a full body disruption of the tyrosinase and golden genes highlighting the efficiency of the technique.

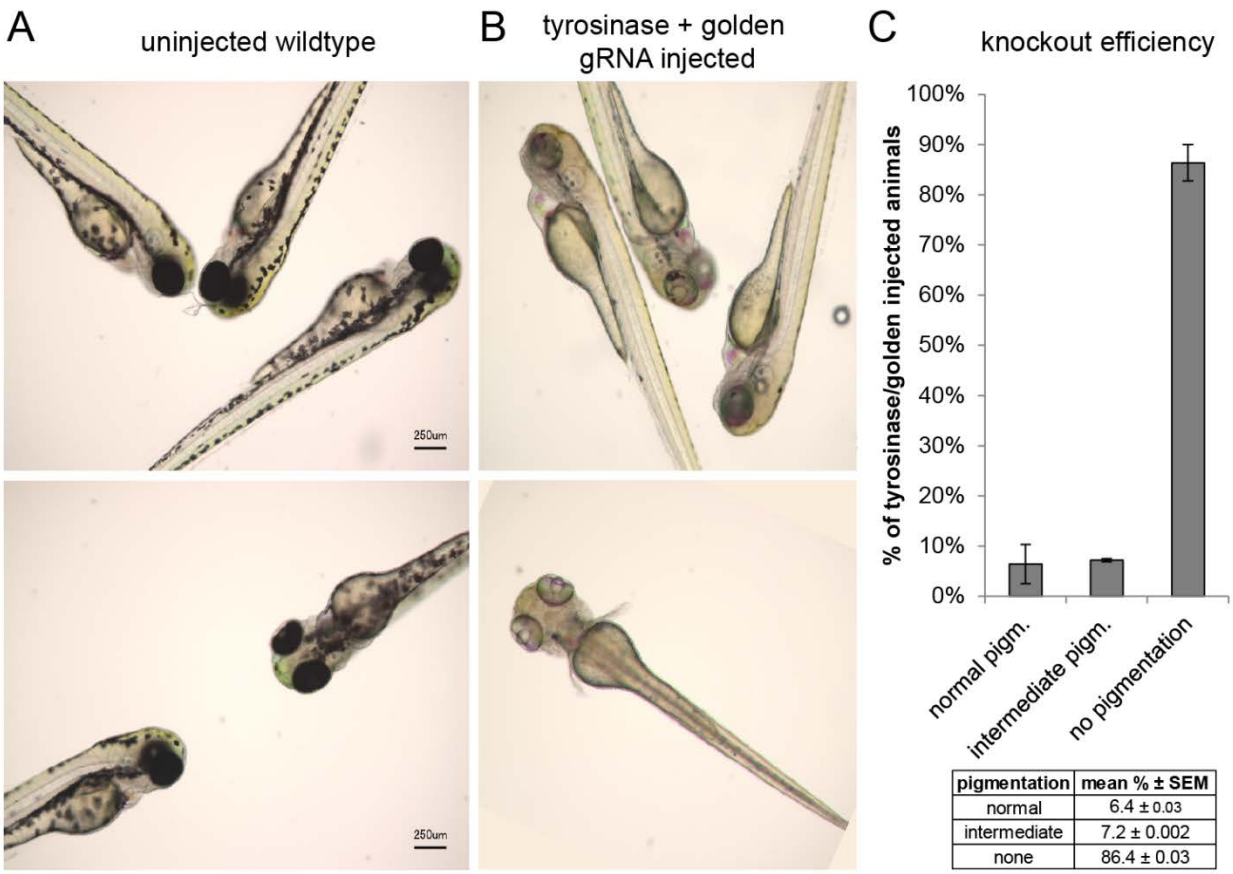

Figure 3.25: Loss of pigmentation in CRISPR/Cas9-induced knock-out of pigmentation related genes tyrosinase and golden A) Uninjected wildtype embryos show a characteristic pigmentation patterns of the skin and have highly pigmented eyes. B) Embryos injected with Cas9 protein and gRNAs targeting the pigmentation related genes tyrosinase and golden show a loss of pigmentation in skin and eyes. C) Over 86 % of the injected embryos show a complete loss of pigmentation. Around 7% of injected larvae display an intermediate pigmentation indicating a partial or mosaic knock-out. 6.4% of the embryos show no loss of pigmentation, when compared to wildtype embryos.

3.4.4 Choice of CRISPR/Cas9 target sites for TAAR13c

The positive control experiments showed a genome editing rate above 90 % using pigmentation related genes tyrosinase and golden (see previous chapter). We now sought to knock-out the cadaverine receptor TAAR13c from the zebrafish genome. An earlier study (V. Krishna, 2017) revealed the challenges finding appropriate target sites for TAAR13 genes. As all of the members show high sequence homology, between 86.6 % and 94 %, most target sites will display off-target effects by binding to multiple members of the TAAR13 family or even other TAARs. The 5´UTR and 3´UTR display a much lower sequence homology with 37.8-52 % and 45.2-57.3 %, respectively. See appendix for identity matrices obtained from multiple sequence alignments of TAAR13 members 5´UTRs, exons, and 3´UTRs. To avoid off-target effects within the family gRNA target sites were searched in the 5´and 3´UTRs of TAAR13c. Initially, the target sites were chosen with the online tool from the Zhang lab (crispr.mit.edu). Subsequently CHOPCHOP (http://chopchop.cbu.uib.no/), a more recent and convenient tool for target site design, was used (Labun et al., 2016). It allows the variation of different parameters and lists the potential target site according to their predicted efficiency and off-targets. A complete list of the target sites used in this study including the off-targets and efficiency scores is provided in material and methods, chapter 2.5. Target sites were required to start with GG, as first base transcribed by the T7 RNA-polymerase is a G, which at the same time will represent the first nucleotide binding to the target site. If a target site starts with bases other than GG (i.e. NG or GN), the bases have to be manually changed to GG, to enable the transcription via T7 RNA-polymerase. This was for example the case in the tyrosinase target site used in the positive control experiments.

For the TAAR13c 5´UTR a variety of potential target sites was identified by the CHOPCHOP program. From those, three target sites with high efficiency and minimal off-targets were chosen (5´13c sites 1-3). One additional target site obtained with the crispr.mit.edu-tool was chosen as well (5´13c sites 4). 5´TAAR13c target site 1 displayed the fewest off-targets with only one 20/20 bp match off-target in a non-coding region. Further off-targets had several mismatches.

Surprisingly, only very few potential target sites were found in the 3´UTR. In lack of alternatives two target sites, 3´13c site 1 and 2, were selected although they displayed a relatively high number of off-targets. The 3´UTR has a low GC content (30,4 %), which is reflected in the low number of potential target sites as they require at least two GGs in the correct distance from each other (5´GG and PAM sequence NGG).

However, when searching the TAAR13c exon for specific target sites with the CHOPCHOP program potential target sites not identified by a previous study in the lab (Krishna Subramanian, 2017) were obtained. Three of these sites in the middle of the exon were chosen (exon13c sites 1-3). Exon13c site 2 has no 20/20 bp off-targets, but shares 19 bp with a sequence in taar13e, which might result in off-targeting. Other off-targets had higher numbers of mismatches.

3.4.5 Knock/out of TAAR13c from its genomic locus

After designing the target sites, combinations of gRNAs for two target sites were co-injected with Cas9 in order to excise the DNA fragment between the two double strand brakes introduced by the Cas9 protein. The success of the injections was controlled by PCR of a fragment enclosing the two target sites (see Table 3.1).

Table 3.1: CRISPR/Cas9 TAAR13c target site combinations and size of the knock-out fragments. Two target site gRNAs were co-injected. PCR with genomic DNA of 2-5 dpf larvae (whole body) or adults (fin clip) was used as PCR template to determine the successful excision of the DNA fragment between two target sites.

target site combinations	**size of uncut PCR fragment**	**size of excised fragment**	**size of cut PCR fragment**	**k.o.-PCR fragment amplified**
5´ s1 + 5´ s4	1940 bp	715 bp	1225 bp	**+ (Figure 3.26.C)**
5´ s2 + exon s1	1940 bp	639 bp	1301 bp	- (not shown)
5´ s2 + exon s2	1940 bp	645 bp	1295 bp	- (not shown)
5´ s2 + 3´ s1	2.866 bp	1.994 bp	872 bp	- (not shown)
5´ s2 + 3´ s2	2.866 bp	2.121 bp	745 bp	- (not shown)
5´ s3 + 3´ s1	2.866 bp	2.263 bp	603 bp	- (not shown)
5´ s3 + 3´ s2	2.866 bp	2.376 bp	490 bp	- (not shown)
5´ s3 + exon s1	1940 bp	908 bp	1.032 bp	**+ (Figure 3.26.D)**
5´ s3 + exon s2	1940 bp	914 bp	1.026 bp	+ (not shown)
5´ s4 + 3´ s1	2.866 bp	1.906 bp	960 bp	- (not shown)
5´ s4 + 3´ s2	2.866 bp	2.033 bp	833 bp	- (not shown)

Figure 3.26.A shows the genomic locus of TAAR13c on chromosome 20 of the zebrafish genome. Green arrows indicate the target sites that were shown to generate a knockout. Red arrows indicate the target sites that failed to generate a knockout. Grey target sites were not used in this study, because other target sites in that region were already successfully used. The horizontal blue arrows indicate the position of the confirmation PCR primers. Table 3.1 shows all target site combinations used in this study.

Figure 3.26.B illustrates the knock-out strategy. 1) Specific guide RNAs navigate Cas9 to two adjacent target sites. 2) Two double strand breaks (DSB) are introduced within the region of interest. 3) The loose ends can be joint together by non-homologous end joining (NHEJ) leading to the excision of the DNA sequence between the DSBs. In a PCR targeting this genomic region this results in a shortened PCR amplicon.

In an initial attempt to test the general function and efficiency of the methodological approach, a rather small fragment was chosen to be excised from the 5´UTR, before approaching to targeting the whole gene. 5´ target sites 1 and 4 enclose a 715 bp fragment. Both gRNAs were co-injected with Cas9-NLS into 1-2 cell stage fertilized eggs. 48 h after the injection DNA was extracted from pools of 7-10 embryos were Injection of these two target sites. PCR with the wildtype DNA results in a single band slightly below the 2 kb marker, as was expected for the wildtype (expected: 1.940 bp; Figure 3.26.C). The In 5 out of 9 samples the PCR results in a weak additional band at around 1.200 bp, as would be expected in case of a knock-out of the 715 bp fragment. This illustrates that the method works for those specific target sites.

Although the majority of the samples showed the knock-out band, pooled template DNA does not allow conclusions about homo- or heterozygosity of the knock-out animals nor does it allow estimating the knock-out efficiency. Thus, after determining whether or not a combination of guide RNAs works, genomic DNA of single larvae was used for PCR in order to determine the genotype of the larvae or even adults. Table 3.1 depicts which guide RNA combinations resulted in knock-out PCR fragments and which did not.

Three out of four 5´UTR target sites worked in at least one combination. Similarly, two out of two target sites within the exon led to a knock-out fragment in at least one combination. Unfortunately, none of the 3´UTR target sites led to an identifiable knock-out fragment regardless of the target site they were paired with (compare Table 3.1).

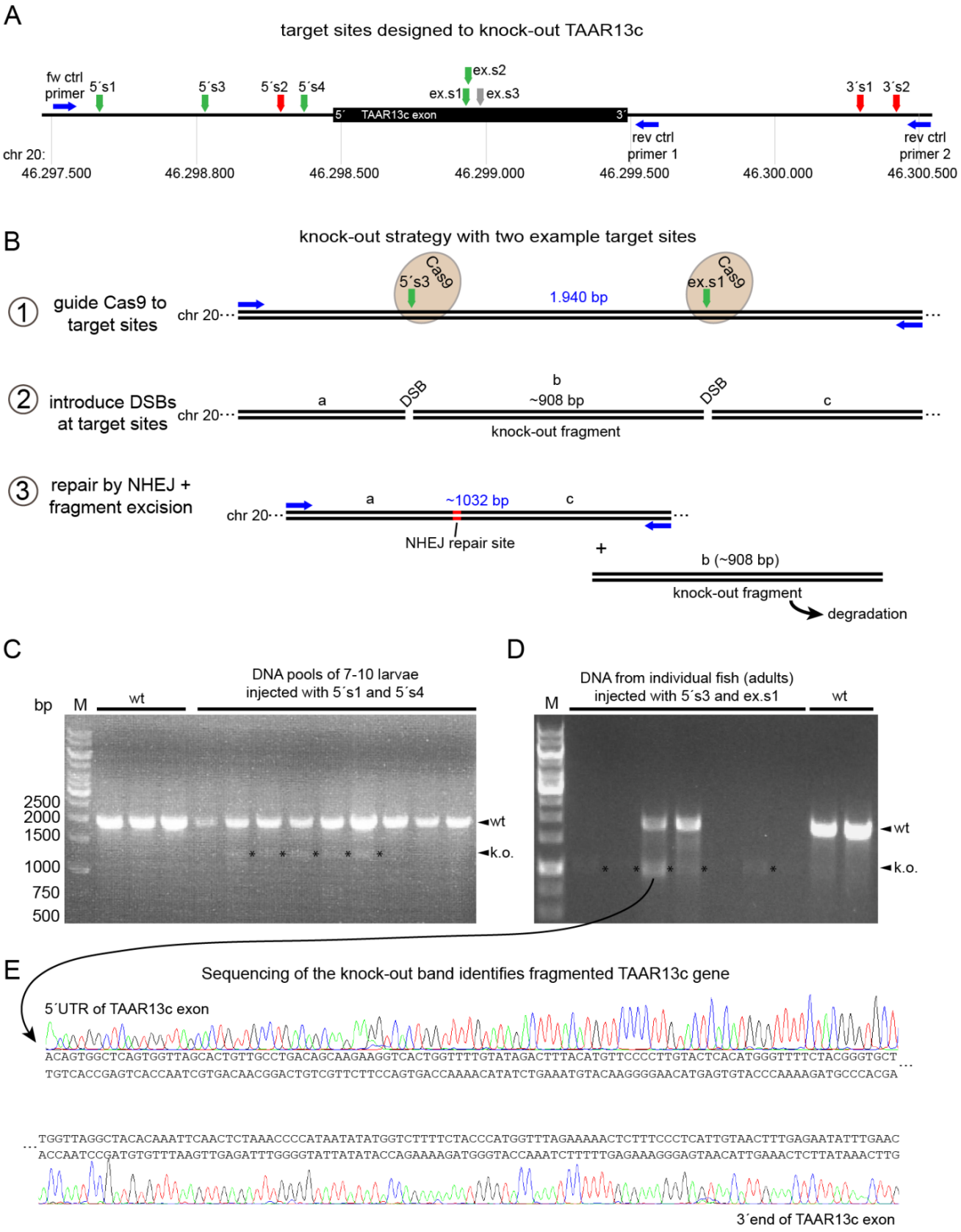

Figure 3.26: CRISPR/Cas9-mediated knock-out of TAAR13c (legend on next page)

Figure 3.26: CRISPR/Cas9-mediated knock-out of TAAR13c. A) Genomic locus of the TAAR13c gene on chromosome 20. Black bar indicates the TAAR13c exon. Vertical arrows indicate the location of the gRNA target sites designed in this study. Target sites marked green have created knock-out bands in at least one target site combination. Target sites marked red did not result in knock-out bands. Blue arrows indicate the position of the control PCR primers. B) Knock-out strategy: 1) Specific guide RNAs navigate Cas9 to two adjacent target sites. 2) Two double strand breaks (DSB) are introduced within the region of interest. 3) The loose ends can be joint together by non-homologous end joining (NHEJ) leading to the excision of the DNA sequence enclosed by the DSBs. C) Cas9 co-injection of target sites 5´s1 and 5´s4 results in knock-out PCR amplicons in 5/9 pooled DNA samples. The knock-out band is absent in the wildtype control. D) Cas9 co-injection of target sites 5´s3 and exon-s1 results in knock-out PCR amplicons in 5/7 fin-clip DNA samples from individual adults. 3/7 samples show only the knock-out band, suggesting a homozygous knock-out. E) Sequencing result from one of the knock-out bands shows, that it is the shortened TAAR13c fragment, lacking the cutout sequence.

Therefore, guide RNAs for 3´UTR target sites were combined with those for exon-targeting guide RNAs in order to knock out at least half of the TAAR13c exon sequence and thereby prevent its expression. 5´UTR site 3 in combination with either site within the exon led to a knock-out band in the PCR control (compare Table 3.1).

As exon-targeting site 2 had the fewest predicted off-targets, this site was used for further experiments. Injected larvae were raised to adulthood. Genomic DNA from single fish was isolated from a fin clip biopsy and tested for knock-out bands with the control primers. Figure 3.26.D shows the PCR fragments obtained with fin clip DNA of seven injected fish and two wildtype fish. Five out of seven injected animals showed the expected knock-out band of around 1.000 bp. The band was in some cases very weak but still visible. Three of these five animals showed only the knock-out band but the wildtype band expected to appear slightly below the 2.000 bp marker band. The knock-out band was absent in the wildtype control DNA from the uninjected siblings, which only showed the wildtype band (1.940 bp). The knock-out bands were cut out from the gel, purified and sequenced from both ends using the control primers, which also had been used for the PCR. In fact the sequencing results revealed that the sequenced fragment in deed is a shortened piece of the targeted TAAR13c gene in all fragments analyzed, strongly suggesting that the targeted sequence between the target sites has been knocked-out from the genome. For animals showing only the knock-out band in the PCR a homozygous, bi-allelic knock-out can be assumed. For animals showing both the knock-out band and the wildtype band a heterozygous, mono-allelic knock-out can be assumed.

Given a germline transmission of the knock-out event, the animals obtained in these experiments can be used as founders for a TAAR13c knock-out line, which can be used for the further analysis of the physiological role of TAAR13c and the underlying neuronal circuitry.

Taken together these results show the suitability and functionality of this knock-out approach for the TAAR13c gene. A specific knock-out using the CRISPR/Cas9 system with only one target site might also be applicable as new and seemingly specific target sites seem to be available despite the high homology of the TAAR13 genes.

3.5 Evolution of trace amine-associated receptors in the fish lineage

Olfactory receptors of the TAAR family regulate several important behaviors both in tetrapods and teleosts (Ferrero et al., 2011, Ferrero et al., 2012, Li et al., 2013, Hussain et al., 2013). Aversive behavior seems to be generated by class II TAARs both in tetrapod and teleost species. Remarkably, class II appeared to be lost in more modern fish based on a study in five fish genomes (Hussain et al., 2009). In the meantime many more genomes have become available and a few studies looking at subsets of species have been published (Libants et al., 2009, Azzouzi et al., 2015), but in general the evolution of this important receptors family is not very well understood yet.

Here, a systematic study of TAAR gene evolution in fish has been performed to determine the evolutionary origin of TAARs and to trail the evolutionary fate of class II TAARs in modern fish.

The results represent a thorough analysis of all fish genomes currently (February 2017) available in NCBI. The respective species cover a wide evolutionary range, from jawless vertebrates (2 species) over cartilaginous fish (3 species) and early-diverging bony fish (*Lepisosteus oculatus*, *Scleropages formosus*) to a broad range of teleost species representing many of the major phylogenetic subdivisions in this most numerous clade of all vertebrates.

3.5.1 Overview of TAAR gene evolution with emphasis on origin and class II TAARs

The NCBI genome databases of all available fish species have been searched using zebrafish TAAR13c as query sequence for tBLASTn search. Predicted amino acid sequences of candidate genes matching our criteria (E-value of 10-20 or lower, min. 200 amino acids sequence length) were used to generate a phylogenetic tree (PhyML) using known TAAR genes of class I, II, and III, ORs and several aminergic receptors as references in a first step. In that way potential members of TAAR class II were identified and archived. All newly found class II TAARs were put into one final phylogenetic tree (Figure 3.27).

Interestingly, in almost all fish species we also found a gene ancestral to TAARs, which did not fall into either of the known TAAR classes. In the two jawless fish - both are lampreys, *Petromyzon marinus* and *Lethenteron camtschaticum* - this ancestral gene underwent a heavy expansion, which is typical for olfactory receptors. Lampreys do not possess any TAARs though.

We termed these ancestral genes, TAAR-like genes (TARL), because they do not exhibit the characteristic TAAR motif (compare Figure 3.28), but they clearly share a common ancestor with all TAARs. All TARL genes found were also included into the final phylogenetic tree (Figure 3.27).

As the literature about the evolutionary origin of TAARs is inconsistent - the origin was described to be in chordates, vertebrates, or jawed vertebrates -, we also tried to address the question where TAARs (and, as we found, also TARLs) originated from. Therefore ancestral TARLs were used as query in a tBLASTn search in several chordates (lancelets), hemichordates (acorn worms) and echinoderms (incl. sea stars) that were available in the NCBI databases. The resulting sequences were merged into one phylogenetic tree together with several aminergic receptors that served as outgroup in the final tree. The outgroup comprises aminergic receptors from various vertebrate and invertebrate species and include adrenergic, histaminergic, serotonergic, cholinergic and dopaminergic receptors. The choice of outgroup genes is of particular importance as it can lead to incorrect conclusions in case of missing links. A full list of the outgroup genes and their amino acid sequences as well as all other sequences included in the phylogenetic trees below is provided on the supplementary CD.

Figure 3.27 shows the final tree containing all class II TAARs found in this study, all TARLs from lamprey and jawed fish found, several HTR4 genes and an appropriate number of aminergic receptors, that serve as an outgroup.

The search for the right outgroups and ancestral genes for Figure 3.27 already lead to conclusions about the origin of TAARs. TAAR and TARL genes originate from a duplication of the HTR4 (5-hydroxytryptamine receptor 4) gene, which is still present in humans. HTR4 itself can be first found in hemichordates and is absent in ciona, a tunicate. Lancelets, as a representative of the first chordates, possess neither TAARs nor TARLs, while lampreys already have a large number of TARLs. In conclusion, TAARs and TARLs likely have a most recent common ancestor in vertebrates as a single gene, as also suggested by the tree.

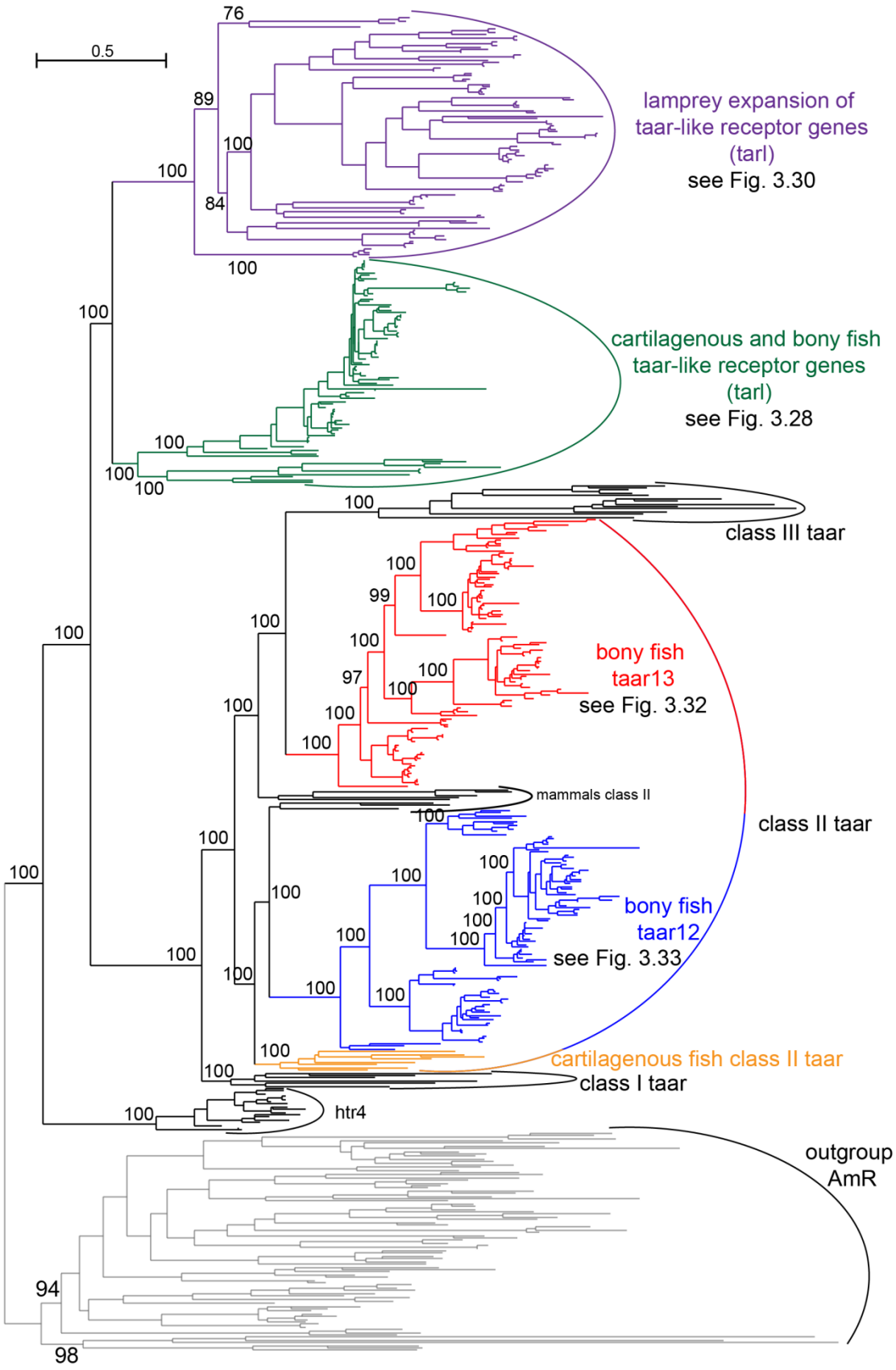

Figure 3.27: The origin of TAARs and fate of class II in a phylogenetic tree (legend on next page).

Figure 3.27: The origin of TAARs and fate of class II in a phylogenetic tree TAARs originate in a duplication of HTR4 and share a MRCA with the ancestral TAAR-like genes (TARL). TARLs expanded heavily in jawless fish (lamprey, purple) but not in other fish (green). TAARs are not present in jawless, but heavily expanded in jawed fish, especially teleosts. Ancestral class II TAARs are already present in cartilaginous fish (orange). TAAR12 (blue) and TAAR13 (red) are the only class II members in bony fish often displaying lineage specific expansions.

3.5.2 Olfactory functionality arose twice independently in the TAAR family

After the initial duplication of their most recent common ancestor gene TARLs and TAARs took a different route in jawless and jawed vertebrates, respectively. While TARLs heavily expanded in the jawless lampreys (for details see Chapter 3.5.3 and Figure 3.29) likely taking up olfactory function (Libants et al., 2009), they show very slow evolutionary dynamics in all jawed vertebrates inspected, where each species usually possesses only one, in some cases two and in one species three TARL genes (for details see Chapter 3.5.4 and Figure 3.30).

TAARs on the other hand underwent a major expansion in the jawed vertebrates. Most of the TAAR genes known to date took up olfactory functions, with the exception of TAAR1 (Borowsky et al., 2001). TAARs can be subdivided into three classes (I, II, III) and often even display species specific expansions (Hussain et al., 2009).

We further investigated the evolution of class II TAARs in the fish lineage, because this class is known to be involved in important behavioral responses to amine stimuli in fish (Hussain et al., 2013, Li et al., 2015). When looking closer at the evolution of this class in fish, we found that, with one exception, class II comprises only two members in all 81 species that were covered. TAAR12 shows early as well as late gene loss events and is absent in all neoteleosts (for details see Chapter 3.5.6 and Figure 3.32). TAAR13 is present in all early-derived fish and, other than suggested previously (Hussain et al., 2009), still can be found in a number of neoteleosts, although it has been lost in the majority (for details see Chapter 3.5.7 and Figure 3.33).

Detailed phylogenetic trees highlighting TARLs in jawless fish and jawed fish, respectively, and class II genes TAAR12 and TAAR13 are given below.

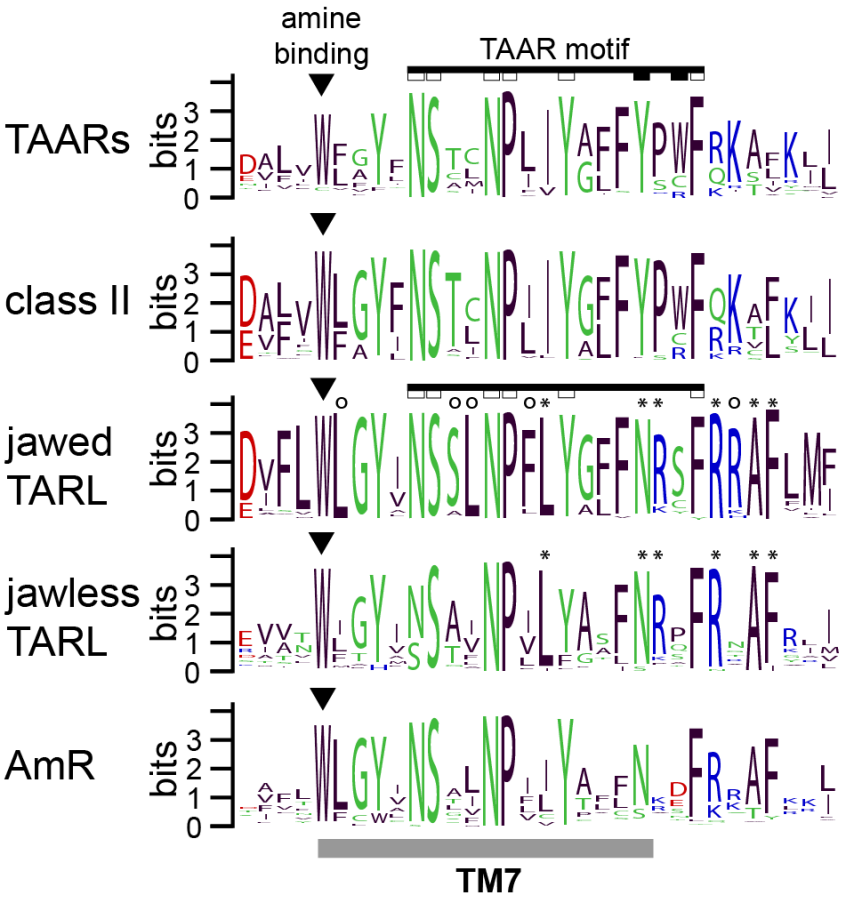

Figure 3.28: Amino acid sequence conservation in TM7 and adjacent regions of TAARs, TARLs and aminergic receptors. Sequences from TAARs in general, class II TAARs in specific, jawed fish TARL, jawless fish TARL and the aminergic receptor outgroup were used to create a sequence logo. The degree of conservation is reflected by the height of the letters in the amino acid code (maximal height = most conserved). The amine binding motif is conserved in all receptor classes shown. The TAAR-defining motif (Lindemann and Hoener, 2005) is not present in TARLs and aminergic receptors.

3.5.3 Lamprey species possess up to 50 TAAR-like genes

Two genomes from jawless fish were available at NCBI. Both of the species are lampreys, the sea lamprey *Petromyzon mariunus (Pm)* and the arctic lamprey *Lethenteron camtschaticum* (*Lec*). Transcriptome data from a third species, the river lamprey *Lampetra fluviatilis (Laf)*, was also available and searched for potential TARL genes. The resulting genes are included into the detailed tree given below (Figure 3.29).

In the arctic lamprey 51 TARLs were found. Such a large expansion is typical for olfactory receptors and can be found for ORs and TAARs in other lineages. In fact one of the sea lamprey TARL genes (misidentified as TAAR) was shown to be expressed in the OE (Libants et al., 2009). 32 TARL genes were found in the sea lamprey and 9 TARL genes in the river lamprey transcriptome. Often orthologous genes were found in at least two of the lamprey species. Additional species specific duplications may have led to a higher number of TARL genes in the arctic lamprey when compared to the number of TARL genes in the other lamprey species.

3.5.4 Slow dynamic in the evolution of TAAR-like genes in jawed vertebrates

In contrast to the jawless fish, TARLs did not undergo an expansion in the jawed fish species analyzed. Usually each of the jawed fish species contained only one TARL gene (66/73 jawed fish). In some cases two copies of this gene (6/73 jawed fish) and in one case 3 copies (salmon, *Salmo salar*) were found. There seemed to be an early gene duplication event before the divergence of cartilaginous and bony fish, as both a shark (*Rhincodon typus*) and several bony fish (e.g. eel, salmon, and tuna) possess the second TARL gene. Salmon is the only species with three TARL genes, with a duplication of TARL1.

After the duplication most of the species seem to have lost the second copies of the gene. Note that the TARL gene is also present in tetrapods, here two frog species (*Xenopus laevis* and *Xenopus tropicalis*) and does not expand there either. A detailed phylogenetic tree highlighting the jawed fish TARL gene relationships is provided in Figure 3.30.

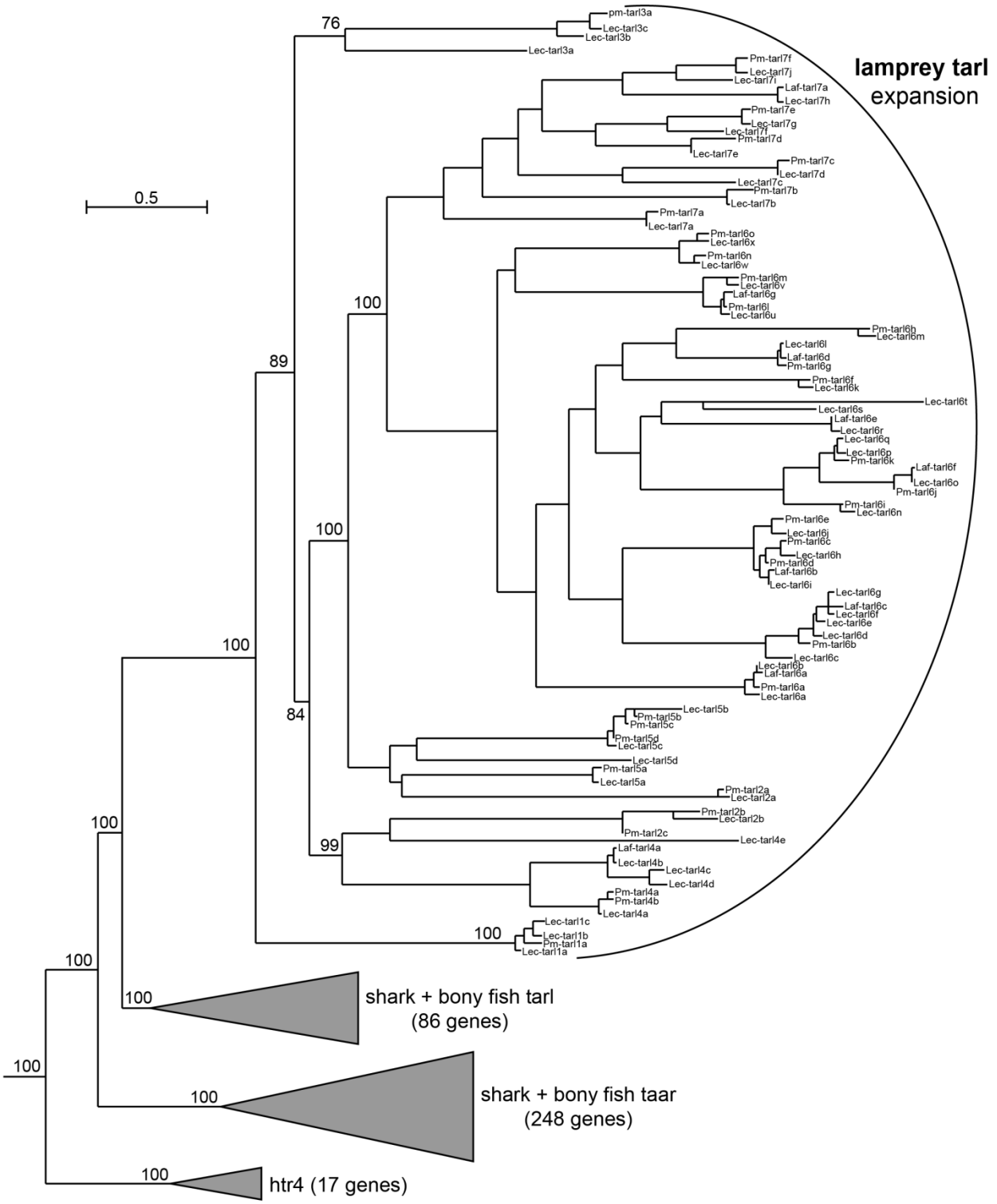

Figure 3.29: Expansion of TAAR-like genes in 2 lamprey species, a family of jawless fish. 51 genes were found in the arctic lamprey (*Lec*). 32 genes were found in the sea lamprey (*Pm*). 9 genes could be derived from river lamprey (*Laf*) transcriptome data. Scale bar = 50 % amino acid substitutions per site.

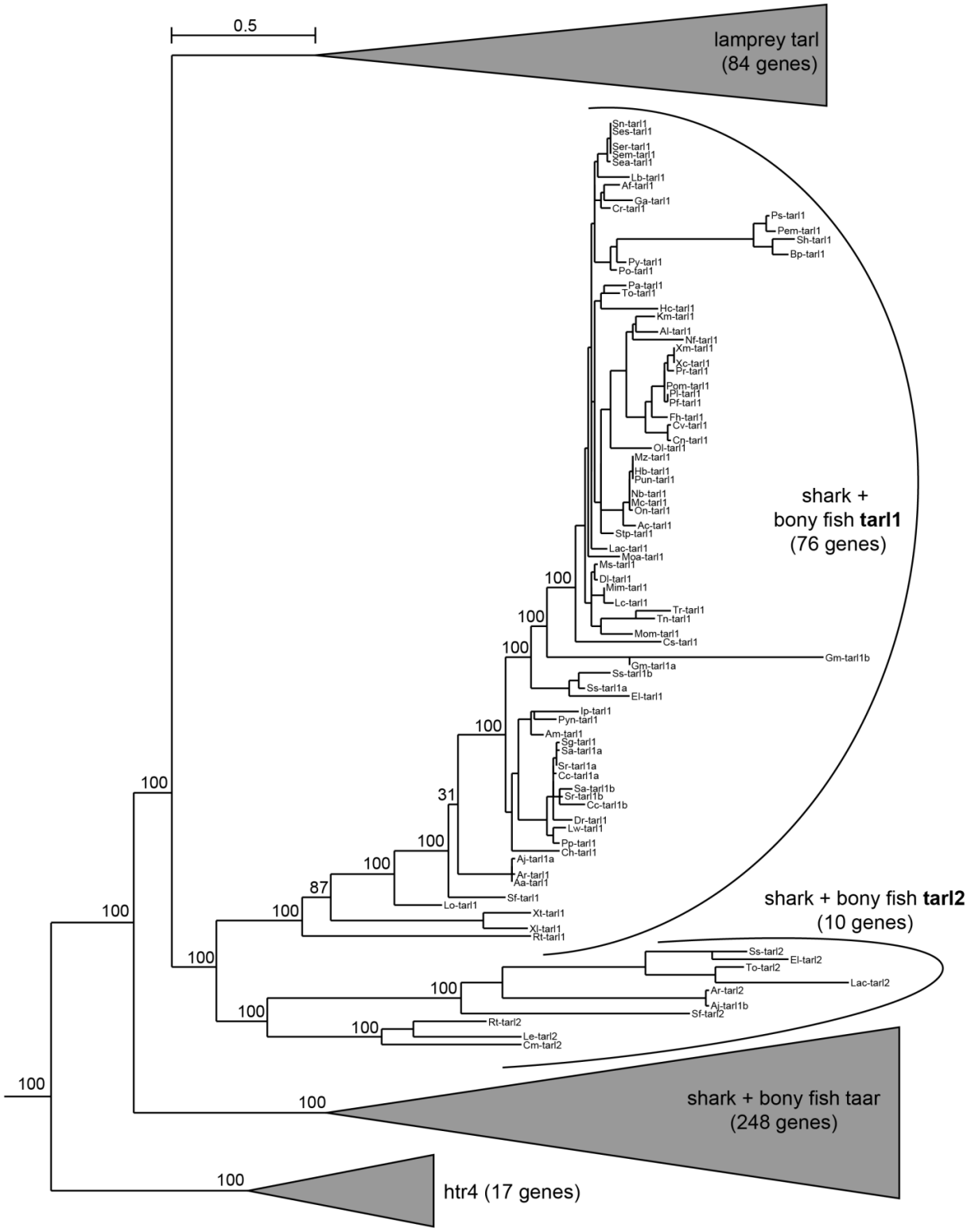

Figure 3.30: Slow dynamic in the evolution of TAAR-like genes in jawed vertebrates. Jawed fish possess either one, maximum two members of the TARL gene family. After an early duplication the second copy was lost in most of the species analyzed. The salmon is the only species here with a third TARL gene as a result of a species-specific duplication. Two frog species (*Xenopus laevis* and *tropicalis*) also possess a TARL gene. Scale bar = 50 % amino acid substitutions per site.

3.5.5 The zebrafish TAAR-like gene is expressed in the brain and other organs

Our phylogenetic study found that the zebrafish genome harbors one TARL gene, hence called TARL1. Because TARL genes have not been studied at all in jawed fish, we wanted to find out if and where TARL1 is expressed in our model organism.

Primers targeting the gene were used to perform a reverse transcriptase PCR (RT-PCR) with cDNA obtained from RNA of different organs of the zebrafish. As aminergic receptors as well as TAARs are known to be primarily expressed in neuronal tissue and the olfactory epithelium, respectively, we first focused on the brain and the olfactory epithelium (OE). cDNA obtained from the trunk was used to check, whether TARL1 is expressed in other parts of the body in general.

The RT-PCR shows that TARL1 is clearly and primarily expressed in the brain. Weaker bands and therefore lower expression levels can be observed in the OE and also the trunk (see Figure 3.31.A; first three lanes). Primers against actin (actb1) were used as a measure for the input cDNA levels. Actin expression levels are equal in all three tissues tested, supporting the reliability of the differences observed in the expression levels of TARL1. To exclude the possibility of genomic DNA (gDNA) contaminations in the cDNA samples, a PCR using gDNA together with the actin primers was performed as well. The amplicon includes an intron and is therefore bigger than the actin amplicon obtained with cDNA as a template (see Figure 3.31.A; right side). As the larger band is absent in the cDNA PCR, a contamination with gDNA can be excluded. Zebrafish TARL1 is mono-exonic. Therefore, if a PCR with TARL1 primers is set up with gDNA, the band appears at the same height as when cDNA is used.

To find out where exactly TARL1 is expressed a DIG-labelled *in situ* hybridization RNA probe against TARL1 was generated using the same primers as used for the RT-PCR, but now containing a T3 promotor site. In that way antisense (to show the gene expression) and sense (negative control) probe could be generated using T3 RNA polymerase (Figure 3.31.B).

These probes were used for *in situ* hybridizations in the adult OE as well as 5 dpf whole mount zebrafish larvae (Figure 3.31.C + D, respectively). Using these probes no TARL1 expression could be observed in the adult OE.

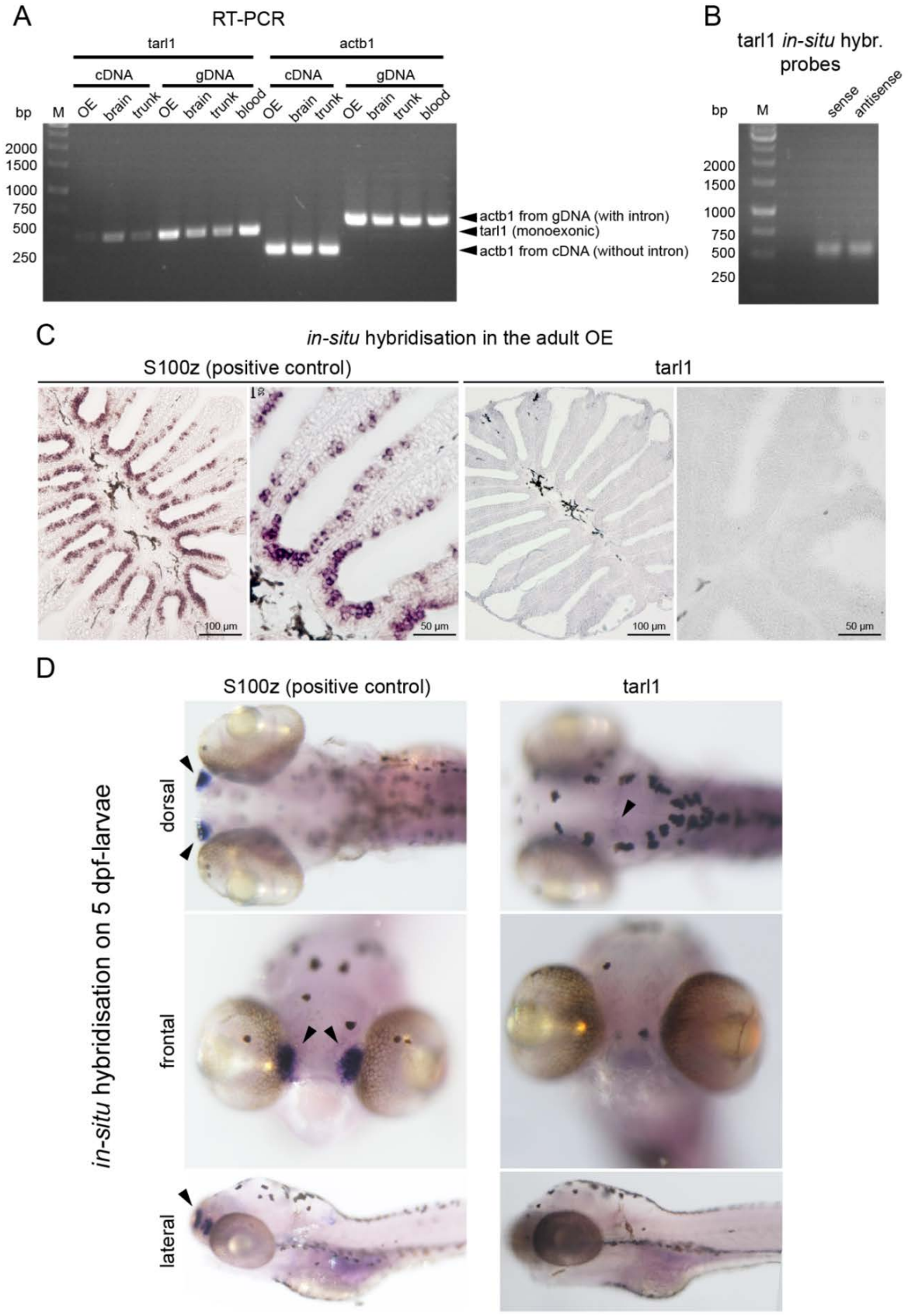

Figure 3.31: Expression of the zebrafish TARL1 gene (legend on next page).

Figure 3.31: Expression of the zebrafish TARL1 gene. A) RT-PCR using cDNA from different tissues to determine where TARL1 is expressed. Actin (actb1) was used as a loading control. PCR on gDNA was used to exclude gDNA contaminations in the cDNA. B) *In situ* hybridization probes (sense and antisense) against TARL1. C) *In situ* hybridization on the adult OE. S100z, used as a positive control, is expressed in OSNs. TARL1 is not expressed in the OE. D) *In situ* hybridization on 5 dpf larval zebrafish. S100z, used as a positive control, is expressed in the nose. TARL1 has a low expression profile. TARL1 might be expressed at the midbrain-hindbrain boundary.

Similarly no clear expression pattern could be observed in the larvae. In some of the larvae there appeared to be a weak staining of distinct cells at the midbrain hindbrain boundary (see Figure 3.31.D, dorsal view). In both the OE and the larvae a probe against the OE-specific gene S100z was used as a positive control. S100z is strongly expressed in OSNs of the adult as well as larval OE.

A second primer pair designed for TARL1 also showed the expression in a RT-PCR, but failed to provide a clear expression pattern when used for *in situ* hybridization (data not shown).

Taken together the RT-PCR clearly shows the expression of TARL1 in the brain and at lower levels in the OE and lower body, but the *in situ* hybridization failed to further determine the expression pattern of TARL1.

3.5.6 Early and late losses of the ancestral *taar12* class II gene during ray-finned fish evolution

Class II TAARs are involved in the generation of physiologically relevant behaviors in mice and fish (Li et al., 2013, Hussain et al., 2013). We found ancestral class II TAAR genes in three different species of cartilaginous fish, including a true shark (whale shark, *Rhincodon typus*), a chimaera (Australian ghostshark, *Callorhinchus milii*), and a ray (little skate, *Leucoraja erinaceae*). Cartilaginous fish class II TAARs form a separate clade within the fish class II and do not have any direct orthologues in bony fish (compare Figure 3.32; labelled orange)

One of the two TAAR class II members in bony fish is TAAR12. A phylogenetic tree of TAAR12 genes found in the 81 fish species genomes available on NCBI is provided in Figure 3.32. The origin of TAAR12 is to be found after the divergence of lobe- and ray-finned fish, as TAAR12 is absent in the tetrapod lineage.

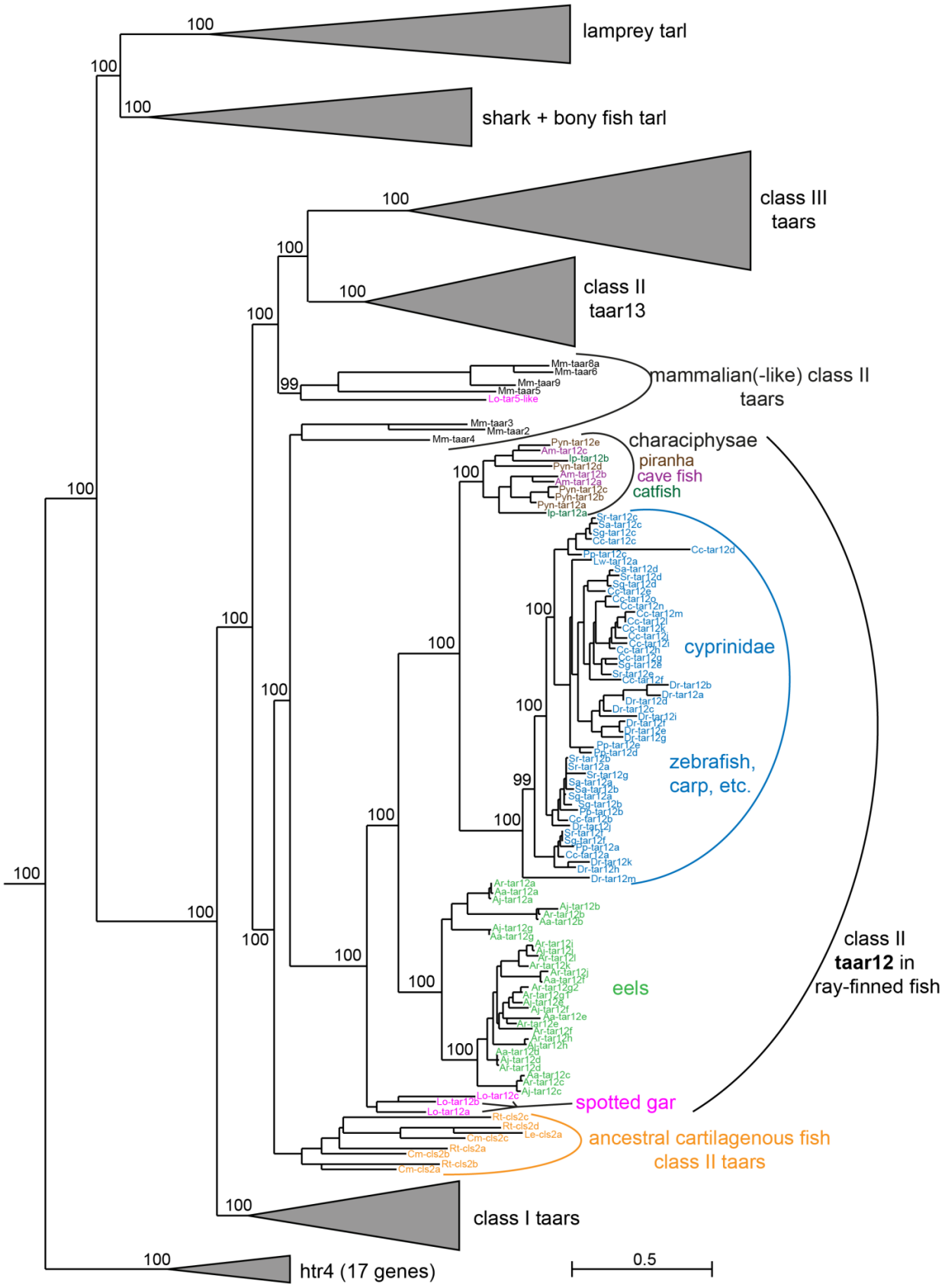

Figure 3.32: Phylogenetic tree of TAAR12 genes found in fish genomes (legend next page).

Figure 3.32: Phylogenetic tree of TAAR12 genes found in fish genomes. TAAR12 is present in most early-derived bony fish, with some exceptions, where it has been lost individually. The MRCA of all euteleostomorpha also lost TAAR12, leading to the absence of TAAR12 in all recent neoteleosts. Spotted gar, eels, cyprinidae and characiphysae (piranha, cavefish, catfish) display genus- or family-specific expansions of TAAR12. Cartilaginous fish possess ancestral class II TAARs different from TAAR12 and TAAR13. Scale bar = 50 % amino acid substitutions per site.

TAAR12 is present in the majority of early-derived bony fish like spotted gar (*Lepisosteus oculatus*), eels (*Anguilla*), all cyprinidae and characiphysae, but has been lost independently in some of them, e.g. the Asian bonytongue (*Scleropages formosus*) and the herring (*clupea harengus*). Importantly, none of the fish in the late-derived neoteleost lineage possesses the TAAR12 gene. In fact the TAAR12 gene must have been lost shortly after the emergence of the Eueleosteomorpha, which include a vast number of recent species. Figure 3.34 illustrates which of the considered species have and don´t have TAAR12.

Genus or family specific expansions of the TAAR12 gene are very common in those clades that retained the gene. Such expansions can for example be found in the rather archaic spotted gar (3 genes) and in eels (up to 13 genes), but also in the families of cyprinidae (including zebrafish, carp, etc.) and characiphysae (piranha, catfish, cavefish), which together form the clade of otophysi (see Figures 3.33 and 3.34).

3.5.7 The ancestral *taar13* gene is conserved in all early-derived fish and is still present in genomes several neoteleost species

The second class II member known in fish to date is TAAR13. In zebrafish this class is responsible for the detection of several diamines and mediates aversive behavior (Li et al., 2015, Hussain et al., 2013).

A phylogenetic tree of TAAR13 genes found in the 81 fish species genomes available on NCBI is provided in Figure 3.33. The origin of TAAR13 is to be found in a duplication of a class I TAAR gene in the early jawed fish lineage, which later on underwent another duplication resulting in a lobe-finned class II branch (harboring TAAR5-9) and the TAAR13 branch.

TAAR13 is present in all bony fish, starting from spotted gar (*Lepisosteus oculatus*) up to cod *(Gadus Morhua)*. Pike (*Esox Lucius*), salmon (*Salmo salar*), and cod possess TAAR13 genes, while their MRCA already had lost TAAR12, the other class II member present in fish.

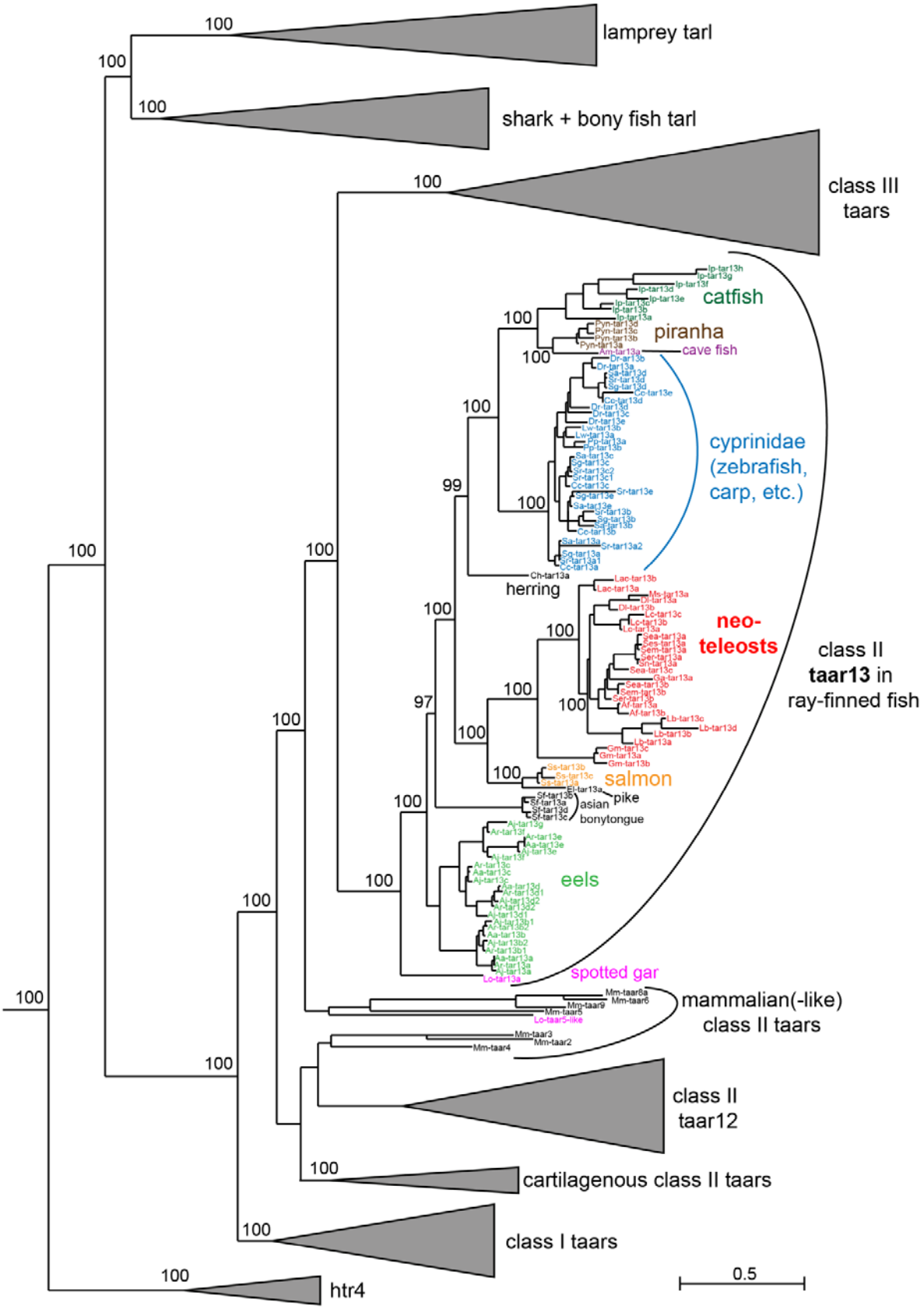

Figure 3.33: Phylogenetic tree of TAAR13 genes found in fish genomes (legend on next page).

Figure 3.33: Phylogenetic tree of TAAR13 genes found in fish genomes. The TAAR13 branch emerged from an early TAAR class I duplicant. TAAR13 is present in all early-derived bony fish. In the closely related cyprinidae it displays family specific expansions. Otherwise TAAR13 mostly expanded genus- or even species-specific (eels, asian bonytongue, salmon, piranha, catfish). In some species only one gene was found (e.g. spotted gar, pike, cavefish). Importantly, several neoteleosts have retained and some even expanded TAAR13. Side note: Spotted gar features a mammalian-like TAAR5 gene, highlighting its phylogenetic proximity to the lobe finned lineage. Scale bar = 50 % amino acid substitutions per site.

Surprisingly, we also found TAAR13 in several neoteleost species, which, in a study on only 5 bony fish genomes, were previously reported to have lost class II TAARs completely (Hussain et al., 2009). Looking at dozens of species our study allows more certain statements about the losses and retention of these genes.

We even found TAAR13 in the stickleback, which was also looked at in the earlier study. Although it could be a pseudogene (see appendix for full amino acid sequence predictions) we are still certain about the retention of TAAR13 in the neoteleosts, as we found fully intact TAAR13 gene sequences in 11 out of 56 neoteleost species (percomorphaceae). This also entails, that TAAR13 has been lost at different points in the neoteleost lineage. At least six independent gene loss events are required to account for the situation found in this clade. Some of these TAAR13 gene loss events occurred rather early, e.g. in the MRCA of all ovalentaria, other loss events occurred later, maybe even genus-specific, e.g. in *Miichthys miiuy*.

Figure 3.34 illustrates which of the considered species have and don´t have TAAR13.

Interestingly the spotted gar, a very archaic bony fish closely related to the lobe finned (tetrapod) lineage ancestors, features a mammalian-like TAAR5 gene, highlighting its phylogenetic proximity to the lobe finned lineage.

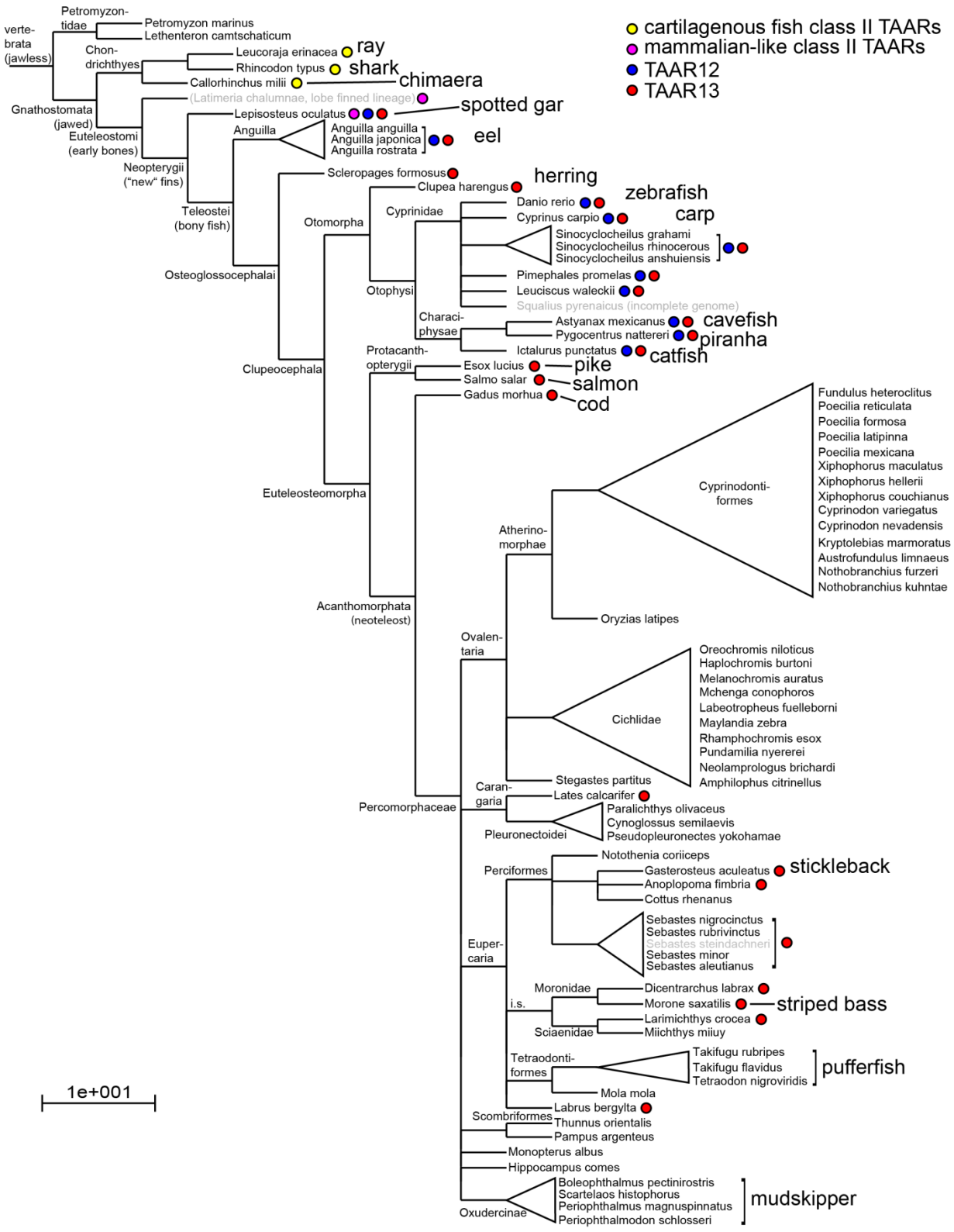

Figure 3.34: Summarizing phylogenetic tree on the evolution of class II TAARs in the fish lineage. Tree was obtained from NCBI taxonomy browser and includes all species, whose genomes were searched for class II TAARs here. Colors indicate if class II members were found in the respective species (yellow = cartilaginous type, magenta = mammalian like, blue = TAAR12, red = TAAR13).

4 DISCUSSION

The olfactory system of fish is capable of detecting a variety of different odor classes, many of which elicit distinct behavioral outputs. The study at hand investigates the perception of amine and diamine stimuli and the neuronal basis for behaviors induced by these odorants in the olfactory system of the zebrafish *Danio rerio*, which is a widely used model organism in biological research.

4.1 Amine and diamine odor stimuli are primarily processed by ciliated olfactory sensory neurons

Amines and polyamines represent an important odor class in aquatic organisms and often induce a behavioral response (Rolen et al., 2003, Hussain et al., 2013, Li et al., 2015). Amines were shown to activate trace amine-associated receptors (TAARs) in fish as well as tetrapods (Ferrero et al., 2012, Hussain et al., 2013). In mammals TAARs were shown to be expressed in ciliated neurons (Zhang et al., 2013), one of five (and possibly more) types of olfactory sensory neurons (Ahuja et al., 2014, Wakisaka et al., 2017). However, it was not known which OSN type expresses the large family of TAAR genes in fish.

Here we have analyzed the cellular localization of TAAR13c, which is of special interest, because it was the first fish TAAR to be deorphanized and linked to a specific behavior. TAAR13c is a high-affinity cadaverine receptor and mediates the aversive response to that odor (Hussain et al., 2013).

Co-localization of an antibody against TAAR13c with accepted markers for three different populations of OSNs - ciliated, microvillous and crypt neurons - showed that TAAR13c is indeed expressed only in ciliated neurons. Cells expressing TAAR13c are OMP-positive, a feature exclusive to ciliated neurons in zebrafish (Sato et al., 2005). Acetylated tubulin is a structural element of cilia and has been widely used to visualize cilia in OSNs and other cell types (Arikawa and Williams, 1993, Reiten et al., 2017). Using confocal microscopy on double IHC olfactory epithelia we confirmed, that TAAR13c OSNs express acetylated tubulin in their cilia. TAARs rely on second messenger signaling using the specialized $G\alpha_{olf}$ subunit, which distinguishes them from V1Rs and V2Rs for instance, which use a different Gα protein (Zhang et al., 2013). A preliminary study from another graduate student in the lab had suggested that G_{olf} is

co-localized with TAAR13c (Krishna Subramanian, 2017). We have repeated these experiments and re-assessed the co-localization of TAAR13c and $G\alpha_{olf}$ using higher resolution imaging. Indeed the dendritic knob of TAAR13c OSNs co-localized with the $G\alpha_{olf}$ signal. Taken together these results show the ciliated nature of the OSNs expressing the cadaverine-receptor TAAR13c.

We also wanted to know, whether the same is true for OSNs responsive to other amines. In close collaboration with the group of Prof. Dr. Ivan Manzini we developed a straightforward Ca^{2+}-imaging technique enabling us to visualize the changes in intracellular calcium levels as an indicator for neuronal activity to an odor in a tissue explant of the olfactory epithelium. This is the first time odor-evoked activity in single OSNs has been measured *in situ* in any fish species.

In short, OEs were sliced horizontally to be able to access a layer of OSNs with a confocal microscope. Then, cells were loaded with a calcium sensitive dye and repeatedly stimulated with odorant solutions while keeping them in a constant flow of fluid. We observed that the composition of this extracellular solution was crucial for obtaining cellular responses. We were not able to detect any signals using the Ringer solution commonly used for *Xenopus laevis* explants. Instead we found artificial cerebrospinal fluid (ACSF) to be the optimal solution. Indeed, ACSF was previously used successfully for activity imaging in zebrafish OB preparations (Friedrich and Korsching, 1997). ACSF contains glucose, which provides an additional but seemingly essential energy source to the cells in the explant. Odors were delivered into the constant flow of ACSF with a concentration of 10 - 100 µM.

Using this technique we could detect odor-mediated neuronal activity in single OSNs within the OE. Especially a mix of amines was found to represent a reliable stimulus, repeatedly evoking stable signals in a large number of OSNs. The diamines cadaverine and putrescine rarely generated Ca^{2+}-increases, but these signals were never reproducible upon repeated stimulation. This, and the fact that also single amine odorants often failed to evoke signals (data not shown), could be based in the sparse expression of individual TAAR receptors, including the cadaverine receptor TAAR13c (Hussain et al., 2013). ATP was used as a positive control odor, as it had already been used in studies of the olfactory system of the frog *Xenopus laevis* (Dittrich et al., 2014). ATP activated a population of horizontal basal cells in our experiments, which appeared very similar to cells labelled the stem cell marker α-PCNA. A similar population of basal cells was activated in the frog nose upon ATP stimulation (Dittrich et al., 2014). Surprisingly, we did not obtain reliable signals in response to amino acid odors, which are thought to be an important

odor class in aquatic animals and have already been shown to activate specific subsets of cells in the zebrafish OE (Friedrich and Korsching, 1998). The reason remains elusive, although it is conceivable that the AM ester-based method of dye loading employed here may be less efficient for amino acid-responsive cells.

In total we were able to record amine- and ATP-responses from several hundreds, respectively thousands of cells from the zebrafish OE. In order to find out, if the amine response is indeed carried by ciliated neurons - as shown by us in another set of experiments for cadaverine - we determined morphological parameters of the activated OSNs and compared them to fluorescently labelled OSNs of known types. In specific, we measured the laminar height of microvillous and ciliated OSNs, expressing fluorescent reporter genes under the control of TRPC2 and OMP promoter, respectively, and compared the cumulative distributions (ECDFs) to the laminar height of amine sensitive OSNs from the Ca^{2+}-imaging. The average laminar height is clearly different for each of the three main OSN types (ciliated, microvillous, and crypt) (Ahuja et al., 2014). The results showed that the ECDFs for laminar height of ciliated and amine sensitive neurons are essentially the same, strongly suggesting that the amine responses are indeed carried by ciliated neurons. Similarly we compared the distributions of ATP-sensitive and PCNA-labelled horizontal cells and also found them to be the same, suggesting that both correspond to the same population. Of course a direct co-labelling is still required to have the ultimate proof, which unfortunately is not possible with Ca^{2+}-imaging. Horizontal basal cells serve as stem cells for the regeneration of olfactory sensory tissue in case of injury (Joiner et al., 2015) and in tetrapods might rely on ATP-signaling (Hassenklover et al., 2009). Further research in the topic of olfactory regeneration is needed to answer these questions.

To sum up, using two independent approaches we showed that the sensation of monoamine and diamine stimuli in zebrafish both rely on the activation of ciliated OSNs, similar to the situation in tetrapods. This constitutes a remarkable degree of conservation across at least 430 million years of diverging evolution (Blair and Hedges, 2005).

4.2 Amine and diamine representations in the olfactory bulb

Axons from OSNs expressing the same olfactory receptor project into the olfactory bulb via the olfactory nerve and converge onto so called glomeruli. In these glomeruli the sensory information is transferred to second order neurons, which transmit the signal into the higher brain areas (Kermen et al., 2013). Therefore, the OB is the first important relay station for olfactory processing in the central nervous system.

Some progress has been made in the morphological and functional characterization of the glomerular map in zebrafish (Sato et al., 2005, Braubach et al., 2012). Several studies have identified glomeruli being activated by specific ligands and in some cases even connected these findings to a behavioral response. For example PGF2α, a steroid hormone, activates a large ventral glomerulus (Friedrich and Korsching, 1998) and induces male courtship behavior (Yabuki et al., 2016). The lateral glomerulus lG2 is activated by adenosine and induces feeding associated behavior (Wakisaka et al., 2017). Glomeruli of the lateral chain have been found to process amino acid stimuli (Friedrich and Korsching, 1997). The zebrafish OB contains several clusters of glomeruli of different sizes. Immunohistochemical stainings have been used to visualize the distribution and cluster-like organisation of glomeruli in the zebrafish OB, finding that glomeruli are located in fixed clusters with several large glomeruli being re-identifiable across individual animals (Braubach et al., 2012).

Here, we set out to identify the glomerular clusters responsible for the detection of amines in zebrafish and furthermore, if possible, pinpoint specific glomeruli processing cadaverine stimuli. Because we knew that pERK is a reliable marker for odor-induced neuronal activity in the OE at least for cadaverine (Hussain et al., 2013), we extended this method to the OB in order to identify the glomeruli processing specific odorant stimuli. Because of the high sensitivity of olfactory receptors, it is of major importance to guarantee experimental conditions free of any inadvertent stimuli, which might lead to a false positive result. We reevaluated the experimental conditions for odor stimulation, as we experienced high background pERK levels and inconsistencies in the glomerular labelling, probably due to unwanted odors present in the water. Distilled water, ran through a reverse osmosis filter and re-supplemented with sea salts turned out to minimize pERK background levels and ensure a reproducible pERK signal in response to stimulation with different odors or odor mixes. Different from previous experimental procedures (Krishna Subramanian, 2017), fish were not stimulated in falcon tubes, but in glass vessels containing 150

ml of water. This precaution was taken to reduce stress in the animal during the acclimatization and stimulation phase.

Using this setup we were able to identify a single glomerulus in the dorso-lateral cluster of glomeruli (dlG) of the zebrafish olfactory bulb being activated in response to stimulation with low concentrations of cadaverine (3µM). The glomerulus had a fixed position and was identifiable by its relative coordinates in the anterio-posterior and ventro-dorsal dimensions. As TAAR13c was found to be the receptor with the highest affinity for cadaverine (Hussain et al., 2013), we suppose that this glomerulus is formed by TAAR13c expressing axons. A direct co-labeling, e.g. expression of a fluorescent reporter gene in TAAR13c OSNs, has to be provided yet. The TAAR13c antibody was not able to label the glomerulus. With the rise of CRISPR/Cas9 knock-in techniques, transgenic labeling of single receptor OSN populations is becoming increasingly interesting in general and could provide a practical tool for the delineation of axonal projections in future experiments.

In order to exclusively label the single cadaverine-responsive glomerulus with pERK we had to decrease the cadaverine concentrations, which were used in an earlier study to activate TAAR13c expressing neurons (from 10 µM to 3 µM) (Hussain et al., 2013). Using cadaverine concentrations higher than 3 µM we observed multiple dlG glomeruli being labelled by pERK. Stimulation with 100 µM of cadaverine resulted in a pERK signal covering almost the entire dlG cluster. At concentrations this high other receptors with a lower cadaverine-affinity might be activated by the ligand in a less specific manner. This additional receptor recruitment is selective for OSNs projecting only to the dorso-lateral cluster though. The additional receptors recruited might be other amine receptors, presumably TAARs. The dorso-lateral cluster of glomeruli was also activated by a mix of 12 different monoamines, which had already been used in the Ca^{2+}-imaging experiments and was shown to activate ciliated type OSNs. Knowing that one of the major projection targets of ciliated OSNs is the dlG cluster (Sato et al., 2005), we can now propose that the dlG cluster of glomeruli is formed by axons from amine-sensing and thus most likely TAAR-expressing, ciliated OSNs. Fitting to this conclusion and to the fact that TAARs are one of the largest olfactory receptor families in zebrafish (Hashiguchi and Nishida, 2007) another study showed, that the dlG cluster harbors a large number of rather small glomeruli (Braubach et al., 2012), which could represent the clustered entity of TAAR glomeruli. PGF2α was used as a positive control in our pERK experiments. It was found to robustly activate a ventral glomerulus,

which had already been shown using another technique (Friedrich and Korsching, 1998). Water served as a negative control and did not lead to increased pERK levels in all but one cases.

It is unknown, if odor representations in the olfactory bulb are evolutionary conserved along the fish lineage. Therefore we chose the three-spined stickleback, a neoteleost species native to Europe, to serve as a comparative subject of study. The lineages of zebrafish and stickleback have evolved separately for an estimated time of 250 million years (Betancur et al., 2013). Labeling of synaptic vesicle protein 2 (SV2) provided a general overview of the glomerular organisation patterns in the stickleback OB. Similar to the zebrafish OB, it comprises several large clusters of glomeruli, among them a dorso-lateral cluster, a rather medial dorsal cluster, several anterior glomeruli, a ventro-lateral and a large ventro-medial cluster. A difference is the absence of glomeruli in the posterior medio-dorsal region of the OB - in zebrafish occupied by the mdG cluster - , which instead seemed to be packed with interneurons that get activated upon odor stimulation.

Regardless of the long-term evolutionary separation we observed conserved odor representations in the OBs of both model animals in a pERK based neural activity assay. As shown by us for zebrafish, amines and high cadaverine concentrations activated primarily the dorso-lateral and dorsal glomeruli in the stickleback OB. Food odor (corresponding to amino acid stimuli) mainly activated ventro-lateral glomeruli. Low concentrations of cadaverine (3 µM) induced pERK signal in a small dorso-lateral OB area, possibly corresponding to a single glomerulus. More studies are needed to describe the formation of odor maps in this interesting evolutionary context. Even in mice amine representations seem to be assigned to dorsal OB regions (Dewan et al., 2013).

4.3 Methods for analysis of the neuronal circuit activated by the death-associated diamine odor cadaverine

Deciphering the neuronal circuits leading to a defined behavioral output is one of the major tasks ahead in the studies of sensory systems. To this point most of the studies, as well as the analysis discussed so far in this study, have addressed the peripheral components of the neuronal circuits underlying olfactory mediated behaviors.

After the identification of amine and diamine-responsive OSNs and glomeruli, we wanted to know which brain areas are involved in the further olfactory processing of these stimuli. In a first set of experiments we again turned to pERK as an indicator for neuronal activity, as it was shown to successfully map whole-brain activity in response to sensory stimuli in the larval zebrafish (Randlett et al., 2015). Several studies have contributed to the identification of olfactory pathways (reviewed in Kermen et al., 2013) and also provided a nearly complete projectome of second-order neurons in the olfactory system of larval zebrafish (Miyasaka et al., 2014). Intriguingly, this projectome is missing the subset of dlG neuron projections, because the promoters used in that study to specifically express fluorescent markers are obviously not used by neurons in this cluster. As we found, the dlG cluster is mainly responsible for the detection of amines and might be targeted by TAAR-expressing neurons. Stimulation of 6-dpf zebrafish with cadaverine followed by pERK labeling provided an insight into the neuronal circuit activated by this diamine odor. Food odor was used as a positive control stimulus. For both odors we observed highly increased numbers of activated cells in the olfactory bulbs and the dorsal telencephalon, the latter representing a part of the brain also heavily targeted by projections from other glomeruli (Miyasaka et al., 2014). We were not able to image the deeper brain areas (e.g. hypothalamus and posterior tubercle) in whole-mount larval preparations due to microscope limitations. A more powerful microscope (e.g. multi-photon) will allow whole-brain imaging of these specimens.

Technical advancements in the field of microscopy (multi-photon and light sheet microscopes) and tissue clearing have enabled scientists to image larger tissues up to whole brains (Ahrens et al., 2013, Schultz et al., 2017, Jahrling et al., 2017). Combined with use of genetically encoded calcium indicators (GECIs), like GCaMP6, these advancements allow the analysis of complete neuronal circuits as has been done in the larval zebrafish brain (Quirin et al., 2016, Winter et al., 2017).

Here, we employed Ca^{2+}-imaging in the larval brain using GCaMP6s expressed under control of the pan-neuronal promotor *elavl3*. The GCaMP6 zebrafish lines were kindly provided by the group of Misha B. Ahrens from the Janelia Research Campus (Ashburn, USA). Using a conventional confocal microscope we were able to detect cadaverine-induced as well as spontaneous neuronal activity on a cellular level in different brain regions (OB, telencephalon, habenula) with a temporal resolution sufficient to visualize neuronal activity patterns. In future our lab will use these techniques to gain insight into the neuronal circuits activated by specific

odors. The “z-brain” atlas maps the expression of dozens of important marker genes onto a standardized 6-dpf larval brain (Randlett et al., 2015) and could be used to map the signals from Ca^{2+}-imaging experiments done in our lab in order to identify specific brain areas.

4.4 Cadaverine-induced behavior in juvenile versus adult zebrafish

As we employed techniques to map neuronal activity imaging in the 6 dpf larvae we wanted to know if the behavioral response to cadaverine is also already present at that age. The most important neuronal projections of the olfactory system are already present at 6 dpf (Miyasaka et al., 2014) and a variety of behaviors are already displayed (reviewed by Sumbre and Depolavieja (2014)).

Cadaverine was shown to induce an innate aversive behavior in adult zebrafish (Hussain et al., 2013). However, a previous study in our lab encountered manifold problems using a flow-channel behavior apparatus with larval zebrafish (Krishna Subramanian, 2017). Therefore, we wanted to establish a simpler behavioral test, similar to the setup used by Hussain et al. 2013, but now scaled down to smaller dimensions fitting the size of the zebrafish larvae.

After a short acclimatization 6 dpf zebrafish larvae were shown to display a normal swimming behavior in a 20 cm tank holding 10 ml of odor-neutral water. Stimuli were carefully applied through a tube by an experimenter not visible to the larvae. An odor solution volume of 0.5 ml was found to only minimally disturb the animals at the point of application. Larger volumes tended to mechanically “push” the larvae away from the odor source, which lead to freezing behavior in some cases (data not shown).

Food odor was used as a positive control odor, which indeed elicited attraction in the majority of the larvae with a significant shift of the positioning towards the odor source when looked at the pooled results from 10 animals. In contrast to the results obtained for adult zebrafish, the 6 dpf animals did not show an aversive behavior in response to cadaverine, but were instead rather attracted to the odor. They displayed a significant shift of their position towards the odor source when looked at the pooled data from 10 animals. The shift was smaller than for food odor, but still significant. Water, which was used as a negative control, did not result in any change of the larval behavior, neither on the individual level nor in the analysis of the pooled data from 10 animals.

It is possible, that zebrafish change the evaluation of cadaverine as a potential source of danger throughout their lifetime. Predators, which might be attracted to cadaverine, might not consider the larval zebrafish as prey, which could explain why cadaverine is not yet seen as an aversive stimulus in the larvae. Another possibility is, that aversion is not included into the behavioral repertoire of 6 dpf larvae yet and only emerges later in the ontogenetic development. The onset of the aversive behavioral response has to be identified in future experiments.

4.5 Generation of TAAR13c knock-out zebrafish lines

The use of the CRISPR/Cas9 system drastically improved and facilitated genome editing compared to TALEN and ZFN techniques, which have been available before (Xiao et al., 2013, Gaj et al., 2013).

The system uses an RNA guide harboring a target site specific 20 bp sequence and a RNA scaffold, which forms a complex with Cas9 nuclease. If brought into a cell, the complex is guided to the target site locus and will introduce a double strand break (Jinek et al., 2012). Non-homologous DNA repair mechanisms can lead to small insertions or deletions, which disrupt gene function and thereby lead to a knock-out.

In positive control experiments, where we knocked out the pigmentation related genes *tyrosinase* and *golden*, we observed knock-out frequencies of nearly 90 %. The use of *sp*Cas9 protein carrying a nuclear localization sequence is definitely to be preferred over the injection of Cas9 mRNA, which was done in previous studies in the lab (Ivandic, 2015, Krishna Subramanian, 2017).

An alternative approach has been used to excise fragments of up to 7 kb from the genome of zebrafish (Ota et al., 2014). Two target sites flanking a genomic region of interest were used to induce two double strand breaks and excising the fragment in between by non-homologous end joining repair. Similar approaches have been used in mammalian cells (Cong et al., 2013).

Here, we used the same approach to excise the TAAR13c gene from the genome. Because the members of the TAAR13 family show a very high sequence identity it is difficult to design gRNA target sites, which only target the desired gene. Therefore we intended to design target sites in the 5´and 3´UTRs flanking the TAAR13c gene and thereby excising the gene from its

locus. In the 5´UTR we were able to identify several target sites with no or very few off targets, that were able to introduce a double strand break when injected with Cas9 protein. However, in the 3´UTR we observed a lack of suitable target sites within 1.000 bp following the STOP codon. The target sites, which could be obtained, displayed very high off-target scores and are thereby likely to induce a number of off-target mutations in other genes. Despite that, we were able to identify three target sites within the TAAR13c exon using up-to-date target site design algorithms (Labun et al., 2016). These target sites were now used in combination with the 3´UTR target sites to excise around 1 kb including around half of the TAAR13c coding sequence.

Using different target site combinations we observed an excision of the fragment between the two target sites. Sequencing with primers flanking the region of interest confirmed, that the shortened PCR product is indeed the target locus. If the mutation was transferred to the germline these adult fish can now be used as founders of a TAAR13c knock-out line. This technique can be a valuable tool in targeting olfactory receptor genes, as members of these large gene families usually display strong sequence conservation.

4.6 Evolutionary origin and olfactory functionality of TAARs

TAARs have undergone large expansions in the fish lineage, especially in zebrafish (Hashiguchi and Nishida, 2007, Gloriam et al., 2005, Hussain et al., 2009). These earlier studies looked either at single genomes or a handful of available fish genomes at that time. Today we have access to an increasing number of published genomes in the NCBI database, including more than 80 fish genomes (as of February 2017) and hundreds of other genomes from different branches of the tree of life. This enables us to more precisely recreate the phylogeny of single gene families in the course of evolution.

The evolutionary origin of TAARs has already been looked at closer in the tetrapod lineage with only minor consideration of the fish genomes available (Eyun et al., 2016). One study claimed that jawless lamprey already possess TAAR genes, which might function as olfactory receptors (Libants et al., 2009), while another study determined these genes do not possess the TAAR defining motif, which only evolved later, and considered these genes as aminergic receptors (Hussain et al., 2009). TAARs were described to have emerged from a duplication of a serotonin receptor family member (HTR4), but the study did not include enough genomes to identify the

MRCA (Spielman et al., 2015). Several steps in the TAAR evolution remain elusive, which is why we started a large scale analysis of all fish genomes available in the database and included aminergic receptors from invertebrate species (hemichordates and chordates) to pinpoint the evolutionary origin of TAARs.

We could confirm that the origin of TAARs is indeed a duplication of the HTR4 gene. Including also hemichordates and chordates into our analysis, we found that this duplication must have occurred after the emergence of chordates, but before the emergence of jawed fish. Interestingly, another gene duplication then gave raise to two independently evolving gene families, TARL and TAAR, which both have gained olfactory functionality.

This on the one hand occurred in the TAAR-like receptor family (TARL), members of which were found in (almost) all fish genomes searched, but only underwent expansion in the lamprey, i.e. jawless fish. These genes were originally described as a subclass of TAARs (Hashiguchi and Nishida, 2007, Spielman et al., 2015), but do not possess the TAAR motif and clearly form a separate branch in our thorough phylogenetic analysis. Nonetheless, some of the TARL members were shown to be expressed in the lamprey OE (Libants et al., 2009). Phylogenetic relations within the TARLs were only incompletely and somewhat inaccurately described earlier (Eyun et al., 2016) and could be depicted more accurately and with higher branch supports in our analysis.

The second gene family is the TAAR family, which underwent expansions in all vertebrate species except the lamprey, where no member of this family was found. Nothing is known about the function of TAARs in jawed fish yet. Using RT-PCR we found that zebrafish TARL1 is expressed in the brain and to lesser extent also in the nose and lower body. We were not able to identify the exact areas of expression in the brain by *in situ* hybridization up to this point. Additional studies are required to study expression profiles and possible functions of this gene. It could serve as a biogenic amine receptor in the nervous system, like was described for TAAR1, which is the only known TAAR not to be expressed in the olfactory system (Liberles and Buck, 2006).

4.7 Evolution of class II TAARs in the fish lineage

In zebrafish class II TAARs comprise two subfamily members, TAAR12 and TAAR13, with 5 and 13 members respectively (Hussain et al., 2009). TAAR13 members have been shown to be activated by diamines, some of which induce aversive behaviors (Hussain et al., 2013, Li et al., 2015). Because of this interesting role in fish behavior, we searched for class II TAAR genes in 81 fish genomes in the NCBI database and reconstructed the phylogeny of this TAAR class in the fish lineage.

Importantly no TAARs at all were found in jawless fish (lampreys), although they possess a large expansion of TARL genes as discussed in the previous chapter. We found early members of class II TAARs in cartilaginous fish (shark, ray, chimaera), which conforms with an earlier study, where the emergence of TAARs was identified to have happened after the segregation of jawed from jawless fish (Hussain et al., 2009).

Both TAAR12 and TAAR13 have emerged in the ray-finned fish lineage shortly after the segregation of tetrapod (lobe-finned) and fish (ray-finned) lineages. Tetrapods possess their own subset of class II TAARs, which was lost very early in ray-finned fish evolution. With one exception this repertoire does not overlap with fish class II TAAR members. In fact, the only fish found retaining a mammalian-like TAAR5 gene is the spotted gar, a very archaic ray-finned fish. The MRCA of all other fish, i.e. the forefather of all teleosts, has lost this class II gene and only retained TAAR12 and TAAR13 as members of class II.

TAAR12 and TAAR13 are present in almost all early derived bony fish. TAAR12 has been lost individually in 2 species and then abruptly in the MRCA of all Euteleostomorpha, which still include species like pike, salmon and cod.

TAAR13 has been retained more constantly and also longer. All early derived bony fish possess TAAR13 genes, even pike, salmon and cod, which have lost TAAR12. In the more recently evolved clades the situation is more complex. An earlier study with 5 teleost genomes suggested the loss of class II TAARs in all neoteleosts, which include the percomorphaceae (Hussain et al., 2009). In our large scale analysis we now found, that TAAR13 was indeed lost in most of these species. But we also found fully intact TAAR13 genes in 11 out of 56 neoteleost species, meaning that TAAR13 was indeed retained in the neoteleost lineage and then individually lost in

several clades within the neoteleosts. In accordance, similarly frequent gene gains and losses have been reported for mammalian ORs (Niimura and Nei, 2007) and V1Rs (Grus et al., 2005).

The reason for this seemingly random gene loss and gain patterns in class II TAARs remains elusive. A low evolutionary pressure might have led to random gene loss events in many species. Other TAARs - e.g. class III TAARs, which underwent a large expansion in neoteleosts - might have gained functions originally fulfilled by class II genes.

4.8 Outlook

Our results strongly suggest that amine as well as diamine stimuli are processed by ciliated OSNs in the zebrafish olfactory system. Cadaverine in particular is perceived by TAAR13c-expressing, ciliated OSNs. In the olfactory bulb amine and diamine odors activate a specific glomerular cluster (dlG). Low concentrations of cadaverine activate a single invariant glomerulus in this cluster. Olfactory bulb odor representations seem to be evolutionary conserved, at least from the early-derived teleost zebrafish to the neoteleosts stickleback. This hypothesis has to be verified by more studies on odor representations in additional species from different branches of vertebrate evolution.

We observe a behavioral response to cadaverine stimuli present in larval zebrafish (attraction). However, this response is, for reasons unknown yet, different from the response reported in adult fish (aversion). We employed different techniques to study neuronal circuits related to odor-induced behaviors in the larval zebrafish. pERK can be used as a general neuronal activity marker in the larval brain and GCaMP6 Ca^{2+}-imaging can be used to detect neuronal activity *in vivo*. Combined with our CRISPR/Cas9 knock-out approaches for olfactory receptors these techniques will serve as powerful tools for the delineation of odor-processing neuronal circuits.

The TAAR family of olfactory receptors originates from a duplication of the HTR4 gene before the emergence of jawed fish. From there both gene copies evolved to become olfactory receptors. TARLs expanded and developed olfactory function in jawless, but not jawed fish. TAARs evolved into a large family of olfactory receptors in the jawed lineage and greatly expanded in many recent fish taxa. Frequent gene gain and loss events are shown here for TAAR12 and TAAR13 in the fish lineage. Similar gene-specific analysis for other receptor families could elucidate if this is a common feature within olfactory receptors.

5 REFERENCES

ADLER, J. 1969. Chemoreceptors in bacteria. *Science,* 166**,** 1588-97.

AGETSUMA, M., AIZAWA, H., AOKI, T., NAKAYAMA, R., TAKAHOKO, M., GOTO, M., SASSA, T., AMO, R., SHIRAKI, T., KAWAKAMI, K., HOSOYA, T., HIGASHIJIMA, S. & OKAMOTO, H. 2010. The habenula is crucial for experience-dependent modification of fear responses in zebrafish. *Nat Neurosci,* 13**,** 1354-6.

AHRENS, M. B., ORGER, M. B., ROBSON, D. N., LI, J. M. & KELLER, P. J. 2013. Whole-brain functional imaging at cellular resolution using light-sheet microscopy. *Nature Methods,* 10**,** 413-+.

AHUJA, G., BOZORG NIA, S., ZAPILKO, V., SHIRIAGIN, V., KOWATSCHEW, D., OKA, Y. & KORSCHING, S. I. 2014. Kappe neurons, a novel population of olfactory sensory neurons. *Sci Rep,* 4**,** 4037.

AHUJA, G., IVANDIC, I., SALTURK, M., OKA, Y., NADLER, W. & KORSCHING, S. I. 2013. Zebrafish crypt neurons project to a single, identified mediodorsal glomerulus. *Sci Rep,* 3**,** 2063.

AKERBOOM, J., RIVERA, J. D. V., GUILBE, M. M. R., MALAVE, E. C. A., HERNANDEZ, H. H., TIAN, L., HIRES, S. A., MARVIN, J. S., LOOGER, L. L. & SCHREITER, E. R. 2009. Crystal Structures of the GCaMP Calcium Sensor Reveal the Mechanism of Fluorescence Signal Change and Aid Rational Design. *Journal of Biological Chemistry,* 284**,** 6455-6464.

ALIOTO, T. S. & NGAI, J. 2005. The odorant receptor repertoire of teleost fish. *BMC Genomics,* 6**,** 173.

ALIOTO, T. S. & NGAI, J. 2006. The repertoire of olfactory C family G protein-coupled receptors in zebrafish: candidate chemosensory receptors for amino acids. *BMC Genomics,* 7**,** 309.

ARIKAWA, K. & WILLIAMS, D. S. 1993. Acetylated alpha-tubulin in the connecting cilium of developing rat photoreceptors. *Invest Ophthalmol Vis Sci,* 34**,** 2145-9.

AZZOUZI, N., BARLOY-HUBLER, F. & GALIBERT, F. 2015. Identification and characterization of cichlid TAAR genes and comparison with other teleost TAAR repertoires. *BMC Genomics,* 16**,** 335.

BAIER, H. & KORSCHING, S. 1994. Olfactory glomeruli in the zebrafish form an invariant pattern and are identifiable across animals. *J Neurosci,* 14**,** 219-30.

BAKALYAR, H. A. & REED, R. R. 1990. Identification of a specialized adenylyl cyclase that may mediate odorant detection. *Science,* 250**,** 1403-6.

BARRANGOU, R., FREMAUX, C., DEVEAU, H., RICHARDS, M., BOYAVAL, P., MOINEAU, S., ROMERO, D. A. & HORVATH, P. 2007. CRISPR provides acquired resistance against viruses in prokaryotes. *Science,* 315**,** 1709-12.

BARTH, A. L., DUGAS, J. C. & NGAI, J. 1997. Noncoordinate expression of odorant receptor genes tightly linked in the zebrafish genome. *Neuron,* 19**,** 359-69.

BEAR, D. M., LASSANCE, J. M., HOEKSTRA, H. E. & DATTA, S. R. 2016. The Evolving Neural and Genetic Architecture of Vertebrate Olfaction. *Curr Biol,* 26**,** R1039-R1049.

BEHRENS, M., FRANK, O., RAWEL, H., AHUJA, G., POTTING, C., HOFMANN, T., MEYERHOF, W. & KORSCHING, S. 2014. ORA1, a zebrafish olfactory receptor ancestral to all mammalian V1R genes, recognizes 4-hydroxyphenylacetic acid, a putative reproductive pheromone. *J Biol Chem,* 289**,** 19778-88.

BELLUSCIO, L., GOLD, G. H., NEMES, A. & AXEL, R. 1998. Mice deficient in G(olf) are anosmic. *Neuron,* 20**,** 69-81.

BEPARI, A. K., WATANABE, K., YAMAGUCHI, M., TAMAMAKI, N. & TAKEBAYASHI, H. 2012. Visualization of odor-induced neuronal activity by immediate early gene expression. *BMC Neurosci,* 13**,** 140.

BETANCUR, R. R., BROUGHTON, R. E., WILEY, E. O., CARPENTER, K., LOPEZ, J. A., LI, C., HOLCROFT, N. I., ARCILA, D., SANCIANGCO, M., CURETON II, J. C., ZHANG, F., BUSER, T., CAMPBELL, M. A., BALLESTEROS, J. A., ROA-VARON, A., WILLIS, S., BORDEN, W. C., ROWLEY, T., RENEAU, P. C., HOUGH, D. J., LU, G., GRANDE, T., ARRATIA, G. & ORTI, G. 2013. The tree of life and a new classification of bony fishes. *PLoS Curr,* 5.

BIECHL, D., TIETJE, K., GERLACH, G. & WULLIMANN, M. F. 2016. Crypt cells are involved in kin recognition in larval zebrafish. *Sci Rep,* 6**,** 24590.

BIECHL, D., TIETJE, K., RYU, S., GROTHE, B., GERLACH, G. & WULLIMANN, M. F. 2017. Identification of accessory olfactory system and medial amygdala in the zebrafish. *Scientific Reports,* 7.

BLAIR, J. E. & HEDGES, S. B. 2005. Molecular phylogeny and divergence times of deuterostome animals. *Mol Biol Evol,* 22**,** 2275-84.

BOEKHOFF, I. & BREER, H. 1992. Termination of second messenger signaling in olfaction. *Proc Natl Acad Sci U S A,* 89**,** 471-4.

BOROWSKY, B., ADHAM, N., JONES, K. A., RADDATZ, R., ARTYMYSHYN, R., OGOZALEK, K. L., DURKIN, M. M., LAKHLANI, P. P., BONINI, J. A., PATHIRANA, S., BOYLE, N., PU, X., KOURANOVA, E., LICHTBLAU, H., OCHOA, F. Y., BRANCHEK, T. A. & GERALD, C. 2001. Trace amines: identification of a family of mammalian G protein-coupled receptors. *Proc Natl Acad Sci U S A,* 98**,** 8966-71.

BRAUBACH, O. R., FINE, A. & CROLL, R. P. 2012. Distribution and functional organization of glomeruli in the olfactory bulbs of zebrafish (Danio rerio). *J Comp Neurol,* 520**,** 2317-39, Spc1.

BROUNS, S. J., JORE, M. M., LUNDGREN, M., WESTRA, E. R., SLIJKHUIS, R. J., SNIJDERS, A. P., DICKMAN, M. J., MAKAROVA, K. S., KOONIN, E. V. & VAN DER OOST, J. 2008. Small CRISPR RNAs guide antiviral defense in prokaryotes. *Science,* 321**,** 960-4.

BRUNET, L. J., GOLD, G. H. & NGAI, J. 1996. General anosmia caused by a targeted disruption of the mouse olfactory cyclic nucleotide-gated cation channel. *Neuron,* 17**,** 681-93.

BUCK, L. & AXEL, R. 1991. A novel multigene family may encode odorant receptors: a molecular basis for odor recognition. *Cell,* 65**,** 175-87.

BUNDSCHUH, S. T., ZHU, P., SCHARER, Y. P. & FRIEDRICH, R. W. 2012. Dopaminergic modulation of mitral cells and odor responses in the zebrafish olfactory bulb. *J Neurosci,* 32**,** 6830-40.

BUSHDID, C., MAGNASCO, M. O., VOSSHALL, L. B. & KELLER, A. 2014. Humans Can Discriminate More than 1 Trillion Olfactory Stimuli. *Science,* 343**,** 1370-1372.

CALFUN, C., DOMINGUEZ, C., PEREZ-ACLE, T. & WHITLOCK, K. E. 2016. Changes in Olfactory Receptor Expression Are Correlated With Odor Exposure During Early Development in the zebrafish (Danio rerio). *Chem Senses,* 41**,** 301-12.

CAO, Y., OH, B. C. & STRYER, L. 1998. Cloning and localization of two multigene receptor families in goldfish olfactory epithelium. *Proc Natl Acad Sci U S A,* 95**,** 11987-92.

CHEN, T. W., WARDILL, T. J., SUN, Y., PULVER, S. R., RENNINGER, S. L., BAOHAN, A., SCHREITER, E. R., KERR, R. A., ORGER, M. B., JAYARAMAN, V., LOOGER, L. L., SVOBODA, K. & KIM, D. S. 2013. Ultrasensitive fluorescent proteins for imaging neuronal activity. *Nature,* 499**,** 295-300.

CHEN, T. Y. & YAU, K. W. 1994. Direct modulation by Ca(2+)-calmodulin of cyclic nucleotide-activated channel of rat olfactory receptor neurons. *Nature,* 368**,** 545-8.

CHO, S. W., KIM, S., KIM, Y., KWEON, J., KIM, H. S., BAE, S. & KIM, J. S. 2014. Analysis of off-target effects of CRISPR/Cas-derived RNA-guided endonucleases and nickases. *Genome Res,* 24**,** 132-41.

CONG, L., RAN, F. A., COX, D., LIN, S. L., BARRETTO, R., HABIB, N., HSU, P. D., WU, X. B., JIANG, W. Y., MARRAFFINI, L. A. & ZHANG, F. 2013. Multiplex Genome Engineering Using CRISPR/Cas Systems. *Science,* 339**,** 819-823.

CROOKS, G. E., HON, G., CHANDONIA, J. M. & BRENNER, S. E. 2004. WebLogo: a sequence logo generator. *Genome Res,* 14**,** 1188-90.

DEWAN, A., PACIFICO, R., ZHAN, R., RINBERG, D. & BOZZA, T. 2013. Non-redundant coding of aversive odours in the main olfactory pathway. *Nature,* 497**,** 486-9.

DHALLAN, R. S., YAU, K. W., SCHRADER, K. A. & REED, R. R. 1990. Primary structure and functional expression of a cyclic nucleotide-activated channel from olfactory neurons. *Nature,* 347**,** 184-7.

DING, Q., REGAN, S. N., XIA, Y., OOSTROM, L. A., COWAN, C. A. & MUSUNURU, K. 2013. Enhanced efficiency of human pluripotent stem cell genome editing through replacing TALENs with CRISPRs. *Cell Stem Cell,* 12**,** 393-4.

DITTRICH, K., SANSONE, A., HASSENKLOVER, T. & MANZINI, I. 2014. Purinergic receptor-induced Ca2+ signaling in the neuroepithelium of the vomeronasal organ of larval Xenopus laevis. *Purinergic Signal,* 10**,** 327-36.

DRAGUNOW, M. & FAULL, R. 1989. The Use of C-Fos as a Metabolic Marker in Neuronal Pathway Tracing. *Journal of Neuroscience Methods,* 29**,** 261-265.

DREOSTI, E., LLOPIS, N. V., CARL, M., YAKSI, E. & WILSON, S. W. 2014. Left-Right Asymmetry Is Required for the Habenulae to Respond to Both Visual and Olfactory Stimuli. *Current Biology,* 24**,** 440-445.

DULAC, C. & AXEL, R. 1995. A novel family of genes encoding putative pheromone receptors in mammals. *Cell,* 83**,** 195-206.

EDWARDS, J. G. & MICHEL, W. C. 2002. Odor-stimulated glutamatergic neurotransmission in the zebrafish olfactory bulb. *J Comp Neurol,* 454**,** 294-309.

EYUN, S. I., MORIYAMA, H., HOFFMANN, F. G. & MORIYAMA, E. N. 2016. Molecular Evolution and Functional Divergence of Trace Amine-Associated Receptors. *PLoS One,* 11**,** e0151023.

FERRANDO, S., BOTTARO, M., GALLUS, L., GIROSI, L., VACCHI, M. & TAGLIAFIERRO, G. 2006. Observations of crypt neuron-like cells in the olfactory epithelium of a cartilaginous fish. *Neurosci Lett,* 403**,** 280-2.

FERRERO, D. M., LEMON, J. K., FLUEGGE, D., PASHKOVSKI, S. L., KORZAN, W. J., DATTA, S. R., SPEHR, M., FENDT, M. & LIBERLES, S. D. 2011. Detection and avoidance of a carnivore odor by prey. *Proc Natl Acad Sci U S A,* 108**,** 11235-40.

FERRERO, D. M., WACKER, D., ROQUE, M. A., BALDWIN, M. W., STEVENS, R. C. & LIBERLES, S. D. 2012. Agonists for 13 trace amine-associated receptors provide insight into the molecular basis of odor selectivity. *ACS Chem Biol,* 7**,** 1184-9.

FRIEDRICH, R. W. & KORSCHING, S. I. 1997. Combinatorial and chemotopic odorant coding in the zebrafish olfactory bulb visualized by optical imaging. *Neuron,* 18**,** 737-52.

FRIEDRICH, R. W. & KORSCHING, S. I. 1998. Chemotopic, combinatorial, and noncombinatorial odorant representations in the olfactory bulb revealed using a voltage-sensitive axon tracer. *J Neurosci,* 18**,** 9977-88.

FULLER, C. L., YETTAW, H. K. & BYRD, C. A. 2006. Mitral cells in the olfactory bulb of adult zebrafish (Danio rerio): morphology and distribution. *J Comp Neurol,* 499**,** 218-30.

FUSS, S. H. & KORSCHING, S. I. 2001. Odorant feature detection: activity mapping of structure response relationships in the zebrafish olfactory bulb. *J Neurosci,* 21**,** 8396-407.

GAGNON, J. A., VALEN, E., THYME, S. B., HUANG, P., AKHMETOVA, L., PAULI, A., MONTAGUE, T. G., ZIMMERMAN, S., RICHTER, C. & SCHIER, A. F. 2014. Efficient mutagenesis by Cas9 protein-mediated oligonucleotide insertion and large-scale assessment of single-guide RNAs. *PLoS One,* 9**,** e98186.

GAJ, T., GERSBACH, C. A. & BARBAS, C. F., 3RD 2013. ZFN, TALEN, and CRISPR/Cas-based methods for genome engineering. *Trends Biotechnol,* 31**,** 397-405.

GASIUNAS, G., BARRANGOU, R., HORVATH, P. & SIKSNYS, V. 2012. Cas9-crRNA ribonucleoprotein complex mediates specific DNA cleavage for adaptive immunity in bacteria. *Proc Natl Acad Sci U S A,* 109**,** E2579-86.

GERKIN, R. C. & CASTRO, J. B. 2015. The number of olfactory stimuli that humans can discriminate is still unknown. *Elife,* 4.

GERMANA, A., MONTALBANO, G., LAURA, R., CIRIACO, E., DEL VALLE, M. E. & VEGA, J. A. 2004. S100 protein-like immunoreactivity in the crypt olfactory neurons of the adult zebrafish. *Neurosci Lett,* 371**,** 196-8.

GLIEM, S., SYED, A. S., SANSONE, A., KLUDT, E., TANTALAKI, E., HASSENKLOVER, T., KORSCHING, S. I. & MANZINI, I. 2013. Bimodal processing of olfactory information in an amphibian nose: odor responses segregate into a medial and a lateral stream. *Cell Mol Life Sci,* 70**,** 1965-84.

GLORIAM, D. E., BJARNADOTTIR, T. K., YAN, Y. L., POSTLETHWAIT, J. H., SCHIOTH, H. B. & FREDRIKSSON, R. 2005. The repertoire of trace amine G-protein-coupled receptors: large expansion in zebrafish. *Mol Phylogenet Evol,* 35**,** 470-82.

GODFREY, P. A., MALNIC, B. & BUCK, L. B. 2004. The mouse olfactory receptor gene family. *Proc Natl Acad Sci U S A,* 101**,** 2156-61.

GREER, P. L., BEAR, D. M., LASSANCE, J. M., BLOOM, M. L., TSUKAHARA, T., PASHKOVSKI, S. L., MASUDA, F. K., NOWLAN, A. C., KIRCHNER, R., HOEKSTRA, H. E. & DATTA, S. R. 2016. A Family of non-GPCR Chemosensors Defines an Alternative Logic for Mammalian Olfaction. *Cell,* 165**,** 1734-1748.

GRUS, W. E., SHI, P., ZHANG, Y. P. & ZHANG, J. Z. 2005. Dramatic variation of the vomeronasal pheromone receptor gene repertoire among five orders of placental and marsupial mammals. *Proceedings of the National Academy of Sciences of the United States of America,* 102**,** 5767-5772.

GUINDON, S., DUFAYARD, J. F., LEFORT, V., ANISIMOVA, M., HORDIJK, W. & GASCUEL, O. 2010. New algorithms and methods to estimate maximum-likelihood phylogenies: assessing the performance of PhyML 3.0. *Syst Biol,* 59**,** 307-21.

HANCHATE, N. K., KONDOH, K., LU, Z., KUANG, D., YE, X., QIU, X., PACHTER, L., TRAPNELL, C. & BUCK, L. B. 2015. Single-cell transcriptomics reveals receptor transformations during olfactory neurogenesis. *Science,* 350**,** 1251-5.

HANSEN, A., ROLEN, S. H., ANDERSON, K., MORITA, Y., CAPRIO, J. & FINGER, T. E. 2003. Correlation between olfactory receptor cell type and function in the channel catfish. *J Neurosci,* 23**,** 9328-39.

HANSEN, A. & ZEISKE, E. 1998. The peripheral olfactory organ of the zebrafish, Danio rerio: an ultrastructural study. *Chem Senses,* 23**,** 39-48.

HASHIGUCHI, Y. & NISHIDA, M. 2006. Evolution and origin of vomeronasal-type odorant receptor gene repertoire in fishes. *BMC Evol Biol,* 6**,** 76.

HASHIGUCHI, Y. & NISHIDA, M. 2007. Evolution of trace amine associated receptor (TAAR) gene family in vertebrates: lineage-specific expansions and degradations of a second class of vertebrate chemosensory receptors expressed in the olfactory epithelium. *Mol Biol Evol,* 24**,** 2099-107.

HASHIGUCHI, Y. & NISHIDA, M. 2009. Screening the V2R-type putative odorant receptor gene repertoire in bitterling Tanakia lanceolata. *Gene,* 441**,** 74-9.

HASSENKLOVER, T., SCHWARTZ, P., SCHILD, D. & MANZINI, I. 2009. Purinergic signaling regulates cell proliferation of olfactory epithelium progenitors. *Stem Cells,* 27**,** 2022-31.

HERRADA, G. & DULAC, C. 1997. A novel family of putative pheromone receptors in mammals with a topographically organized and sexually dimorphic distribution. *Cell,* 90**,** 763-73.

HUSSAIN, A., SARAIVA, L. R., FERRERO, D. M., AHUJA, G., KRISHNA, V. S., LIBERLES, S. D. & KORSCHING, S. I. 2013. High-affinity olfactory receptor for the death-associated odor cadaverine. *Proc Natl Acad Sci U S A,* 110**,** 19579-84.

HUSSAIN, A., SARAIVA, L. R. & KORSCHING, S. I. 2009. Positive Darwinian selection and the birth of an olfactory receptor clade in teleosts. *Proc Natl Acad Sci U S A,* 106**,** 4313-8.

HWANG, W. Y., FU, Y., REYON, D., MAEDER, M. L., TSAI, S. Q., SANDER, J. D., PETERSON, R. T., YEH, J. R. & JOUNG, J. K. 2013. Efficient genome editing in zebrafish using a CRISPR-Cas system. *Nat Biotechnol,* 31**,** 227-9.

IHARA, S., YOSHIKAWA, K. & TOUHARA, K. 2013. Chemosensory signals and their receptors in the olfactory neural system. *Neuroscience,* 254**,** 45-60.

IRION, U., KRAUSS, J. & NUSSLEIN-VOLHARD, C. 2014. Precise and efficient genome editing in zebrafish using the CRISPR/Cas9 system. *Development,* 141**,** 4827-30.

IVANDIC, I. 2015. CRISPR/Cas9 knockout and functional characterization of *gnav1*. *Dissertation*.

JAHRLING, N., BECKER, K., SAGHAFI, S. & DODT, H. U. 2017. Light-Sheet Fluorescence Microscopy: Chemical Clearing and Labeling Protocols for Ultramicroscopy. *Methods Mol Biol,* 1563**,** 33-49.

JENSEN, M. C. & RIDDELL, S. R. 2015. Designing chimeric antigen receptors to effectively and safely target tumors. *Curr Opin Immunol,* 33**,** 9-15.

JINEK, M., CHYLINSKI, K., FONFARA, I., HAUER, M., DOUDNA, J. A. & CHARPENTIER, E. 2012. A programmable dual-RNA-guided DNA endonuclease in adaptive bacterial immunity. *Science,* 337**,** 816-21.

JOINER, A. M., GREEN, W. W., MCINTYRE, J. C., ALLEN, B. L., SCHWOB, J. E. & MARTENS, J. R. 2015. Primary Cilia on Horizontal Basal Cells Regulate Regeneration of the Olfactory Epithelium. *Journal of Neuroscience,* 35**,** 13761-13772.

JONES, D. T. & REED, R. R. 1989. Golf: an olfactory neuron specific-G protein involved in odorant signal transduction. *Science,* 244**,** 790-5.

JUNEK, S., CHEN, T. W., ALEVRA, M. & SCHILD, D. 2009. Activity correlation imaging: visualizing function and structure of neuronal populations. *Biophys J,* 96**,** 3801-9.

KARLSON, P. & LUSCHER, M. 1959. Pheromones': a new term for a class of biologically active substances. *Nature,* 183**,** 55-6.

KE, M. T., FUJIMOTO, S. & IMAI, T. 2013. SeeDB: a simple and morphology-preserving optical clearing agent for neuronal circuit reconstruction. *Nat Neurosci,* 16**,** 1154-61.

KERMEN, F., FRANCO, L. M., WYATT, C. & YAKSI, E. 2013. Neural circuits mediating olfactory-driven behavior in fish. *Front Neural Circuits,* 7**,** 62.

KLEENE, S. J. 1993. Origin of the chloride current in olfactory transduction. *Neuron,* 11**,** 123-32.

KOIDE, T., MIYASAKA, N., MORIMOTO, K., ASAKAWA, K., URASAKI, A., KAWAKAMI, K. & YOSHIHARA, Y. 2009. Olfactory neural circuitry for attraction to amino acids revealed by transposon-mediated gene trap approach in zebrafish. *Proceedings of the National Academy of Sciences of the United States of America,* 106**,** 9884-9889.

KOO, T., LEE, J. & KIM, J. S. 2015. Measuring and Reducing Off-Target Activities of Programmable Nucleases Including CRISPR-Cas9. *Mol Cells,* 38**,** 475-81.

KRESS, S. & WULLIMANN, M. F. 2012. Correlated basal expression of immediate early gene egr1 and tyrosine hydroxylase in zebrafish brain and downregulation in olfactory bulb after transitory olfactory deprivation. *Journal of Chemical Neuroanatomy,* 46**,** 51-66.

KRISHNA SUBRAMANIAN, V. 2017. Characterization of an olfactory receptor mediating aversive behaviour to a death-associated odour. *Dissertation*.

KRISHNAN, S., MATHURU, A. S., KIBAT, C., RAHMAN, M., LUPTON, C. E., STEWART, J., CLARIDGE-CHANG, A., YEN, S. C. & JESUTHASAN, S. 2014. The right dorsal habenula limits attraction to an odor in zebrafish. *Curr Biol,* 24**,** 1167-75.

LABUN, K., MONTAGUE, T. G., GAGNON, J. A., THYME, S. B. & VALEN, E. 2016. CHOPCHOP v2: a web tool for the next generation of CRISPR genome engineering. *Nucleic Acids Res,* 44**,** W272-6.

LEIBMAN, R. S. & RILEY, J. L. 2015. Engineering T Cells to Functionally Cure HIV-1 Infection. *Mol Ther,* 23**,** 1149-59.

LEINDERS-ZUFALL, T., BRENNAN, P., WIDMAYER, P., S, P. C., MAUL-PAVICIC, A., JAGER, M., LI, X. H., BREER, H., ZUFALL, F. & BOEHM, T. 2004. MHC class I peptides as chemosensory signals in the vomeronasal organ. *Science,* 306**,** 1033-7.

LEINDERS-ZUFALL, T., ISHII, T., CHAMERO, P., HENDRIX, P., OBOTI, L., SCHMID, A., KIRCHER, S., PYRSKI, M., AKIYOSHI, S., KHAN, M., VAES, E., ZUFALL, F. & MOMBAERTS, P. 2014. A family of nonclassical class I MHC genes contributes to ultrasensitive chemodetection by mouse vomeronasal sensory neurons. *J Neurosci,* 34**,** 5121-33.

LEINDERS-ZUFALL, T., ISHII, T., MOMBAERTS, P., ZUFALL, F. & BOEHM, T. 2009. Structural requirements for the activation of vomeronasal sensory neurons by MHC peptides. *Nat Neurosci,* 12**,** 1551-8.

LI, Q., KORZAN, W. J., FERRERO, D. M., CHANG, R. B., ROY, D. S., BUCHI, M., LEMON, J. K., KAUR, A. W., STOWERS, L., FENDT, M. & LIBERLES, S. D. 2013. Synchronous evolution of an odor biosynthesis pathway and behavioral response. *Curr Biol,* 23**,** 11-20.

LI, Q. & LIBERLES, S. D. 2015. Aversion and attraction through olfaction. *Curr Biol,* 25**,** R120-9.

LI, Q., TACHIE-BAFFOUR, Y., LIU, Z., BALDWIN, M. W., KRUSE, A. C. & LIBERLES, S. D. 2015. Non-classical amine recognition evolved in a large clade of olfactory receptors. *Elife,* 4.

LIBANTS, S., CARR, K., WU, H., TEETER, J. H., CHUNG-DAVIDSON, Y. W., ZHANG, Z., WILKERSON, C. & LI, W. 2009. The sea lamprey Petromyzon marinus genome reveals the early origin of several chemosensory receptor families in the vertebrate lineage. *BMC Evol Biol,* 9**,** 180.

LIBERLES, S. D. & BUCK, L. B. 2006. A second class of chemosensory receptors in the olfactory epithelium. *Nature,* 442**,** 645-650.

LIN, J., ZHOU, Y., LIU, J., CHEN, J., CHEN, W., ZHAO, S., WU, Z. & WU, N. 2017. Progress and Application of CRISPR/Cas Technology in Biological and Biomedical Investigation. *J Cell Biochem,* 118**,** 3061-3071.

LINDEMANN, L. & HOENER, M. C. 2005. A renaissance in trace amines inspired by a novel GPCR family. *Trends Pharmacol Sci,* 26**,** 274-81.

LIPSCHITZ, D. L. & MICHEL, W. C. 2002. Amino acid odorants stimulate microvillar sensory neurons. *Chem Senses,* 27**,** 277-86.

LIU, J. F., SIEMIAN, J. N., SEAMAN, R., ZHANG, Y. N. & LI, J. X. 2017a. Role of TAAR1 within the Subregions of the Mesocorticolimbic Dopaminergic System in Cocaine-Seeking Behavior. *Journal of Neuroscience,* 37**,** 882-892.

LIU, Z., CHEN, S., JIN, X., WANG, Q., YANG, K., LI, C., XIAO, Q., HOU, P., LIU, S., WU, S., HOU, W., XIONG, Y., KONG, C., ZHAO, X., WU, L., LI, C., SUN, G. & GUO, D. 2017b. Genome editing of the HIV co-receptors CCR5 and CXCR4 by CRISPR-Cas9 protects CD4+ T cells from HIV-1 infection. *Cell Biosci,* 7**,** 47.

LUPTON, C., SENGUPTA, M., CHENG, R. K., CHIA, J., THIRUMALAI, V. & JESUTHASAN, S. 2017. Loss of the Habenula Intrinsic Neuromodulator Kisspeptin1 Affects Learning in Larval Zebrafish. *eNeuro,* 4.

LUU, P., ACHER, F., BERTRAND, H. O., FAN, J. & NGAI, J. 2004. Molecular determinants of ligand selectivity in a vertebrate odorant receptor. *J Neurosci,* 24**,** 10128-37.

MALNIC, B., GODFREY, P. A. & BUCK, L. B. 2004. The human olfactory receptor gene family. *Proc Natl Acad Sci U S A,* 101**,** 2584-9.

MATHURU, A. S. & JESUTHASAN, S. 2013. The medial habenula as a regulator of anxiety in adult zebrafish. *Front Neural Circuits,* 7.

MATSUNAMI, H. & BUCK, L. B. 1997. A multigene family encoding a diverse array of putative pheromone receptors in mammals. *Cell,* 90**,** 775-84.

MIWA, N. & STORM, D. R. 2005. Odorant-induced activation of extracellular signal-regulated kinase/mitogen-activated protein kinase in the olfactory bulb promotes survival of newly formed granule cells. *J Neurosci,* 25**,** 5404-12.

MIYASAKA, N., ARGANDA-CARRERAS, I., WAKISAKA, N., MASUDA, M., SUMBUL, U., SEUNG, H. S. & YOSHIHARA, Y. 2014. Olfactory projectome in the zebrafish forebrain revealed by genetic single-neuron labelling. *Nat Commun,* 5**,** 3639.

MIYASAKA, N., MORIMOTO, K., TSUBOKAWA, T., HIGASHIJIMA, S., OKAMOTO, H. & YOSHIHARA, Y. 2009. From the olfactory bulb to higher brain centers: genetic visualization of secondary olfactory pathways in zebrafish. *J Neurosci,* 29**,** 4756-67.

MOMBAERTS, P. 2004. Genes and ligands for odorant, vomeronasal and taste receptors. *Nat Rev Neurosci,* 5**,** 263-78.

MORI, K. & SAKANO, H. 2011. How Is the Olfactory Map Formed and Interpreted in the Mammalian Brain? *Annual Review of Neuroscience, Vol 34,* 34**,** 467-499.

MORI, K., TAKAHASHI, Y. K., IGARASHI, K. M. & YAMAGUCHI, M. 2006. Maps of odorant molecular features in the Mammalian olfactory bulb. *Physiol Rev,* 86**,** 409-33.
MUELLER, T. 2012. What is the Thalamus in Zebrafish? *Front Neurosci,* 6**,** 64.
MUNGER, S. D., LANE, A. P., ZHONG, H., LEINDERS-ZUFALL, T., YAU, K. W., ZUFALL, F. & REED, R. R. 2001. Central role of the CNGA4 channel subunit in Ca2+-calmodulin-dependent odor adaptation. *Science,* 294**,** 2172-5.
MUTO, A., LAL, P., AILANI, D., ABE, G., ITOH, M. & KAWAKAMI, K. 2017. Activation of the hypothalamic feeding centre upon visual prey detection. *Nature Communications,* 8.
NAKAI, J., OHKURA, M. & IMOTO, K. 2001. A high signal-to-noise Ca2+ probe composed of a single green fluorescent protein. *Nature Biotechnology,* 19**,** 137-141.
NATHAN, F. M., OGAWA, S. & PARHAR, I. S. 2015. Kisspeptin1 modulates odorant-evoked fear response via two serotonin receptor subtypes (5-HT1A and 5-HT2) in zebrafish. *J Neurochem,* 133**,** 870-8.
NIIMURA, Y. & NEI, M. 2007. Extensive gains and losses of olfactory receptor genes in mammalian evolution. *PLoS One,* 2**,** e708.
OHLOFF, G. 1994. Scent and Fragrances: The fascination of odors and their chemical perspectives. *Springer-Verlag; Berlin***,** pp. 154–158.
OKA, Y., SARAIVA, L. R. & KORSCHING, S. I. 2012. Crypt neurons express a single V1R-related ora gene. *Chem Senses,* 37**,** 219-27.
OKAMOTO, H., AGETSUMA, M. & AIZAWA, H. 2012. Genetic dissection of the zebrafish habenula, a possible switching board for selection of behavioral strategy to cope with fear and anxiety. *Dev Neurobiol,* 72**,** 386-94.
OTA, S., HISANO, Y., IKAWA, Y. & KAWAHARA, A. 2014. Multiple genome modifications by the CRISPR/Cas9 system in zebrafish. *Genes Cells,* 19**,** 555-64.
PACIFICO, R., DEWAN, A., CAWLEY, D., GUO, C. & BOZZA, T. 2012. An olfactory subsystem that mediates high-sensitivity detection of volatile amines. *Cell Rep,* 2**,** 76-88.
PFISTER, P. & RODRIGUEZ, I. 2005. Olfactory expression of a single and highly variable V1r pheromone receptor-like gene in fish species. *Proc Natl Acad Sci U S A,* 102**,** 5489-94.
QUIRIN, S., VLADIMIROV, N., YANG, C. T., PETERKA, D. S., YUSTE, R. & AHRENS, M. B. 2016. Calcium imaging of neural circuits with extended depth-of-field light-sheet microscopy. *Opt Lett,* 41**,** 855-8.
RAMIREZ, C. L., FOLEY, J. E., WRIGHT, D. A., MULLER-LERCH, F., RAHMAN, S. H., CORNU, T. I., WINFREY, R. J., SANDER, J. D., FU, F., TOWNSEND, J. A., CATHOMEN, T., VOYTAS, D. F. & JOUNG, J. K. 2008. Unexpected failure rates for modular assembly of engineered zinc fingers. *Nat Methods,* 5**,** 374-5.
RAN, F. A., HSU, P. D., WRIGHT, J., AGARWALA, V., SCOTT, D. A. & ZHANG, F. 2013. Genome engineering using the CRISPR-Cas9 system. *Nature Protocols,* 8**,** 2281-2308.
RANDLETT, O., WEE, C. L., NAUMANN, E. A., NNAEMEKA, O., SCHOPPIK, D., FITZGERALD, J. E., PORTUGUES, R., LACOSTE, A. M., RIEGLER, C., ENGERT, F. & SCHIER, A. F. 2015. Whole-brain activity mapping onto a zebrafish brain atlas. *Nat Methods,* 12**,** 1039-46.
REINIG, S., DRIEVER, W. & ARRENBERG, A. B. 2017. The Descending Diencephalic Dopamine System Is Tuned to Sensory Stimuli. *Current Biology,* 27**,** 318-333.
REITEN, I., USLU, F. E., FORE, S., PELGRIMS, R., RINGERS, C., DIAZ VERDUGO, C., HOFFMAN, M., LAL, P., KAWAKAMI, K., PEKKAN, K., YAKSI, E. & JURISCH-YAKSI, N. 2017. Motile-Cilia-Mediated Flow Improves Sensitivity and Temporal Resolution of Olfactory Computations. *Curr Biol,* 27**,** 166-174.

RINK, E. & WULLIMANN, M. F. 2001. The teleostean (zebrafish) dopaminergic system ascending to the subpallium (striatum) is located in the basal diencephalon (posterior tuberculum). *Brain Res,* 889**,** 316-30.

RINK, E. & WULLIMANN, M. F. 2004. Connections of the ventral telencephalon (subpallium) in the zebrafish (Danio rerio). *Brain Res,* 1011**,** 206-20.

ROLEN, S. H., SORENSEN, P. W., MATTSON, D. & CAPRIO, J. 2003. Polyamines as olfactory stimuli in the goldfish Carassius auratus. *J Exp Biol,* 206**,** 1683-96.

RYBA, N. J. & TIRINDELLI, R. 1997. A new multigene family of putative pheromone receptors. *Neuron,* 19**,** 371-9.

SABO, D. L., BOEKER, E. A., BYERS, B., WARON, H. & FISCHER, E. H. 1974. Purification and physical properties of inducible Escherichia coli lysine decarboxylase. *Biochemistry,* 13**,** 662-70.

SARAIVA, L. R., AHUJA, G., IVANDIC, I., SYED, A. S., MARIONI, J. C., KORSCHING, S. I. & LOGAN, D. W. 2015. Molecular and neuronal homology between the olfactory systems of zebrafish and mouse. *Sci Rep,* 5**,** 11487.

SARAIVA, L. R. & KORSCHING, S. I. 2007. A novel olfactory receptor gene family in teleost fish. *Genome Res,* 17**,** 1448-57.

SATO, Y., MIYASAKA, N. & YOSHIHARA, Y. 2005. Mutually exclusive glomerular innervation by two distinct types of olfactory sensory neurons revealed in transgenic zebrafish. *J Neurosci,* 25**,** 4889-97.

SATO, Y., MIYASAKA, N. & YOSHIHARA, Y. 2007. Hierarchical regulation of odorant receptor gene choice and subsequent axonal projection of olfactory sensory neurons in zebrafish. *J Neurosci,* 27**,** 1606-15.

SCHMACHTENBERG, O. 2006. Histological and electrophysiological properties of crypt cells from the olfactory epithelium of the marine teleost Trachurus symmetricus. *J Comp Neurol,* 495**,** 113-21.

SCHULTZ, S. R., COPELAND, C. S., FOUST, A. J., QUICKE, P. & SCHUCK, R. 2017. Advances in Two-Photon Scanning and Scanless Microscopy Technologies for Functional Neural Circuit Imaging. *Proceedings of the Ieee,* 105**,** 139-157.

SCHWOB, J. E., JANG, W., HOLBROOK, E. H., LIN, B., HERRICK, D. B., PETERSON, J. N. & HEWITT COLEMAN, J. 2017. Stem and progenitor cells of the mammalian olfactory epithelium: Taking poietic license. *J Comp Neurol,* 525**,** 1034-1054.

SERIZAWA, S., ISHII, T., NAKATANI, H., TSUBOI, A., NAGAWA, F., ASANO, M., SUDO, K., SAKAGAMI, J., SAKANO, H., IJIRI, T., MATSUDA, Y., SUZUKI, M., YAMAMORI, T., IWAKURA, Y. & SAKANO, H. 2000. Mutually exclusive expression of odorant receptor transgenes. *Nat Neurosci,* 3**,** 687-93.

SERIZAWA, S., MIYAMICHI, K. & SAKANO, H. 2004. One neuron-one receptor rule in the mouse olfactory system. *Trends Genet,* 20**,** 648-53.

SHI, P. & ZHANG, J. 2007. Comparative genomic analysis identifies an evolutionary shift of vomeronasal receptor gene repertoires in the vertebrate transition from water to land. *Genome Res,* 17**,** 166-74.

SHIRASU, M., YOSHIKAWA, K., TAKAI, Y., NAKASHIMA, A., TAKEUCHI, H., SAKANO, H. & TOUHARA, K. 2014. Olfactory receptor and neural pathway responsible for highly selective sensing of musk odors. *Neuron,* 81**,** 165-78.

SILVA TEIXEIRA, C. S., CERQUEIRA, N. M. & SILVA FERREIRA, A. C. 2016. Unravelling the Olfactory Sense: From the Gene to Odor Perception. *Chem Senses,* 41**,** 105-21.

SPECA, D. J., LIN, D. M., SORENSEN, P. W., ISACOFF, E. Y., NGAI, J. & DITTMAN, A. H. 1999. Functional identification of a goldfish odorant receptor. *Neuron,* 23**,** 487-98.

SPIELMAN, S. J., KUMAR, K. & WILKE, C. O. 2015. Comprehensive, structurally-informed alignment and phylogeny of vertebrate biogenic amine receptors. *PeerJ,* 3**,** e773.

STEPHAN, A. B., SHUM, E. Y., HIRSH, S., CYGNAR, K. D., REISERT, J. & ZHAO, H. 2009. ANO2 is the cilial calcium-activated chloride channel that may mediate olfactory amplification. *Proc Natl Acad Sci U S A,* 106**,** 11776-81.

SULLIVAN, S. L., ADAMSON, M. C., RESSLER, K. J., KOZAK, C. A. & BUCK, L. B. 1996. The chromosomal distribution of mouse odorant receptor genes. *Proc Natl Acad Sci U S A,* 93**,** 884-8.

SUMBRE, G. & DEPOLAVIEJA, G. G. 2014. The world according to zebrafish: how neural circuits generate behavior. *Frontiers in Neural Circuits,* 8.

SUZUKI, J., SAKURAI, K., YAMAZAKI, M., ABE, M., INADA, H., SAKIMURA, K., KATORI, Y. & OSUMI, N. 2015. Horizontal Basal Cell-Specific Deletion of Pax6 Impedes Recovery of the Olfactory Neuroepithelium Following Severe Injury. *Stem Cells Dev,* 24**,** 1923-33.

SYED, A. S., SANSONE, A., HASSENKLOVER, T., MANZINI, I. & KORSCHING, S. I. 2017. Coordinated shift of olfactory amino acid responses and V2R expression to an amphibian water nose during metamorphosis. *Cell Mol Life Sci,* 74**,** 1711-1719.

TAKEUCHI, H. & SAKANO, H. 2014. Neural map formation in the mouse olfactory system. *Cell Mol Life Sci,* 71**,** 3049-57.

TALBOT, J. C. & AMACHER, S. L. 2014. A streamlined CRISPR pipeline to reliably generate zebrafish frameshifting alleles. *Zebrafish,* 11**,** 583-5.

TRELOAR, H. B., FEINSTEIN, P., MOMBAERTS, P. & GREER, C. A. 2002. Specificity of glomerular targeting by olfactory sensory axons. *J Neurosci,* 22**,** 2469-77.

VON DER WEID, B., ROSSIER, D., LINDUP, M., TUBEROSA, J., WIDMER, A., COL, J. D., KAN, C., CARLETON, A. & RODRIGUEZ, I. 2015. Large-scale transcriptional profiling of chemosensory neurons identifies receptor-ligand pairs in vivo. *Nat Neurosci,* 18**,** 1455-63.

VON NIEDERHAUSERN, V., KASTENHUBER, E., STAUBLE, A., GESEMANN, M. & NEUHAUSS, S. C. 2013. Phylogeny and expression of canonical transient receptor potential (TRPC) genes in developing zebrafish. *Dev Dyn,* 242**,** 1427-41.

WAGNER, S., GRESSER, A. L., TORELLO, A. T. & DULAC, C. 2006. A multireceptor genetic approach uncovers an ordered integration of VNO sensory inputs in the accessory olfactory bulb. *Neuron,* 50**,** 697-709.

WAKISAKA, N., MIYASAKA, N., KOIDE, T., MASUDA, M., HIRAKI-KAJIYAMA, T. & YOSHIHARA, Y. 2017. An Adenosine Receptor for Olfaction in Fish. *Curr Biol,* 27**,** 1437-1447 e4.

WEI, J., WAYMAN, G. & STORM, D. R. 1996. Phosphorylation and inhibition of type III adenylyl cyclase by calmodulin-dependent protein kinase II in vivo. *J Biol Chem,* 271**,** 24231-5.

WEI, J., ZHAO, A. Z., CHAN, G. C., BAKER, L. P., IMPEY, S., BEAVO, J. A. & STORM, D. R. 1998. Phosphorylation and inhibition of olfactory adenylyl cyclase by CaM kinase II in Neurons: a mechanism for attenuation of olfactory signals. *Neuron,* 21**,** 495-504.

WETZKER, R. & BOHMER, F. D. 2003. Transactivation joins multiple tracks to the ERK/MAPK cascade. *Nat Rev Mol Cell Biol,* 4**,** 651-7.

WIEDENHEFT, B., STERNBERG, S. H. & DOUDNA, J. A. 2012. RNA-guided genetic silencing systems in bacteria and archaea. *Nature,* 482**,** 331-8.

WINTER, M. J., WINDELL, D., METZ, J., MATTHEWS, P., PINION, J., BROWN, J. T., HETHERIDGE, M. J., BALL, J. S., OWEN, S. F., REDFERN, W. S., MOGER, J., RANDALL, A. D. & TYLER, C. R. 2017. 4-dimensional functional profiling in the convulsant-treated larval zebrafish brain. *Sci Rep,* 7**,** 6581.

WONG, S. T., TRINH, K., HACKER, B., CHAN, G. C., LOWE, G., GAGGAR, A., XIA, Z., GOLD, G. H. & STORM, D. R. 2000. Disruption of the type III adenylyl cyclase gene leads to peripheral and behavioral anosmia in transgenic mice. *Neuron,* 27**,** 487-97.

XIAO, A., WANG, Z., HU, Y., WU, Y., LUO, Z., YANG, Z., ZU, Y., LI, W., HUANG, P., TONG, X., ZHU, Z., LIN, S. & ZHANG, B. 2013. Chromosomal deletions and inversions mediated by TALENs and CRISPR/Cas in zebrafish. *Nucleic Acids Res,* 41**,** e141.

YABUKI, Y., KOIDE, T., MIYASAKA, N., WAKISAKA, N., MASUDA, M., OHKURA, M., NAKAI, J., TSUGE, K., TSUCHIYA, S., SUGIMOTO, Y. & YOSHIHARA, Y. 2016. Olfactory receptor for prostaglandin F2alpha mediates male fish courtship behavior. *Nat Neurosci,* 19**,** 897-904.

YAN, C., ZHAO, A. Z., BENTLEY, J. K. & BEAVO, J. A. 1996. The calmodulin-dependent phosphodiesterase gene PDE1C encodes several functionally different splice variants in a tissue-specific manner. *J Biol Chem,* 271**,** 25699-706.

YOSHIHARA, Y. 2014. *Chapter 5 - Zebrafish Olfactory System,* Springer.

ZAPILKO, V. & KORSCHING, S. I. 2016. Tetrapod V1R-like ora genes in an early-diverging ray-finned fish species: the canonical six ora gene repertoire of teleost fish resulted from gene loss in a larger ancestral repertoire. *BMC Genomics,* 17**,** 83.

ZHANG, J., PACIFICO, R., CAWLEY, D., FEINSTEIN, P. & BOZZA, T. 2013. Ultrasensitive detection of amines by a trace amine-associated receptor. *J Neurosci,* 33**,** 3228-39.

ZHANG, X. & FIRESTEIN, S. 2002. The olfactory receptor gene superfamily of the mouse. *Nat Neurosci,* 5**,** 124-33.

ZOHAR, Y., MUNOZ-CUETO, J. A., ELIZUR, A. & KAH, O. 2010. Neuroendocrinology of reproduction in teleost fish. *Gen Comp Endocrinol,* 165**,** 438-55.

ZUCCOLO, J., BAU, J., CHILDS, S. J., GOSS, G. G., SENSEN, C. W. & DEANS, J. P. 2010. Phylogenetic analysis of the MS4A and TMEM176 gene families. *PLoS One,* 5**,** e9369.

6 SUPPLEMENTARY INFORMATION

6.1 TAAR13 family sequence homology

Multiple sequence alignments were carried out with CLUSTAL OMEGA and cover 600 bp of 5´and 3´UTRs as well as the entire TAAR13 family members exonic sequence.

Table 6.1: % identity matrix and average GC content of TAAR13 exons

% identity	exon 13a	exon 13d	exon 13b	exon 13c	exon 13e
exon 13a	100	89.28	94.05	88.3	87.72
exon 13d	89.28	100	87.72	89.67	88.79
exon 13b	94.05	87.72	100	87.72	86.65
exon 13c	88.3	89.67	87.72	100	89.47
exon 13e	87.72	88.79	86.65	89.47	100

min %id	max %id	%gc	%at
86.65	94.05	40.307513	59.692487

Table 6.2: % identity matrix and average GC content of TAAR13 5´UTRs

% identity	5´13e	5´13d	5´13a	5´13b	5´13c
5´13e	100	39.19	37.83	40.23	40.26
5´13d	39.19	100	42.88	43.81	43.33
5´13a	37.83	42.88	100	45.95	45.89
5´13b	40.23	43.81	45.95	100	52.01
5´13c	40.26	43.33	45.89	52.01	100

min %id	max %id	%gc	%at
37.83	52.01	37.07	62.93

Table 6.3: : % identity matrix and average GC content of TAAR13 3´UTRs

% identity	3´13e	3´13d	3´13c	3´13a	3´13b
3´13e	100	47.27	45.74	45.18	50.29
3´13d	47.27	100	48.58	53.39	57.31
3´13c	45.74	48.58	100	49.64	53.41
3´13a	45.18	53.39	49.64	100	57.18
3´13b	50.29	57.31	53.41	57.18	100

min %id	max %id	%gc	%at
45.18	57.31	30.43	69.57

6.2 TAAR13c knock-out sequencing result

5´13c site3, exon13c site1, ctrl_primer_fw and rev1 (~1032 bp)

TGAACAAATGTCAGGTGCTCGTAATCTGTTAACAACAGAGGTTTTTAAAGATGGTGTGGAACAGTGGCTCAGTGGTTAGCAC
TGTTGCCTGACAGCAAGAAGGTCACTGGTTTTGTATAGACTTTACATGTTCCCCTTGTACTCACATGGGTTTTCTACGGGTG
CTCTGGTTTCCCCCAACGTCAAAAGACATTCGGTATAGGTGAAATGGATGAACTAAATTGGCCGTAGTGCATGTCTGTGTGA
AAGAGAGTGTATTTCCCAGCATTTTGCTGGGTTGCAGCTGGAAAAGCATCAGCTGCGTAAAACATATGCCAAAGTAGCTGGT
GGTTCATTCAGTTGTGGCGAGCCCTGAAGAATTAGGGACTAAGCTGAAGGAAAATAAATGAATGTATAAAGGCATGCTTTTT
AGGCATTGAATCCTTCAAGTTGGAGCATGGCTGCTTTTTATTCTTATGGTGTGGTGTACTCAAAAGCTAACTTGGAAGGACT
GGAGGAATACATTGCATCAGTGTACTGTATGGGAGGATGTACCCTGTATTTCAATGCCTTGTGGTCAGTTTTAGACACATTA
CTAACTTTTTTCTTGCCTTGTTCTGTCATGGTTGGCTTGTATGCAAGAATTTTTGTAGTAGCAAAAAAGCACATAAAGTCAA
TCACTGAGGCAAACCAGAATGAAAATGAGAATGTGTTTAAAAACCCTCGACGGTCTGAAAGAAAAGCAGCAAAAACTCTTGG
TATAGTTGTGGGTGCTTTTATTCTCTGCTGGTTGCCTTTTTTTATTAACTCTCTGGTGGATCCCTACATTAACTTTCCACC
CCATATGCTCTGTTTGATGCATTTGGTTGGTTAGGCTACACAAATTCAACTCTAAACCCCATAATATATGGTCTTTTCTACC
CATGGTTTAGAAAAACTCTTTCCCTCATTGTAACTTTGAGAATATTTGAACCAAACTCATCTGATATCAATTTATTTACGGT
TTGATTTTCATCAATGTTAATTGTTTTGCACTAGCACACTATGTTTGGC

Red = confirmed by sequencing of the knock-out PCR fragment

White letters = TAAR13c exon

Green/cyan = predicted cutting site, has to be sequenced with a more adjacent primer

6.3 TARL RT-PCR with alternative primers

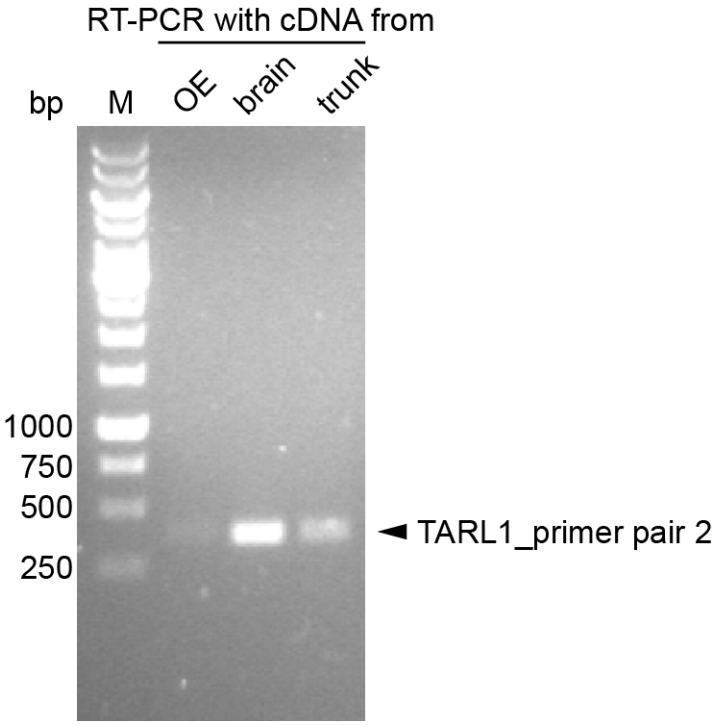

6.4 Species list and name shortcuts

Abbr	Species	Order	higher clades
Ac	*Amphilophus citrinellus*	Cichliformes	Ovalentaria, Percomorphaceae
Aa	*Anguilla anguilla*	Anguilliformes	Elopocephala
Aj	*Anguilla japonica*	Anguilliformes	Elopocephala
Ar	*Anguilla rostrata*	Anguilliformes	Elopocephala
Af	*Anoplopoma fimbria*	Perciformes	Eupercaria, Percomorphaceae
Am	*Astyanax mexicanus*	Characiformes	Otophysa
Al	*Austrofundulus limnaeus*	Cyprinodontiformes	Ovalentaria, Percomorphaceae
Bp	*Boleophthalmus pectinirostris*	Gobiiformes	Percomorphaceae
Cm	*Callorhinchus milii*	Chimaeriformes	Chondrichtyes
Ch	*Clupea harengus*	Clupeiformes	Otomorpha, Clupeocephala
Cr	*Cottus rhenanus*	Perciformes	Eupercaria, Percomorphaceae
Cs	*Cynoglossus semilaevis*	Pleuronectiformes	Carangaria, Percomorphaceae
Cn	*Cyprinodon nevadensis*	Cyprinodontiformes	Ovalentaria, Percomorphaceae
Cv	*Cyprinodon variegatus*	Cyprinodontiformes	Ovalentaria, Percomorphaceae
Cc	*Cyprinus carpio*	Cypriniformes	Ostariophysi, Clupeocephala
Dr	*Danio rerio*	Cypriniformes	Ostariophysi, Clupeocephala
Dl	*Dicentrarchus labrax*	Moronidae	Percomorpharia, Percomorphac.
El	*Esox lucius*	Esociformes	Clupeocephala
Fh	*Fundulus heteroclitus*	Cyprinodontiformes	Ovalentaria, Percomorphaceae
Gm	*Gadus morhua*	Gadiformes	Acanthomorphata
Ga	*Gasterosteus aculeatus*	Perciformes	Eupercaria, Percomorphaceae
Hb	*Haplochromis burtoni*	Cichliformes	Ovalentaria, Percomorphaceae
Hc	*Hippocampus comes*	Syngnathiformes	Percomorphaceae
Ip	*Ictalurus punctatus*	Siluriformes	Otophysa, Otomorpha
Km	*Kryptolebias marmoratus*	Cyprinodontiformes	Ovalentaria, Percomorphaceae
Lb	*Labrus bergylta*	Labriformes	Eupercaria, Percomorphaceae
Lc	*Larimichthys crocea*	Sciaenidae	Eupercaria, Percomorphaceae
LaCa	*Lates calcarifer*	Carangimorphariae	Percomorphaceae
Lo	*Lepisosteus oculatus*	Semionotiformes	Neopterygii
LetCa	*Lethenteron camtschaticum*	Petromyzontiformes	Cyclostomata
Lw	*Leuciscus waleckii*	Cypriniformes	Ostariophysi, Clupeocephala
Le	*Leucoraja erinacea*	Rajiformes	Elasmobranchii, Chondrichtyes
Mz	*Maylandia zebra*	Cichliformes	Ovalentaria, Percomorphaceae
MiMi	*Miichthys miiuy*	Sciaenidae	Eupercaria, Percomorphaceae
Mom	*Mola mola*	Tetraodontiformes	Eupercararia, Percomorpaceae
MoAl	*Monopterus albus*	Synbranchiformes	Anabantaria, Percomorphaceae
Ms	*Morone saxatilis*	Moronidae	Percomorpharia, Percomorphac.
Nb	*Neolamprologus brichardi*	Cichliformes	Ovalentaria, Percomorphaceae
Nf	*Nothobranchius furzeri*	Cyprinodontiformes	Ovalentaria, Percomorphaceae
Nc	*Notothenia coriiceps*	Perciformes	Eupercaria, Percomorphaceae
On	*Oreochromis niloticus*	Cichliformes	Ovalentaria, Percomorphaceae
Ol	*Oryzias latipes*	Beloniformes	Ovalentaria, Percomorphaceae
Po	*Paralichthys olivaceus*	Pleuronectiformes	Carangaria, Percomorphaceae
Pa	*Pampus argenteus*	Scombriformes	Percomorphaceae
Ps	*Periophthalmodon schlosseri*	Gobiiformes	Percomorphaceae
PerMag	*Periophthalmus magnuspinnatus*	Gobiiformes	Percomorphaceae
Pm	*Petromyzon marinus*	Petromyzontiformes	Cyclostomata
Pp	*Pimephales promelas*	Cypriniformes	Ostariophysi, Clupeocephala
Pf	*Poecilia formosa*	Cyprinodontiformes	Ovalentaria, Percomorphaceae
Pl	*Poecilia latipinna*	Cyprinodontiformes	Ovalentaria, Percomorphaceae
Pmex	*Poecilia mexicana*	Cyprinodontiformes	Ovalentaria, Percomorphaceae
Pr	*Poecilia reticulata*	Cyprinodontiformes	Ovalentaria, Percomorphaceae

Abbr	Species	Order	higher clades
Py	*Pseudopleuronectes yokohamae*	Pleuronectiformes	Carangaria, Percomorphaceae
PuNy	*Pundamilia nyererei*	Cichliformes	Ovalentaria, Percomorphaceae
PyNa	*Pygocentrus nattereri*	Characiformes	Otophysa
Rt	*Rhincodon typus*	Orectolobiformes	Chondrichtyes
Ss	*Salmo salar*	Salmoniformes	Clupeocephyla
Sh	*Scartelaos histophorus*	Gobiiformes	Percomorphaceae
Sf	*Scleropages formosus*	Osteoglossiformes	Osteoglossocephala
SeAl	*Sebastes aleutianus*	Perciformes	Eupercaria, Percomorphaceae
SeMi	*Sebastes minor*	Perciformes	Eupercaria, Percomorphaceae
Sn	*Sebastes nigrocinctus*	Perciformes	Eupercaria, Percomorphaceae
SeRu	*Sebastes rubrivinctus*	Perciformes	Eupercaria, Percomorphaceae
Sa	*Sinocyclocheilus anshuiensis*	Cypriniformes	Ostariophysi, Clupeocephala
Sg	*Sinocyclocheilus grahami*	Cypriniformes	Ostariophysi, Clupeocephala
Sr	*Sinocyclocheilus rhinocerous*	Cypriniformes	Ostariophysi, Clupeocephala
StePa	*Stegastes partitus*	incerta sedis	Ovalentaria
Tf	*Takifugu flavidus*	Tetraodontiformes	Eupercararia, Percomorpaceae
Tr	*Takifugu rubripes*	Tetraodontiformes	Eupercararia, Percomorpaceae
Tn	*Tetraodon nigroviridis*	Tetraodontiformes	Eupercararia, Percomorpaceae
To	*Thunnus orientalis*	Scombriformes	Percomorphaceae
Xc	*Xiphophorus couchianus*	Cyprinodontiformes	Ovalentaria, Percomorphaceae
Xh	*Xiphophorus hellerii*	Cyprinodontiformes	Ovalentaria, Percomorphaceae
Xm	*Xiphophorus maculatus*	Cyprinodontiformes	Ovalentaria, Percomorphaceae
Reference species:			
Xt	*Xenopus tropicalis*	Anura	Amphibia, Tetrapod
Xl	*Xenopus laevis*	Anura	Amphibia, Tetrapod
Mm	*Mus musculus*	Rodentia	Mammalia, Tetrapod
Cin	*Ciona intestinalis*	Enterogona	Tunicata, Chordata
Csa	*Ciona savignyi*	Enterogona	Tunicata, Chordata
Alu	*Asymmetron lucayanum*	Amphioxiformes	Cephalochordata
Bbe	*Branchiostoma bennetti*	Amphioxiformes	Cephalochordata
Bfl	*Branchiostoma floridae*	Amphioxiformes	Cephalochordata
Low quality genome:			
Sp	*Squalius pyrenaicus*	Cypriniformes	Ostariophysi, Clupeocephala
Lf	*Labeotropheus fuelleborni*	Cichliformes	Ovalentaria, Percomorphaceae
Mc	*Mchenga conophoros*	Cichliformes	Ovalentaria, Percomorphaceae
Ma	*Melanochromis auratus*	Cichliformes	Ovalentaria, Percomorphaceae
Re	*Rhamphochromis esox*	Cichliformes	Ovalentaria, Percomorphaceae
Nk	*Nothobranchius kuhntae*	Cyprinodontiformes	Ovalentaria, Percomorphaceae
SeSt	*Sebastes steindachneri*	Perciformes	Eupercaria, Percomorphaceae

7 APPENDIX

7.1 Abbreviations

ATP	adenosine triphosphate
bp	basepairs
BSA	bovine serum albumine
CAM	calmodulin
cAMP	cyclic adenosine monophosphate
cDNA	complementary DNA
CNG	cyclic nucleotide gated ion-channel
CRISPR	Clustered Regularly Interspaced Short Palindromic Repeats
DAPI	4',6-Diamidino-2-Phenylindole
DIG	digoxigenin
dlG	dorso-lateral cluster of glomeruli
DMSO	Dimethylsulfoxide
dpf	days post fertilization
GDP	guanine diphosphate
GECI	genetically encoded calcium indicator
GPCR	G-protein coupled receptor
gRNA	guidance ribonucleic acid
GTP	guanine triphosphate
Hb	habenula
IEG	immediate early gene
IHC	immunohistochemistry
ISH	*in situ* hybridization
IVT	*in vitro* transcription
MRCA	most recent common ancestor
OB	olfactory bulb
OE	olfactory epithelium
OR	olfactory receptor
OSN	olfactory sensory neuron
PBS	phosphate buffered saline
PCR	polymerase chain reaction
PDE	phosphodiesterase
pERK	phosphorylated extracellular-signal regulated kinase
rpm	rounds per minute
RT-PCR	reverse transcriptase PCR (on cDNA)
SV2	synaptic vesicle glycoprotein 2
TAAR	trace amine-associated receptor
UTR	untranslated region

V1R/V2R	vomeronasal receptor type 1/2
VNO	vomeronasal organ
kb	kilobasepairs
RT	room temperature
PFA	para-formaldehyde

7.2 Erklärung

Ich versichere, dass ich die von mir vorgelegte Dissertation selbständig angefertigt, die benutzten Quellen und Hilfsmittel vollständig angegeben und die Stellen der Arbeit − einschließlich Tabellen, Karten und Abbildungen −, die anderen Werken im Wortlaut oder dem Sinn nach entnommen sind, in jedem Einzelfall als Entlehnung kenntlich gemacht habe; dass diese Dissertation noch keiner anderen Fakultät oder Universität zur Prüfung vorgelegen hat; dass sie − abgesehen von unten angegebenen Teilpublikationen − noch nicht veröffentlicht worden ist, sowie, dass ich eine solche Veröffentlichung vor Abschluss des Promotionsverfahrens nicht vornehmen werde. Die Bestimmungen der Promotionsordnung sind mir bekannt. Die von mir vorgelegte Dissertation ist von Prof. Dr. Sigrun Korsching betreut worden.

Köln, 23.10.2017

Teilpublikationen

DIERIS, M., AHUJA, G., KRISHNA, V. & KORSCHING, S. I. 2017. A single identified glomerulus in the zebrafish olfactory bulb carries the high-affinity response to death-associated odor cadaverine. Sci Rep, 7, 40892.

7.3 Acknowledgement

First of all I would like to thank my supervisor and mentor Prof. Dr. Sigrun Korsching. She offered me the opportunity to study an interesting field of neurobiology and genetics and pursue my doctoral degree in her lab. As a young researcher I can say it is a great privilege to have a supervisor, who shares her profound knowledge and experience in each and every aspect of science with her students and at the same time cares that much about the students' personal development. Thank you!

I would also like to thank Prof. Dr. Peter Kloppenburg for being part of my thesis advisory committee and for his agreement to serve as thesis referee.

Thanks to Prof. Dr. Tobias Bollenbach for serving as chairman of the examination committee.

A big "thank you" to Prof. Dr. Ivan Manzini, who willingly offered us (Daniel and me) his lab to conduct our Ca^{2+}-imaging experiments on the zebrafish nose. He was also part of my thesis advisory committee and I am thankful for his input and discussions. Thanks also to his postdoc Dr. Thomas Hassenklöver for introducing us to the technique and to data analysis in MATLAB.

I acknowledge my gratitude to the organizers of the graduate school, foremost Dr. Isabell Witt, Dr. Katerina Vlantis and Kathy Jörgens. All of them are doing a great job guiding doctoral students along their path.

As for my lab colleagues I first want to thank Dr. Gaurav Ahuja, who introduced me to many techniques, when I started in the lab at end of 2013. Thanks to Daniel for going on various trips to the Manzini lab and the "Göttinger Altstadt" and for your advice concerning ISH. I´ll also keep the good memories of our adventurous trip to India and Gaurav's and Tripti´s wedding. Thanks, Mehmet, for taking care of our animal facility. To Ivan, thanks for your humor and sarcasm. ☺ Thank you, Adnan, for your advice and for being an excellent travel companion at ACHEMS conference and in the Florida swamps. Thanks to Manish and Kanika for being pleasant lab buddies and friends, to Vladimir for teaching me Russian, to Alex Chockley for reviewing our paper,. Thanks to all the other former lab members, Venky, Sharzad, Veronika, Marco, Alexandra, Adil, for your companionship and thanks to the members of the graduate school for your scientific and non-scientific input.

Finally, thanks to my beloved family for your everlasting support and love.